Lappeenranta
University of Technology

Markku Jokinen

CENTRALIZED MOTION CONTROL OF A LINEAR TOOTH BELT DRIVE: ANALYSIS OF THE PERFORMANCE AND LIMITATIONS

Thesis for the degree of Doctor of Science (Technology) to be presented with due permission for public examination and criticism in the Auditorium 1381 at Lappeenranta University of Technology, Lappeenranta, Finland on the 26th of November, 2010, at noon.

Acta Universitatis
Lappeenrantaensis 407

Supervisors Professor Juha Pyrhönen
Department of Electrical Engineering
Institute of Energy Technology
Lappeenranta University of Technology
Lappeenranta, Finland

Professor Olli Pyrhönen
Department of Electrical Engineering
Institute of Energy Technology
Lappeenranta University of Technology
Lappeenranta, Finland

Reviewers Professor Matti Vilkko
Department of Automation Science and Engineering
Tampere University of Technology
Tampere, Finland

Dr., Docent Marko Hinkkanen
Department of Electrical Engineering
Helsinki University of Technology
Helsinki, Finland

Opponent Professor Matti Vilkko
Department of Automation Science and Engineering
Tampere University of Technology
Tampere, Finland

Dr., Docent Marko Hinkkanen
Department of Electrical Engineering
Helsinki University of Technology
Helsinki, Finland

ISBN 978-952-214-999-2
ISBN 978-952-265-000-9 (PDF)
ISSN 1456-4491
UDC 681.51 : 621.852

Lappeenrannan teknillinen yliopisto
Digipaino 2010

ABSTRACT

Markku Jokinen

Centralized Motion Control of a Linear Tooth Belt Drive: Analysis of the Performance and Limitations

Lappeenranta 2010

149 p.

Acta Universitatis Lappeenrantaensis 407

Diss. Lappeenranta University of Technology

ISBN 978-952-214-999-2, ISBN 978-952-265-000-9 (PDF), ISSN 1456-4491

A centralized robust position control for an electrical driven tooth belt drive is designed in this doctoral thesis. Both a cascaded control structure and a PID based position controller are discussed. The performance and the limitations of the system are analyzed and design principles for the mechanical structure and the control design are given. These design principles are also suitable for most of the motion control applications, where mechanical resonance frequencies and control loop delays are present.

One of the major challenges in the design of a controller for machinery applications is that the values of the parameters in the system model (parameter uncertainty) or the system model it self (non-parametric uncertainty) are seldom known accurately in advance. In this thesis a systematic analysis of the parameter uncertainty of the linear tooth belt drive model is presented and the effect of the variation of a single parameter on the performance of the total system is shown. The total variation of the model parameters is taken into account in the control design phase using a Quantitative Feedback Theory (QFT). The thesis also introduces a new method to analyze reference feedforward controllers applying the QFT.

The performance of the designed controllers is verified by experimental measurements. The measurements confirm the control design principles that are given in this thesis.

Keywords: motion control, robust control, frequency converter, belt drive, flexible load, resonant compensation, fieldbus

UDC 681.51 : 621.852

ACKNOWLEDGMENTS

This research has been carried out during the years 2005–2010 at Lappeenranta University of Technology. The research in this doctoral thesis was carried out within the project *Motion Control* and has been partly funded by ABB.

I would like to thank all the people that made this thesis possible. I am grateful to Professor Juha Pyrhönen and Professor Olli Pyrhönen for the supervision of the thesis, to Dr. Markku Niemelä for the collaboration and encouragement during the years, to Dr. Hanna Niemelä for her help to review and improve the language of this thesis, and to all the laboratory personnel for the arrangements in the laboratory. I also would like to thank Mr. Matti Kauhanen and Mr. Matti Mustonen from ABB for important discussions during the meetings. Special thanks go to the colleagues at LUT who made my working days so much funnier and easier.

I am grateful to the pre-examiners of the thesis, Professor Matti Vilkko and Dr. Marko Hinkkanen for their valuable comments and corrections.

The financial support by Ulla Tuominen Foundation, Lahja and Lauri Hotinen Fund, Walter Ahlström Foundation, and the Finnish Cultural Foundation (South Karelia Regional Fund) is most gratefully appreciated.

Finally, my sincerest appreciation goes to my wife Marika for the understanding and support during the preparation of this thesis.

Helsinki, October 27th, 2010

Markku Jokinen

CONTENTS

ABBREVIATIONS AND SYMBOLS

Roman letters

A	attenuation
a	acceleration
b_1	viscous friction
b_s	damping constant
$C(s)$	transfer function of the controller
$C_{vel}(s)$	velocity controller
D	outer diameter
$D(s)$	disturbance
d	inner diameter
$e(t)$	error
F	force
F_{driven}	driving force
F_{init}	initial tension
$F(s)$	pre-filter
$FF(s)$	feedforward controller
f_i	shape factor
f_{max}	maximum frequency
f_{min}	minimum frequency
f_{res}	resonance frequency
f_{res_min}	minimum resonance frequency
h	curvature error
I_V	torsion modulus of the cross-section
J_1	inertia moment of the pulley
J_2	inertia moment of the pulley
J_{est}	estimated inertia of the system
J_g	inertia of the reducer
J_l	load inertia
J_m	inertia of the motor
J_{meas}	measured inertia
J_{tot}	total inertia of the system
K_1, K_2, K_3	position-dependent elasticity coefficients
K_{eff}	equivalent spring constant
K_P	gain
K_{pf}	gain
k_g	transmission rata of the gearbox
L_{cp}	distance of the centre point
L_{CS}	length of the connection shaft
L_i	length of the movement
$L_{nom}(s)$	nominal loop transfer function
l	length
l_0	initial length
l_{off}	initial length of the offset
M_p	peak overshoot
M_S	robust margin for the sensitivity
M_T	robust margin for the reference
M_{TB}	robust tracking criteria
m_{fix}	evenly distributed mass

m_{fm}	mass that moves
m_L	mass of the load
m_{ufm}	mass that moves but is not evenly distributed
n	order
$P(s)$	process transfer function
$P_{nom}(s)$	nominal model of the process
R	radius of pulley
R_i	radius of the pulley
R_{mL}	inertia ratio of the load and the motor
r	radius
$r(s)$	reference
s	distance
T_{acc}	torque used in acceleration
T_{const}	torque used in constant velocity
T_d	derivation time constant
T_{dec}	torque used in deceleration
T_{fric}	friction torque
T_i	integrator time constant
T_l	torque of the load
T_{max}	maximum torque
T_m	torque of the motor
T_{ref}	torque reference
T_{rest}	torque used in resting
T_{RMS}	RMS torque
$t_{1,end}$	time when first AT message is put into the bus
t_a	amplifier delay
t_{acc}	acceleration time
t_c	controller delay
t_{ca}	delay from the controller to the amplifier
t_{const}	constant velocity time
t_{cyc}	cycle time
t_d	loop delay
t_{dec}	deceleration time
t_{MDT}	transmitting time of MDT message
$t_{p\text{-}to\text{-}p}$	total point-to-point time
t_r	rise time
t_{rest}	resting time
t_s	sensor delay
t_{sc}	delay from the sensor to the controller
$V(s)$	disturbance
v_i	cart velocity
W_i	safety factor or robust bound factor
x	cart position
y	output

Greek letters

α	angle of the curvature
δ	stretched part of the particle

ε	tensile strain
ε_{Abbe}	Abbé error
ξ	damping factor
ξ_z,	damping factor zero
ξ_P	damping factor pole
η_g	efficiency of the gearbox
τ	delay
$\tau_{f1}, \tau_{f2}, f_f$	disturbances to the pulleys and the cart
τ_e	time constant of the torque control
φ_1, φ_2	angular positions of the pulleys
φ_{CS}	angle of the connection shaft
φ_{ref}	angular position reference
ω_0	cut-off frequency
ω_l	angular velocity of the load
ω_m	angular velocity of the motor
ω_P	angular frequency of the pole
ω_{ref}	angular velocity reference
ω_{res}	angular resonance frequency
ω_z	angular frequency of the zero

Acronyms

ADR	drive address
AC	alternating current
AT	drive telegram (amplifier telegram)
BOF	beginning of frame
CNC	computerized numerical controlled
DC	direct current
DTC	direct torque control
EOF	end of frame
ESR	electric service and repair
FCS	frame check sequence
FF_{acc}	acceleration feedforward
FF_{vel}	velocity feedforward
FMS	flexible manufacturing system
GDP	gross domestic product
GM	gain margin
GNP	gross national product
HMI	human machinery interface
IAE	integrated absolute errors
LPMSM	linear permanent magnet synchronous motor
LQG	linear-quadratic-gaussian
LTI	linear-time-invariant
MDT	master data telegram
MIMO	multiple-input multiple-output
MST	master synchronization telegram
NC	numerical controlled
OEM	original equipment manufacturers
P	proportional controller
PC	personal computer

PDF	pseudo-derivative-feedback controller
PID	proportional-integral-derivative controller
PLC	programmable logic controller
PM	phase margin
SISO	single-input single-output
SPC	solution program composer
TDOF	two-degrees-of-freedom
TV	total variation
QFT	quantitative feedback theory
ZPE	zero phase error

1 INTRODUCTION

Manufacturing automation systems have developed rapidly over the last few decades, and numerous new design methods and criteria have evolved in the field. For example, to increase the production rate of processes, the mechanical design of machines has to be lighter, and also the design is made more flexible. Typically, a central master controller calculates the references for the drives. The reference of the drive depends on the application; for instance, it can be a position, velocity, or torque reference. The drives that have been used in the processes have conventionally been servo drives, but nowadays the performance difference between servo drives and alternating current (AC) drives has significantly decreased.

This chapter highlights the background and motivation of the work. First, the history, present, and future of the manufacturing processes are outlined. Next, typical robot topologies are described. Then, control structures of the machinery applications are addressed. After that, the main challenges related to the control of flexible machines are introduced and discussed. Finally, the outline of the thesis is provided and the scientific contributions of the thesis are discussed.

1.1 History, present, and future of manufacturing processes

Manufacturing plays a significant role in the European economy. Approximately 22% of the EU gross national product (GNP) comes from the manufacturing sector, and it is estimated that 75% of the gross domestic product (GDP) and 70% of the employment in Europe is related to the manufacturing business (MANU*FUTURE* 2004). For the economy of the EU, it is important to sustain the competitiveness of the manufacturing sector, which means continuous innovations in both the production and the processes. It is not surprising that a lot of research resources have to be put in this area.

Manufacturing started around 4000 BC, when simple metal tools were made by hammering. From those days, manufacturing has significantly developed: today, almost all manufacturing processes include automation of some kind. The first automated process was launched approximately in 1850, soon after the development of a steam turbine. The first speed-controlled drive was introduced by Harry Ward Leonard, and the first system to control a movement – as we nowadays understand motion control – was developed by Henry Roland in the 1880s (Neugebauer et al. 2007).

The development of consumer goods manufacturing automation can be divided into the phases (paradigms) of *Craft Production* (from circa 1850 onwards), *Mass Production* (from 1913 onwards), *Flexible Production* (from circa 1980 onwards) and *Mass Customization and Personalization* (from circa 2000 onwards) (Jovane et al. 2003). Craft production means that a product is manufactured only once and it is made exactly according to the customer's needs. Typically, a pull-type business model (sell, design, make, and assemble) is applied. To produce the desired product, highly skilled workers and flexible machines are needed. In mass production instead, lots of identical products are made and sold to the customers. This is a much less expensive way to manufacture the products than the one-per-order method. Mass production is based on a push-type business model (design, make, assemble, and sell). This production paradigm was launched in 1913, when Henry Ford introduced a moving assembly line. In the 1970s, demand for more diversified products occurred in the market, and flexible automation was introduced as a response to this. Computer-controlled Flexible Manufacturing System (FMS) robots ensured that the same assembly machines were capable of producing

different kinds of products; a smaller volume per product could be produced at low costs. Today, it is possible to produce a variety of almost customized products at the price of mass production. This production paradigm is called mass production and personalization, and it means that the performance of the production lines has to be known, optimized, and convertible. Here, the technological tool is a reconfigurable manufacturing system (RMS). The RMS can be adapted rapidly to the demands of the market. The development of the manufacturing sector will be rapid in the future; moreover, manufacturing will significantly increase. It is approximated that by 2020 the development of nano, bio, and material technology will enable the *Sustainable Production* paradigm, which is based on society's need for better environment (Jovane et al. 2003).

The rapid evolution of manufacturing automation has produced a lot of research on the control methods of complex machines, as the control is a key factor in the performance of these machines. The first numerical control (NC) of a machine was developed in 1947 just after the World War II, when the United States Air Force and Parsons Company developed a method for moving two axes by using punch cards that included coordinate data required to machine aircraft parts. The first numerically controlled and electrically driven movement of a mechanical structure was performed by a three-axis machine tool, which was developed in a laboratory at MIT in 1952. In the 1960s and 1970s, a huge wiring panel was needed to control the manufacturing systems. The wiring panel included relays, switches, sensors, and the like. The operation logic of the manufacturing systems was designed applying these relays and switches. For describing a combination of electronic and mechanical systems, the term 'mechatronics' was launched by Yaskawa Electronic Corporation in 1969 (Neugebauer et al. 2007). In the same year, the Hydromatic Division of General Motors (GM) introduced the first programmable logic controller (PLC) (Stenerson 1999). The PLC made it possible to decrease the size of the wiring panels, because the relay logic used in the NCs could be replaced by using one program in the PLC. When the first microprocessor-based numerical controllers became available at the end of the 1970s, and almost at the same time, power semiconductors were introduced, the modern era of automation manufacturing was about to begin (Suh et al. 2008).

According to Younkin (2003), brushless direct current (DC) drives were typically used in position control applications in the 1980s; however, Bose (1985) predicted that personal computers and permanent magnet synchronous machines would play a major role in machinery and motion control systems in the future. Indeed, a modern motion control system (Fig 1.1) contains a motion controller PC or PLC, servo drives or high-performance AC drives, sensors, digital and analog inputs and outputs, fieldbus, human machinery interface (HMI), and actuators.

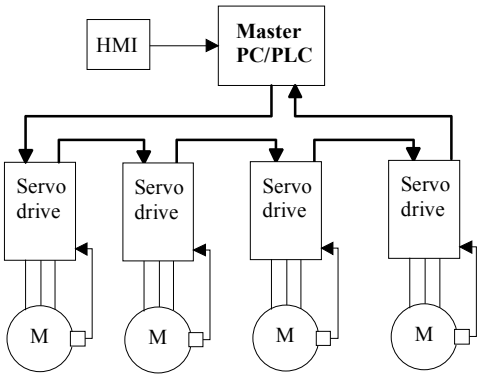

Fig. 1.1. Motion control system with one master PC/PLC that controls four servo drives via fieldbus. The motors are connected to the mechanical structure of the machine. The mechanical structure is not included in the figure.

The development of vector control and its auxiliary systems has significantly decreased the performance difference between basic AC drives and servo drives. In this thesis, 'basic AC drives' refers to industrial frequency converter drives that are mainly used in pump and fan applications. On the other hand, the AC servo drives are designed for high-performance applications such as packaging and manufacturing, and have an advanced control structure. Some applications that were previously controlled by a servo converter can now be handled with a basic AC converter without problems. According to Yaskawa (2005), the high-precision velocity regulation can be served by the vector control and a servo converter, but the high-performance position control applications can be served by a servo converter. Since 2005, however, the difference between AC and servo converters has rapidly reduced.

Nowadays, there are basic AC converters that can be updated with "a servo software package", which includes sophisticated motion calculation, a position control loop, and an interface for a synchronized fieldbus such as SERCOS, EtherCat, Profibus V3, or ProfiNet. The scan times of the AC converters interfaces such as; analog inputs and outputs or fieldbuses are reduced from 5 ms to a few hundred microseconds, and are close to the 125 µs scan times of the servo converters. The sampling times of the AC drives' control loops are decreased to 250–500 µs, whereas the servo controllers provide sampling times of 125–250 µs.

Nowadays, AC drives also support most typical feedback devices, such as pulse encoders, resolvers, SinCos encoders, and synchronous serial interface (SSI) encoders with a high resolution and high bandwidth. Figure 1.2 shows the development of the performance and functionality of the AC and servo drives. Basically, the difference between servo drives and AC drives lies only in the amount of the overloading capability. According to Yaskawa (2005), a Yaskawa Sigma Series servo drive can handle 200–300% torque compared with the 150–200% torque when a basic AC vector control drive is used. The higher amount of torque ensures faster accelerations and decelerations of the process, which reduces the total machining time. However, the situation might be different, if a one size larger AC drive were selected instead.

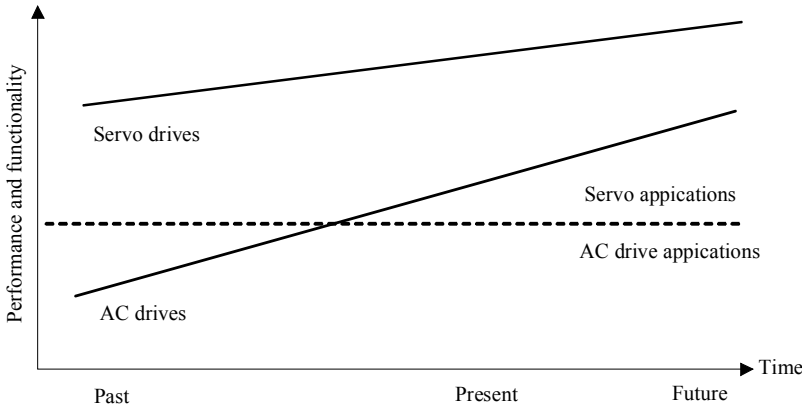

Fig. 1.2. Performance evaluation of servo drives and AC drives.

Figure 1.3 shows the principle of a modern automated process. As it can be seen, there can be several different subprocesses in a system, and every subsystem can comprise several different applications for the servo drives. One application needs a power of 0.5 kW, a rotational speed of 6000 min^{-1}, and a 0.01 mm accuracy of the linear movement. The other application requires 1 kW of power and accurate speed regulation up to the rotational speeds of 10000 min^{-1}. Of course, linear motors can be used in modern applications, and the converter has to be capable of operating with linear motors. The reason for this is that original equipment manufacturers (OEM), which design and produce automation processes, do not usually want to use several different converters.

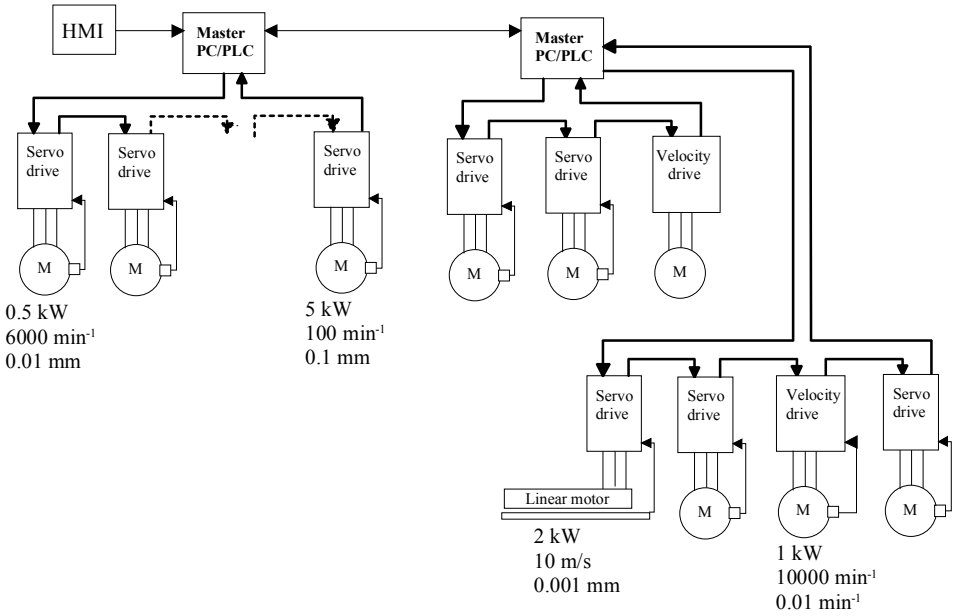

Fig. 1.3. Modern automated process can comprise several subprocesses with different kinds of applications such as accurate positioning of the rotary table, accurate velocity regulation, accurate positioning of the linear motor, and so on.

1.2 Industrial robot topologies

In the past, industrial positioning systems were cam-driven applications (Schneiders et al. 2003). The increasing demand for faster, lighter, more accurate, and more flexible systems forced engineers to design other kinds of solutions. Table 1.1 gathers some performance requirements for different kinds of applications.

Table 1.1. Application fields based on the classification of the VDMA, German Engineering Federation (Kiel 2008).

Application field	Accuracy (mm)	Cycles (1/min)	Power requirements (kW)
Painting and coating	0.1	< 20	< 5
Spot welding	0.1	< 60	< 15
Continuous welding	< 0.1	< 20	< 15
Machining	< 0.1	< 60	< 10
Cutting	< 0.1	< 120	< 5
Assembly of small parts	< 0.01	< 120	< 5
Sorting	< 0.1	< 120	< 5
Picking and palletizing	< 0.5	< 30	< 15

Each application has some special requirements, which means that one robot solution cannot be the right choice for every application. For different kinds of applications, a robot structure is developed that is most effective for purpose. This section introduces the main differences between a Cartesian robot, an articulated industrial robot, and a delta robot.

1.2.1 Articulated industrial robot and delta robot

Articulated industrial robots are used for instance in material handling, machining, painting, welding, and assembly applications. Robots are mainly aimed at general purpose use, but there are robots that are designed for a specific application purpose; for example, ABB offers special robots for painting applications. Articulated industrial robots cannot provide a full working range in every direction. Figure 1.4 shows the working range of an ABB IRB 4600-20/2.50 robot.

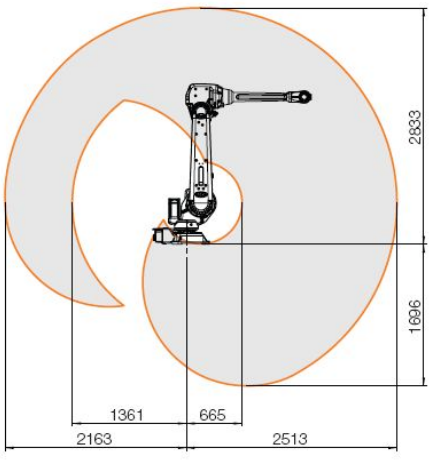

Fig. 1.4. Operation range of IRB 4600-20/2.50 (ABB 2010). Dimensions in mm.

Articulated industrial robots are designed for high accuracy and high repeatability. According to Olabi et al. (2010), the repeatability of robots varies from 0.03 mm to 0.1 mm, but the accuracy is often measured to be within several millimeters. ABB promises that their articulated industrial robots can offer position path repeatabilities between 0.1 and 0.5 mm. The maximum angular velocity of an industrial robot axis varies between 40º/s and 400º/s.

A delta robot structure is the newest comer to the pick and place markets. It was invented in the early 1980s, and the first commercial delta robot, the FlexPicker IRB 340, was launched by ABB in 1998. The design principle is simple; all moving components are made of a lightweight material, and the motors are placed in a separate non-moving base box. All arms are linked in parallel with three degrees of freedom and joined at the delta plate. Also a theta axis is added through the delta plate to give an additional degree of freedom. The theta axis ensures that the robot can rotate 360° around its vertical axis. Figure 1.5 shows the structure of the FlexPicker. The FlexPicker is capable of moving objects up to 2 kg, tolerates accelerations up to 15 m/s^2 and can reach the accuracy of 0.1 mm. Typically, the robot makes 130 pick-and-place operations per minute. (ABB Review 2008).

Fig. 1.5. Delta robot FlexPicker IRB 360 produced by ABB (Parallemic 2010).

According to Laribi et al. (2007), it is challenging to design a parallel manipulator for a given workspace; nevertheless but the authors propose an optimal dimensional synthesis method of the delta parallel robot for a prescribed workspace.

1.2.2 Cartesian robot topology

Cartesian robots are modular robots, where each moving direction is handled with a separate axis, referred to as *x*, *y*, and *z* axis. One, two, or three rotating twist arms can be added to the system. Because of the modular structure, there are lots of different kinds of Cartesian robots. The movement of the axis can be carried out by various kinds of techniques, such as a tooth belt, a lead-screw, rack and pinion, and a linear motor. Pneumatic and hydraulic operations are

naturally also possible. This thesis concentrates only on the electric axis, and the pneumatic and hydraulic axes are left outside the scope of the study. If a tooth belt, a lead-screw, or rack and pinion axis is used, the axis converts the rotational movement of the motor into the linear movement of the axis. Figure 1.6 shows one solution of Cartesian robots, where the x and y directions are handled using two separate guides for both directions, and the z direction is implemented by using only one guide. As Fig. 1.6 shows, the lowest axes must move the weight of the other axes, in other words, they have to move additional weights than just the payload. This will reduce the performance of the system.

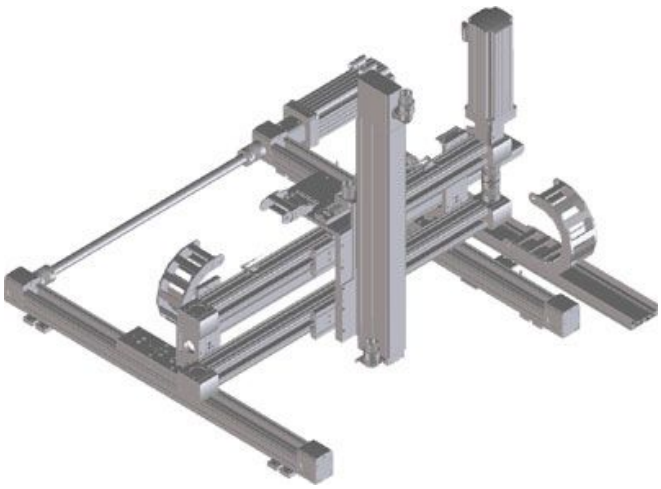

Fig. 1.6. Structure of a Cartesian x, y, z robot (Festo 2006).

The accuracy and performance of the system depend on the selection of the robot structure and also on the linear transmission components of the feed drives. Different transmission components have accuracies and stiffnesses of their own. A higher stiffness ensures a higher resonance frequency, and as a result, a higher gain of the controller can be used. Also higher accelerations can be used, because the resonance frequency of the system will not limit the acceleration and deceleration rates of the system at such low frequencies. For example, a tooth belt axis provides the lowest stiffness, while a lead-screw and a linear drive the highest stiffness. The maximum velocity of the system is, however, limited to be quite low when a lead-screw is used. If a linear motor is used, a mechanical brake is difficult to implement, the position feedback is complex, and the magnetic band tends to pick iron particles. Also the foundation of a linear motor has to be very accurate, because the air gap of the motor has to be constant. When the system is designed, the selection of the linear components depends on the requirements of the robot. The following requirements hold for the linear components:

- Movement has to be made as fast as possible or as fast as necessary
- Movement has to be made as accurate as necessary
- Movement has to be made as affordable as possible

Table 1.2 gathers the typical system parameters of different kinds of transmission components. Figure 1.7 shows the operating ranges between the drives. It should be noted that linear motors are not used in low-speed applications. Operating at low speeds is quite complex, because the detent and thrust forces of a linear motor are usually too significant from the smooth operation

point of view. Tooth belt drives are often selected for material handling applications, because they provide high speed and an accuracy that is sufficient for these kinds of applications (Kiel 2008).

Table 1.2. Parameters of the transmission components (Kiel 2008).

	Transmission components			
Property	Ball screw	Rack and pinion	Linear belt	Linear motor
Traverse path	Limited	Unlimited	Limited	Limited
Speed	2 m/s	5 m/s	10 m/s	15 m/s
Acceleration	Up to 20 m/s^2	40 m/s^2	50 m/s^2	100 m/s^2
Feed force	+++	+++	++	++
Position accuracy	0.01 mm	0.1 mm	0.1 mm	0.001 mm
Stiffness	+++	+++	+	+++
Cost	+	++	+++	-
Application	Machine tools, precision machines, printing	Gantry machine tools, feed axes	Gantry machines, handling devices	Machine tools, handling tools, high-speed machines

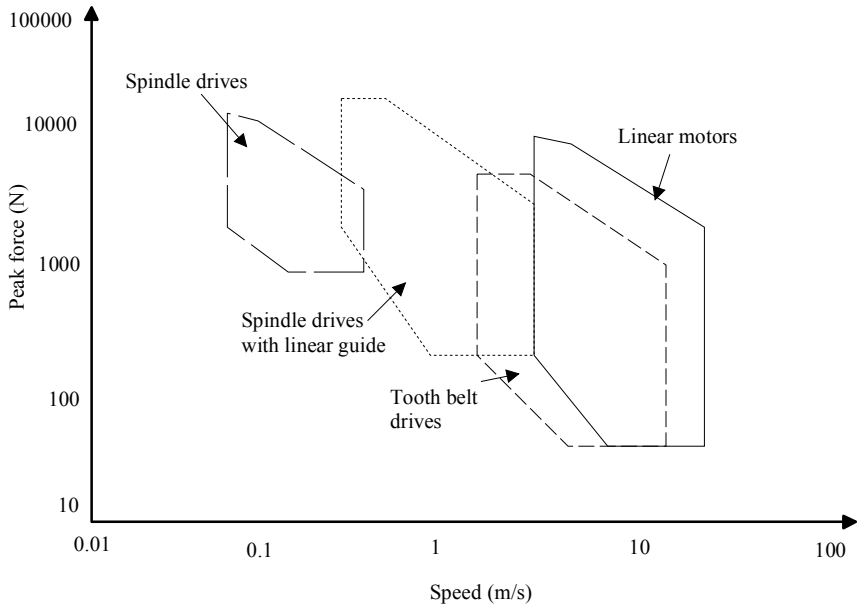

Fig. 1.7. Operating ranges of different linear drive combinations (Kiel 2008).

1.3 Motors in mechatronic applications

There are several different types of motors that are used in mechatronic applications, such as brushless permanent magnet DC motors, stepper motors, induction motors, and permanent magnet synchronous motors. Advantages and drawbacks of different types of motors are discussed for example in (Van de Straete et al. 1998), and (Puranen 2006). Traditionally, a servo motor is selected based on the shaft torque and speed requirements, the reflected load inertia, and thermal dissipation implied by the RMS load torque requirements.

If the load cycle is known, the motor can be chosen based on the speed and torque requirements. The required motor torque T_m can be calculated by

$$T_\mathrm{m} = \underbrace{\left(J_\mathrm{m} + J_\mathrm{g} + J_\mathrm{l}^\mathrm{m}\right)}_{J_\mathrm{tot}}\alpha + T_\mathrm{l}^\mathrm{m}, \tag{1.1}$$

where J_m is the inertia of the motor, J_g is the inertia of the gearbox, J_tot is the total inertia of the system, and α is the angular acceleration of the motor

$$\alpha = \frac{\Delta\omega_\mathrm{m}}{\Delta t}, \tag{1.2}$$

where ω_m is the angular speed of the motor, t is the time. J_l^m is the load inertia referred to the motor shaft

$$J_\mathrm{l}^\mathrm{m} = \left(\frac{1}{k_\mathrm{g}}\right)^2 \frac{J_\mathrm{l}}{\eta_\mathrm{g}}, \tag{1.3}$$

where J_l is the inertia of the load, k_g is the transmission rate of the gearbox, and η_g is efficiency of the gearbox. T_l^m is the load torque referred to the motor shaft

$$T_\mathrm{l}^\mathrm{m} = \frac{T_\mathrm{l}}{k_\mathrm{g}\eta_\mathrm{g}}, \tag{1.4}$$

where T_l is the load torque. The speed requirement for the motor can be calculated based on the load speed requirement

$$\omega_\mathrm{m} = \omega_\mathrm{l} k_\mathrm{g}, \tag{1.5}$$

where ω_m and ω_l are the angular speed requirements of the motor and the load, respectively.

Figure 1.8 shows one cycle of the movement of a system. We see that the rotational speed requirement is 2800 min^{-1} and the torque requirement is 13 Nm.

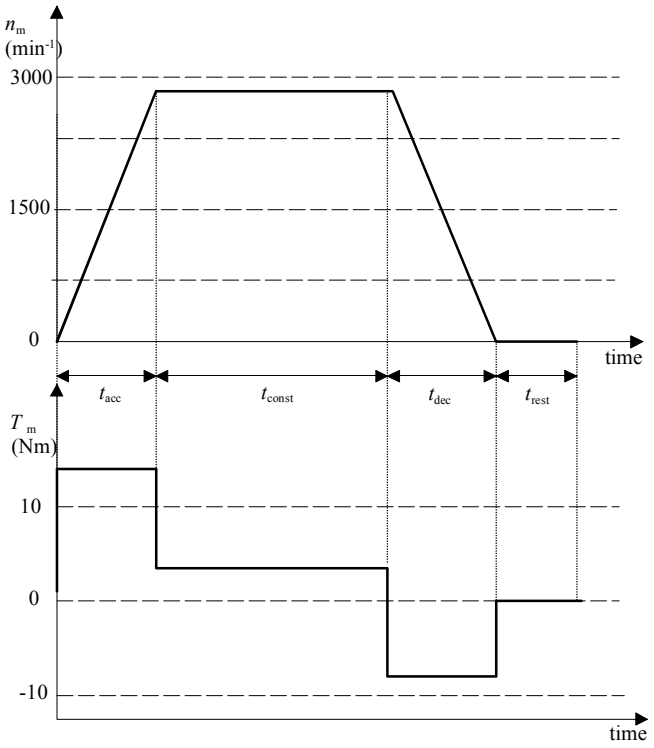

Fig. 1.8. Motor load torque T_m and motor rotational speed requirements n_m.

The RMS torque corresponding to the movement can be calculated (Voss 2007)

$$T_{\mathrm{RMS}} = \sqrt{\frac{T_{\mathrm{acc}}^2 \cdot t_{\mathrm{acc}} + T_{\mathrm{const}}^2 \cdot t_{\mathrm{const}} + T_{\mathrm{dec}}^2 \cdot t_{\mathrm{dec}} + T_{\mathrm{rest}}^2 \cdot t_{\mathrm{rest}}}{t_{\mathrm{acc}} + t_{\mathrm{const}} + t_{\mathrm{dec}} + t_{\mathrm{rest}}}}, \tag{1.6}$$

where T_{acc}, T_{dec}, T_{const}, and T_{rest} are the torque used in acceleration, deceleration, constant velocity, and resting, respectively. The torques used in Eq. (1.6) are referred to the motor axis using Eq. (1.1). Correspondingly, t_{acc}, t_{dec}, t_{const}, and t_{rest} are the times that are needed in acceleration, deceleration, constant velocity, and resting, respectively. If the cooling of the motor is not effective during the resting time, the resting time must be reduced from the denominator of Eq. (1.6). There are multiple studies available concentrating on the selection of the proper motor and the correct transmission rate of the gearbox (Van de Straete et al. 1998; Cusimano 2007), just to mention a few.

In motion control applications, the motions are often fast, and thus, the dynamics are more critical than in a classical drive. According to Younkin et al. (1991), in the case of the load inertia, the motor is often selected to approximately match the reflected load inertia, which minimizes the sensitivity of the total system to load inertia changes. But according to Stephens (2007), however, the 1:1 motor-to-inertia rule applies only to stepper motors, and servomotors that are specified using this rule will be unnecessarily large and expensive. The author claims

that he has successfully tuned systems where the inertia ratios (J_l:J_m) are up to 1600:1, but this needs stiff coupling (no backlash and no compliant).

Almost every motion control system includes some kind of a flexible structure. It could be a coupling that connects a motor and a load, or the mechanical structure of the load may be flexible. This flexible structure behaves as a spring. According to Armstrong (1998), the target of a ballscrew load has traditionally been to keep the reflected inertia under two or three times the motor inertia. Armstrong continues that allowable mismatch may be as high as 5:1 for a short span, servo rated and tensioned belt. The mismatch could be considerably smaller, however, with long spans or improper tensioning.

Sizing a motor for mechatronic applications is not simple, and it seems that especially the selection of the motor-to-load inertia ratio is empirical. In practice, each motor manufacturer has an own motor sizing tool, but these tools are only for "lumped" inertias and apply the rules of thumb listed before. A lot of research has been done in the area of sizing the motor for mechatronic applications, for example Van de Straete et al. (1998), Roos (2007), Voss (2007), Cusimano (2007), Pettersson (2008).

1.4 Features of the frequency converter and the controller

When the control of a multi-axis machine application is designed, first, it should be decided what kind of a synchronizing method is needed for the movements. Of course, some low-performance applications do not need synchronization of any kind, because the amount of contouring error is not critical. The synchronization of the movements can be divided into independent motions (sometimes referred to as a set-point co-ordinate control scheme), a classical master/slave configuration, synchronized motions, co-ordinate motions, and fully co-ordinate motions (Craig 1986) and (Kiong et al. 2008). Figure 1.9 shows the principles of the different synchronization methods. A sequence controller gives only commands such as to go to point A to point B, and a motion controller then calculates the motion profiles for a drive controller, where the position and velocity controller calculates the torque references for the torque controller. According to Lewis et al. (2004), commercial robot controllers can provide motion trajectory generation and following (co-ordinate motions), motion/process integration and sequencing (independent motion, synchronized motion), and human user integration. The last one means that the sequence control or the motion control for each axis is performed by a human user, by using for example a joystick. If separate drive controllers calculate the motion control references by themselves, the system is said to be decentralized. If the motion control and the drive controls are performed in a master controller (PLC or PC), the system is said to be a centralized one. Of course, the motion control can be made in such a way that the control tasks are divided between the master controller and the drive controllers. In that case, the system is said to be a hybrid control system.

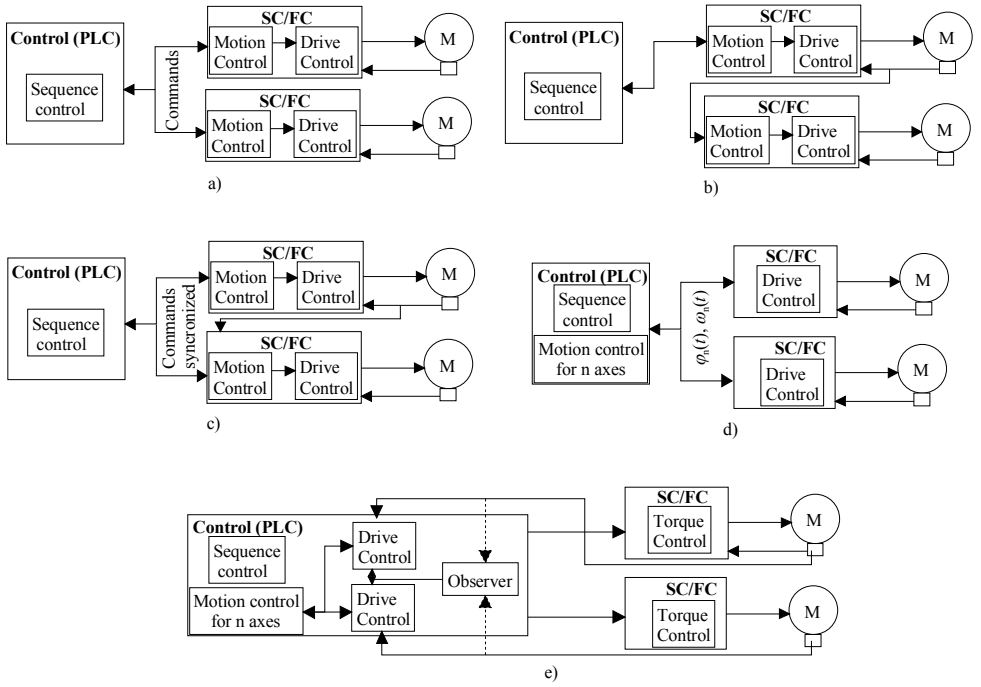

Fig. 1.9. Synchronization methods. a) Independent motions, no synchronizing, b) a classical master/slave configuration, c) synchronized motion, d) co-ordinate motions, and e) fully co-ordinate motions. SC is the servo controller, FC is the frequency converter, $\varphi(t)$ is the motion reference, and $\omega(t)$ is the velocity reference.

Independent motions are common in low-performance pick and place applications. The master controller gives only sequences for each drive, and the drive controllers calculate their own motion profiles. Independent drives operate with no knowledge of the operating conditions of the other drives. The main problem of the independent motions is that if two motors have totally different dynamics, the contouring error will increase significantly, if the dynamic differences are not compensated in the motion control calculation of the drives. In some applications, the sequence control cannot even calculate two movements at the same time, which means that the second axis is not able to start its own sequence until the first axis has finished its own movement. This increases the machinery time unnecessarily. A better option would be to use a synchronized motion or a co-ordinate motion. When synchronized motion is used, the master controller gives command sequences for each drive at the same time. Each drive controller calculates its own motion profiles, but is able to take into account the operating conditions of other drives. For example, if one of the drives cannot accelerate at the desired speed, the other drives can slow down to prevent an increasing contouring error.

When using synchronized motion, the drives need more intelligence. If the drives are not capable of reading the operation conditions of the other drives and using these values in the calculation of their own motion profiles, the motion profile calculation can be carried out in a master controller (co-ordinate motion). Modern master controllers such as PLCs or embedded PCs should at least have an option to perform synchronized motion profiles. According to Kiel (2008), independent motions are used in applications such as conveyor drives, travelling drives, hoist drives, positioning drives, drives for pumps, and ventilators. The synchronized motions are used in winding drives, cycle drives for cross cutters, and flying saws and drives for electronic cam profiles. Co-ordinate motions are used in machinery tools and robot applications.

According to Craig (1986), the classical master slave configuration is used in gantry systems. The problem of this method is that the trajectory of the master motor (motor 1) will never be smooth, and when this is fed as a reference to the second motor (motor 2), the actual trajectory of the second motor will deviate even more from the desired one. Also during a large disturbance in the second motor, the master motor will not be able to take the disturbance into account.

There are a large variety of servo applications; however, this thesis concentrates only on motion control applications, where positioning is needed, meaning that pure velocity servo applications are left outside the scope of the study. Some designers favor decentralized control systems shown in Fig 1.10. In decentralized systems, the position controller is located in the servo drive and the reference given via the fieldbus is a position reference (sequences for each drive). Typically, the sequence controller is located in a separate controller (PLC), but in some cases, one of the servo converters can operate as a master and the other drives are synchronized to the movements of the master drive, which means that a separate controller is not needed. This approach is quite demanding for the synchronization of the characteristics of the fieldbus, and furthermore, most of the fieldbus topologies are not capable of the synchronized position references. If the actual position value of the master drive is fed to the other drives as a reference value using for example encoder emulation or fieldbus, the system performs as a classical master/slave configuration.

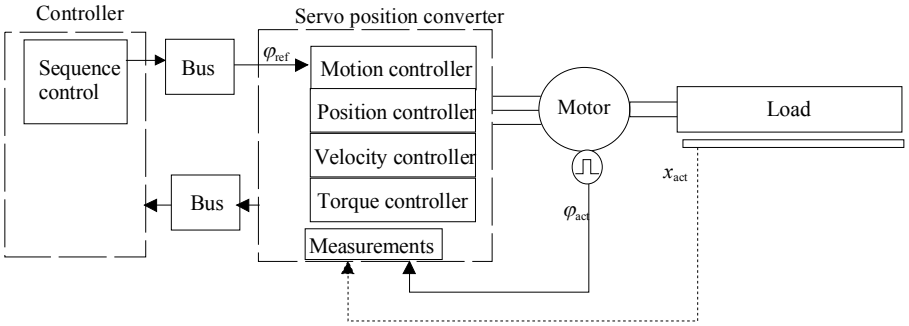

Fig. 1.10. Decentralized control system. Position reference φ_{ref} is given via fieldbus, the motor angle φ_{act} is measured using an encoder and the load position x_{act} is measured from the load using a linear encoder.

Yet another option, shown in Fig. 1.11, is to implement the position controller to a separate controller and provide the velocity reference via a fieldbus. This is a hybrid approach because the control of the machine is divided into two different controllers, a master controller and a servo velocity converter. 'Servo velocity converter' means that the converter is operating in the velocity mode. The reference can be a torque reference, T_{ref}, shown in Fig. 1.12. This means that the separate controller will calculate the motion reference, position, and velocity control, and it gives only the torque command to the drive. This is called a centralized control structure. The control structure can be either a cascaded structure, where there is both a position controller and a velocity controller, or the torque command can be made from the position references using only one controller, for example a PID position controller. If accurate multi-axis co-ordinate motion is needed, the best solution is a centralized control structure where all position and velocity loops can be closed (Kiong et al. 2008). Accurate co-ordinate motion is needed in machine tools such as computerized numerical control (CNC) machining and robot applications.

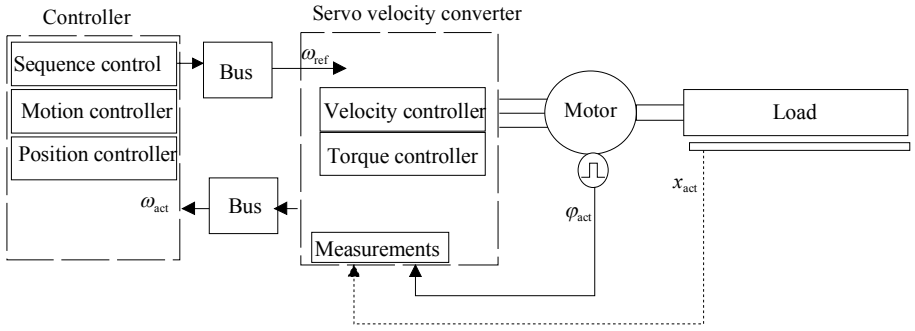

Fig. 1.11. Hybrid approach. The velocity reference ω_{ref} is given via fieldbus, the motor angle φ_{act} is measured using an encoder and the load position x_{act} is measured from the load using a linear encoder. The actual velocity ω_{act} is sent via fieldbus to the controller.

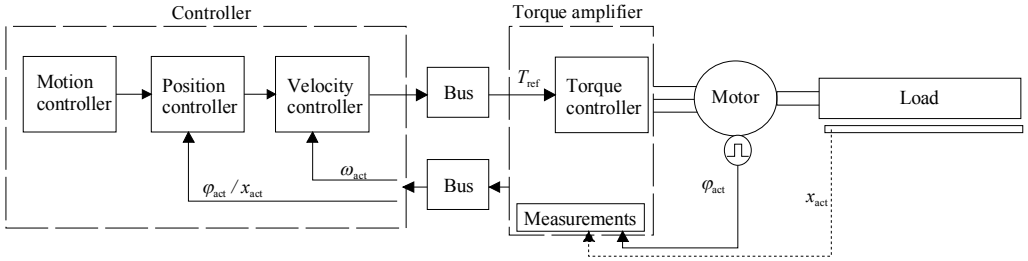

Fig. 1.12. Centralized approach in which the control structure is of a cascaded form.

1.4.1 Control structure of a high-performance frequency converter

As was stated above, there are different kinds of applications, which pose different requirements to the characteristics of frequency converters. This means that there are plenty of different frequency converters and servo converters in the market. Some are designed for "low-performance" applications while others are intended for "high-performance" applications. The most significant difference between low-performance and high-performance drives is that high-performance drives have both more modular interfaces and more complex control algorithms than low-performance drives. It is quite typical that the "high-performance" drives can read all references such as a position, velocity, and torque from the fieldbus at a high sampling rate and provide all the synchronized methods described in Fig 1.09 except the fully co-ordinate motion. Instead, when low-performance drives are used, the sampling rates are much lower and torque reference may not be supported. A lower sampling rate means a lower performance. Synchronized motion and fully co-ordinate motions are also not typically supported.

The control structure of the high-performance frequency converter is a cascaded structure, where the position controller is a P controller with a velocity feedforward (FF_{vel}), shown in Fig. 1.13. A low-pass filter is typically implemented to the velocity feedforward to prevent the high-frequency noise. Some manufactures also provide an option to use an integrator in the position

controller (PI controller) and a pre-filter for filtering the high-frequency reference and for smoothing the reference.

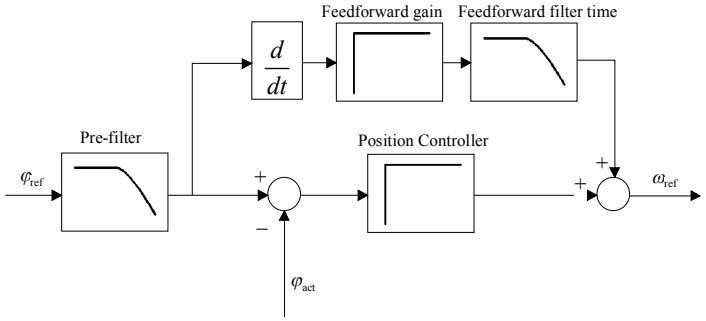

Fig. 1.13. P position controller with a velocity feedforward is a typical position control structure. The output of the controller is the angular velocity reference ω_{ref}.

The output of the position controller is the reference for the velocity control. The velocity controller is typically a PI(D) structure with an acceleration feedforward (FF_{acc}). The derivative part is not always supported. There are some differences in the filtering methods between manufacturers: Some manufacturers provide velocity error filtering, others actual value filtering, and some manufacturers may use both the actual value and reference value filtering. Torque reference filtering may also be provided by using a low-pass filter, and even a notch-filter can in some cases be added to the torque reference to filter out the resonance frequencies. Figure 1.14 illustrates these alternatives.

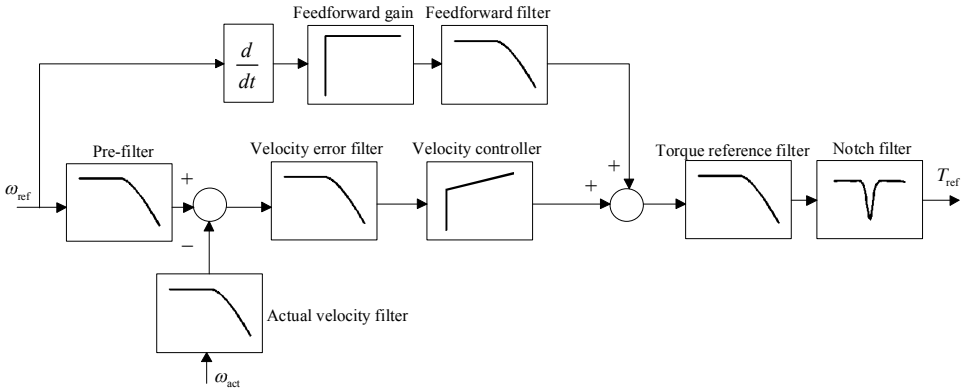

Fig. 1.14. Structure of a velocity controller. The output of the velocity controller is torque reference T_{ref}.

The torque reference is fed to the torque controller, which is a closed-loop vector control or a direct torque control (DTC). Both methods provide a very high performance control with a rise time of torque less than 1 ms. The bandwidth of the torque control seldom decreases the performance of the process, because the mechanical resonances of the system vary between 10 Hz and 200 Hz. If the bandwidth of the torque controller is notably higher than the mechanical resonance frequency is, the torque controller does not degrade the performance of the process. This requirement implies of course that the motor must have a small electric transient time constant (in a permanent magnet synchronous motors without damping L_d/R_s), and the torque controller is either the DTC or a high-performance vector control. The performance of the closed-loop position control depends on the velocity and the position controllers. Typically, the

end-user must tune the parameters of both the position controller and the velocity controller, but nowadays, some auto-tuning methods are also supported. However, these auto-tuning methods may not be practical in the processes that have a limited moving range, significant friction, or mechanical resonances.

There must also be a suitable voltage reserve for the converter to be able to produce fast torque transients. Such a voltage reserve is selected so that the field weakening range of the drive starts earlier than at the point where the motor back emf corresponds to the maximum voltage of the drive. Normally, a 10–30 % voltage reserve is needed to achieve fast torque control.

If we compare the control topologies of a high-performance frequency converter and a servo converter, we can see that there is no significant difference between these two. What is then the main reason for choosing a servo converter rather than a high performance frequency converter if high-performance position control is required? According to Yaskawa (2005), servo converters have faster torque or current loop bandwidths, the velocity and position controls are calculated faster, and the references are read more quickly from the fieldbus or analog inputs than what a frequency converter is capable of. Table 1.3 lists some parameters gathered from the data sheets of some servo converter manufactures and compared with the parameters of the ACSM1 high-performance frequency converter produced by ABB. The present servo converters have faster sampling times of both the position and velocity controllers than the ACSM1. The servo converters provide various tuning tools designed for the end user to tune the controller faster and more accurately; for example, Kollmorgen offers Bode plot calculation for detecting mechanical resonances, and the tuning tool can also calculate tuning parameter values to minimize the effect of the resonance (Wontrop 2010). This is helpful if there is a low frequency resonance present, but a skilful control designer can still design a good or even better controller using more accurate knowledge of the system parameter variations and performance requirements. Auto-tuning will naturally make system commissioning easier and faster.

Table 1.3. Parameter comparison between a high-performance frequency converter and servo converter.

	ACSM1	Servo converters
Position controller	$P + FF_{vel}$	$P + FF_{vel}$
Sampling time of position controller	500 µs	125-250 µs
Velocity controller	$PID + FF_{acc}$	$PID + FF_{acc}$
Sampling time of position controller	250 µs	125-250 µs
Notch filtering	Optional	Standard
Torque control	Fast	Fast
Tuning tools	No	Yes
Reference from fieldbus		
Position reference	500 µs	125-250 µs
Velocity reference	250 µs	125-250 µs
Torque reference	250 µs	125-250 µs
Supported motor type		
Induction motor	Yes	Yes
Permanent magnet	Yes	Yes
Linear motor	No	Yes

1.4.2 Master controller

Functionality of the master controller is one of the key elements of the machine control. Typical solutions are a programmable logic controller (PLC) or a PC-based controller. Even though high-performance servo or AC drives can operate as standalone products, a separate master controller is often chosen when high-performance applications are designed. The main advantage of the PLC or PC is the high computer power capacity. The synchronized motion profile calculations can be performed accurately for several drives, and complex control algorithms can be used for the accurate control of the machine. Also the fully co-ordinate synchronization can be easily carried out.

PLC or PC controller manufacturers have they own function block libraries, where the control designer can find typically used functions, such as a standard PID controller, filters, motion profile calculations, and so on. Thus, the control designer does not have to write own control code anymore. Nowadays, there is also a PLCopen standard (PLCopen 2010), which determines the structures (inputs and outputs) of the standard function blocks. This is very helpful for a control designer.

1.5 Transmitting medium

High-performance multi-axis positioning applications have several technical or commercial requirements for the drive and the operating fieldbus that is used as a transmitting medium between the controller and the drives. According to Hibbard (1995), the fieldbus has to meet the following conditions:

- An open system is required. The users of the products including the bus system should not be restricted to a specific supplier for both the drives and the control.
- The bus must be technology independent, permitting the use of various drive technologies such as brushless DC, vector control, a stepper, and hydraulic and pneumatic systems.
- The fieldbus must be economical.
- The fieldbus must support high-speed and high-resolution operations.
- The fieldbus must support access to internal data in a standardized format – concerning both variables and diagnostics.
- The fieldbus should support single-axis and multi-axis operation.
- The fieldbus should support distributed control.
- The fieldbus must allow the troubleshooting.

There are several fieldbus standards that meet these requirements: for example, SERCOS II, SERCOS III, EtherCat, and ProfiNet.

Properties of the SERCOS II interface are (IEC 61491 2002)

- It provides position, velocity, and torque interfaces. Also interpolation can be handled in the drive controller.
- The fiber optic ring is immune to noise, and it is practically limited to 254 drive controllers on a single ring.
- Master/Slave configuration. CNC is the master, and slave drives are permitted to respond only to CNC requests.

- The telegram type is standardized. For example IDN No 00036 is the velocity command value.
- Cyclic operation guarantees that jitter remains at a low level, and an internal timing sequence is used to ensure that all drives in a loop operate upon their command signals at exact moments. Furthermore, all drives acquire their feedback signals at exactly the same time. The cyclic operation periods can be set to 62.5 µs, 125 µs, 250 µs, 500 µs, 1 ms, and any multiple of 250 µs up to 65 ms.
- Additional information (non-critical) can be transmitted during a cyclic operation. Two bytes of information are set aside of each drive message.
- The interface supports 32 bit data values.

Other important characteristics of the fieldbus are

- Changing limit values on demand
- Changing control loop parameters on demand
- Obtaining detailed status messages from a drive
- Diagnostic functions

The Ethernet-based fieldbus topologies such as SERCOS III, EtherCat, and ProfiNet have gained the most interest in the motion control market because of the very high bandwidth of the buses. These Ethernet-based buses can transmit data using transmission rates up to 100 Mbit/s. For example SERCOS II has only 16 Mbit/s bit rate.

1.6 Control problems related to tooth belt linear drives

This chapter discusses the control problems related to tooth belt linear drives; however, the same problems are present in some form or another in every motion control application. The resonance frequency of the tooth belt linear drives is quite low, and therefore, their accurate control for high dynamic motions is also very demanding.

Position applications typically require high dynamic performance to increase the productivity of the process. The dynamic performance is usually reduced by the mechanical resonances of the system; the resonance frequency depends on the mechanical design. Typically, the natural frequency varies between 10 Hz and 200 Hz (Kiel 2008). If the natural frequency is constant, the easiest solution is to damp it with some kind of a filter or observer; for example Ellis & Lorenz (2000) and Ellis & Gao (2001) compared a low-pass filter, a notch-filter, and different kinds of observers. The best results were reached when observers were used, but the drawback of the observers is that they need an accurate system model, which may not be possible to achieve. For example, the parameters of the tooth belt or lead-screw drive depend on the position of the cart. The resonance frequency is highest when the cart is close to the motor and lowest when the cart is positioned far away from the motor. If the variation is large, linear observers cannot be used.

Tooth belt linear drives are studied by Hace et al. in (1998), (2001), (2004) and (2005). Hace et al. designed a sliding mode controller, a vibration controller, and vibration observer for a linear tooth belt drive. These studies assumed that the parameter of the process model is known and there are no parameter variations during operation, which is seldom true.

Mechanical resonances can be best avoided by using references that do not consist of the resonance frequencies. The references can designed as smooth as possible in such a way that the resonances are not excited (Singhose 1997), (Olabi et al. 2010); nevertheless, if the process has high-amplitude disturbances, resonances may be still occur.

Even though resonance damping and control of flexible loads have attracted a lot of interest in the literature, typically, an accurate process model or complex control algorithms are required. If there are parameter uncertainties or model uncertainties, these algorithms will not work without adaptation to the parameter variation. Some kind of an adaptive or robust control has to be used instead (Åström &Wittenmark 1995).

A lot of effort has been put to increase the tracking capability of the machines. Perhaps the most promising work was provided by Tomizuka (1987), who was the first to present a zero phase tracking algorithm for digital control. The work has encouraged a lot of research in the area. Even though the method is very effective, it requires a lot of measurements of the system to evaluate the phase distortion of the process. The method is still very useful if the process parameters are constant, but in most of the motion control applications this is not the case, and hence, usually other methods have to be used in industrial motion control processes.

1.7 Outline of the thesis

The structure of the thesis is twofold: The first part considers modeling of the system and identification of the system parameters. The second part focuses on the control of the system. The work is organized as follows.

Chapter 1 introduces the history of manufacturing processes and discusses the future trends in the field. The focus is on motion control applications. The chapter introduces the main components and describes the requirements of a typical motion control application. Further, the chapter shows what kind of performance can be achieved by motion control applications, what kinds of problems may occur, and how these can be avoided. Finally, the chapter provides the outline of the thesis and lists the scientific contributions of the work.

Chapter 2 presents an analytical model of a linear tooth belt drive. The uncertainties of the process model are discussed, and the non-linearities of the system are shown. This chapter introduces the reason why traditional control methods are not suitable for linear tooth belts drives. An analysis of the SERCOS fieldbus characteristics is made, and the requirements for the sampling time of the fieldbus are discussed.

Chapter 3 shows the importance of the properly designed and smooth motion profiles. The chapter discusses the advantages and drawbacks of the torque reference filtering techniques, which are very commonly used in the industry. Selection of the feedback control structure is made, and the benefits of reference pre-filtering are discussed. Finally, the implementation of the reference tracking feedforward is introduced.

Chapter 4 discusses the utilization of the robust control method called Quantitative Feedback Theory (QFT) in the motor control application of this doctoral thesis. Two different approaches to control a tooth belt linear motor are compared: a cascaded position and velocity structure and a PID position controller based structure. This chapter shows the advantages and drawbacks of these two approaches and discusses in which applications the

cascaded structure is better, and accordingly, where the PID-based structure is a better choice. Furthermore, feedforward controllers are designed for accurate reference tracking, and the advantages and limitations of the usage of feedforwards are discussed. The chapter shows the importance of the knowledge of the system parameters and discusses the performance limitations caused by the fieldbus delay.

Chapter 5 focuses on the measurement results of the system. The measurements are selected in such a way that the performance and limitations, and also the advantages and drawbacks of the designed control systems can be seen.

Chapter 6 provides the conclusions and makes suggestions for the future work.

1.8 Scientific contributions

In this doctoral thesis, the performance and limitations of a high-performance AC drive in centralized motion control applications is studied. The scientific contributions of this doctoral thesis are:

- The work shows the parameter uncertainties and nonlinearities of the tooth belt linear drive model, introduces the uncertainties of the system in the control designs and succeeds in creating a stable control for a system utilizing the accurate torque control properties of modern high performance frequency converter drives. Justifications for the simplification of the system model for the control design purposes are given.

- The thesis provides a theoretical approach to estimate the loop delay of the centralized motion control system, pointing out the main sources of the loop delay.

- The thesis shows the importance of the properly designed and smooth motion references. The work highlights the main design principles for the design of the motion references.

- The thesis demonstrates the new robust feedback control design of the linear tooth belt drive by applying Quantitative Feedback Theory (QFT).

- The thesis describes in detail the new robust reference feedforward controller design method for the linear tooth belt drive. The work shows the limitations of using the reference feedforward.

- The thesis discusses the effects of variations in the system parameters on the performance of the system. The work suggests new design principles for the selection of the mechanical components and shows the weak points of the old methods.

- The work compares in detail the performances of two different traditional control methods and shows the advantages and drawbacks of these methods.

- By modeling the system, the work points out the main performance limitations of the centralized controller tooth belt drive.

This doctoral thesis is a monograph, and the key scientific contributions are thereby presented in this work.

2 MODELING AND IDENTIFICATION OF THE SYSTEM

This chapter introduces the characteristics of the test setup, including the assembly accuracy of the linear tooth belt drive, the mechanical parameters of the test system, the SERCOS fieldbus interface characteristics, the performed measurements, the torque amplifier, and the embedded PC, where the designed control structure is implemented. In addition to determining the test system and its characteristics, the chapter aims at describing some applications in which the system can be used, and introduces the benefits and drawbacks of the linear tooth belt drive. Furthermore, the chapter addresses the issues of system modeling and performance requirements for a high-performance frequency converter.

2.1 Accuracy and resolution of machinery systems

As the manufacturing processes are evolving, also the performance requirements set for machinery systems increase. Furthermore, production rates are rising and accuracy requirements are tightening up. Figure 2.1 shows the development of machining accuracy over the last few decades. We can see that, nowadays, the typical accuracy of a CNC machine is between 10 and 100 μm, and it is categorized into the *normal machining* class. The *ultra precision machining* class comprises machines, the accuracy of which is better than 0.001 μm. For example, the thickness of an average human hair is approximately 100 μm and the diameter of an atom is 0.0001 μm. However, this dissertation studies cases where the position accuracy is above 100 μm; machinery included in this context are turning and milling machines and packaging and cutting machines. In this chapter, different types of misalignments of the linear drives are considered, and the term 'accuracy' is determined.

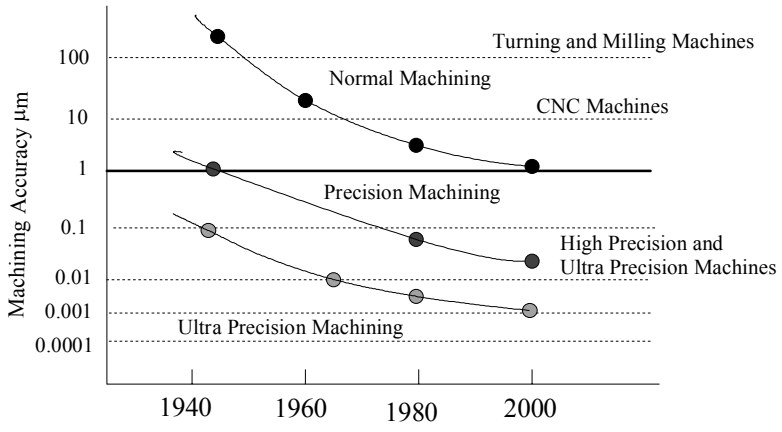

Fig. 2.1. Development of machining accuracy over the last few decades (Byrne et al. 2003).

Because of the small series production, the accuracy of the machines itself has become increasingly important. Geometrical errors of the machine have to be compensated for each product series, if the errors are not linear. The geometric errors can be compensated with error mapping, but it is time consuming and requires good understanding of the sources and effects of

geometric errors in machines. According to Rahman et al. (2000) and Schwenke et al. (2008), the most common sources of position error in multi-axis machine tools are

- Kinematic errors
- Resolution and accuracy of the linear measuring system
- Elastic deformation of drive components
- Inertia forces when braking or accelerating
- Friction and stick slip motion
- Control system
- Cutting force
- Vibration

When a three-axis tooth belt linear drive is considered, all the error sources have to be taken into account. Schwenke et al. (2008) estimate that in 2012, 30–50% of all new machine tools will be compensated for positioning, straightness, and rotation, which means that new and faster compensation methods have to be designed.

Accuracy can be divided into the accuracy of the way (path) itself and the linear position accuracy along the way (McCarthy 1991). The former describes the degree to which the ways provide an ideal single-axis translation, while the latter is concerned with the precision of increment motion along the axis including the accuracy of the mechanical structures, such as leadscrews, belt drives, and encoders. Typically, previous studies include only ideal single-axis translation when the control performance of a system is described, or only the compensation of geometrical errors is studied. An exception can be found in (Ramesh et al. 2005), which concerns both tracking and contouring error compensation methods. Measurement methods of geometric errors are gathered in (Schwenke et al. 2008; Rahman et al. 2000; Fan & Chen 2000).

Kinematic errors may result from a change in the component geometry of the *structural loop* of the machine, axis misalignment, and errors in the measuring systems of the machinery. The structural loop is defined as an assembly of mechanical components that maintains a relative position between specified objects (Schwenke et al. 2008). In linear tooth belt drives, the structural loop consists of bearings, belts, pulleys, the housing, guideways and the frame, drives and the tool, and its holders. Because of the inaccuracy of the structural loop of the linear drives, the actual end position may differ from the nominal end position, which causes a relative positioning error between the machine structures of the same kind. If the position of the axis affects the location of another axis, the error will be a function of positions similarly as is the case in multi-axis robots, which makes the machining errors more complex and challenging to compensate.

It should be pointed out that resolution, accuracy, and repeatability are not the same thing. These terms can be defined as follows: *Resolution* is the smallest resolvable increment of measurement or motion. It corresponds to the smallest increment of motion that can be measured with an encoder (Dornfeld & Lee 2008). This could be a software limit or a mechanical limit. In our test setup, the resolution of the linear encoders is 100 μm and the resolution of the motor SinCos encoder is 2^{13} line per revolution at each sine-wave and 512 waves per revolution, which gives a total resolution of over 4 million per revolution ($2^{13} \cdot 512$): However, because of the frequency converter, the fieldbus, and the motion controller, the final resolution used in the control system is 0.000025 rad, which corresponds to 0.5 μm in the linear scale in this case. *Repeatability* describes the ability to repeat the same motion or measurement within a certain definable limit. *Accuracy* can be represented as a bias between the nominal value (reference setpoint) and the actual value (actual setpoint)

$$\Delta = D_{\text{nom}} - D_{\text{act}} , \tag{2.1}$$

which should be as small as possible. In our test system, the accuracy given by the manufacturer of the SinCos encoder is 60'' (arcsecond), which corresponds to 0.06 μm in the linear scale. Other accuracy reductions are generated by the structure loop of the linear drives, assembly accuracy, and accuracy of the control. The terms are illustrated in Fig. 2.2, where the difference between accuracy and repeatability is shown.

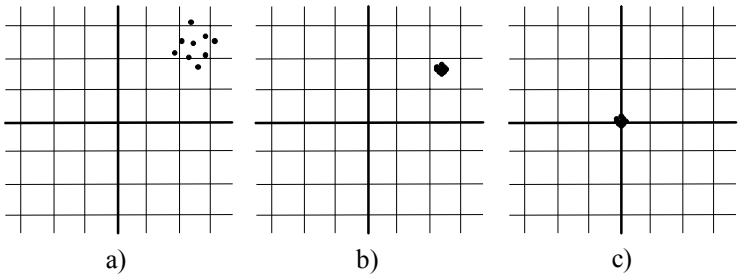

Fig. 2.2. Differences between repeatability and accuracy. The desired point is in the origin. a) Low accuracy and low repeatability, b) low accuracy and high repeatability, and c) high accuracy and high repeatability.

It should be noticed that our measurement system can measure only ideal single-axis translation and one-degree-of-freedom error; the error is measured by a motor encoder or a linear encoder. It describes only the position of the motor angle or the position of the linear axis read head. It does not include the assembly inaccuracies of the mechanical structure. The measurement error between the motor encoder and the linear encoder is caused by the inaccuracy of the measurement, the assembly of the linear encoder, and the inaccuracy of the structural loop of the tooth belt drives. During movement, the belt also stretches, which can be detected by the linear encoder.

When linear movement is considered, there can be six components of position error, which corresponds to the degrees of freedom. Figure 2.3 shows these inaccuracies. There are two linear transitional errors, a roll error, and two tilt errors called pitch and yaw errors, respectively. Transitional errors, such as a backlash or linear misalignment of the linear drives are typically minor, but in the position tables there may occur some vertical and horizontal angular errors referred to as flatness and straightness, respectively.

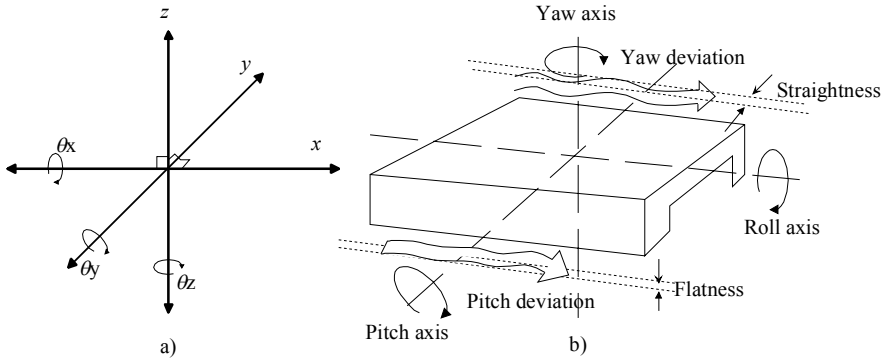

Fig. 2.3. a) Six-degrees-of-freedom, b) geometric error courses in linear movement.

Pitch and yaw errors are the main reasons for the Abbé error, which can be a significant source of error in position tables (McCarthy 1991). The Abbé error refers to a linear error caused by the combination of an underlying angular error and a dimensional offset between the object being measured and the accuracy-determining element. This phenomenon is shown in Fig. 2.4, where typical inaccuracies of the assembly are shown. Inaccuracy caused by the Abbé error can be calculated

$$\varepsilon_{\text{Abbe}} = l_{\text{off}} \cdot \tan(\alpha), \tag{2.2}$$

where l_{off} is the initial length of the offset arm and α is the angle of the curvature. The angle of the curvature can be solved from

$$\frac{h}{l}\alpha + \cos\frac{\alpha}{2} = 1, \tag{2.3}$$

where l is the initial length of the linear drive, and h is the curvature error. The calculation of the angle of the curvature can simplified

$$\alpha = 2 \cdot \arctan\left(\frac{2h}{0.5 \cdot l}\right). \tag{2.4}$$

The Abbé error of the test system can be calculated if the assembly accuracy is known. The manufacturer of the belt drives used in our test system gives the value of 0.1 mm for the assembly accuracy (=> h = 0.1 mm). Because the initial length l of the x-axis is 1600 mm, the angular error can be up to 0.0286 degrees. The maximum length of the offset arm l_{off} (y-axis length) is 1200 mm, resulting in a yaw error of 0.6 mm and a pitch error of 0.23 mm (length of the z-axis offset arm is 450 mm). These errors can be plus or minus depending on the direction of the curvature. The maximum values of the different angular errors of the test system are collected in Table 2.1. Even though the accuracy of the control system is high, these errors can occur in the system because of assembly inaccuracies.

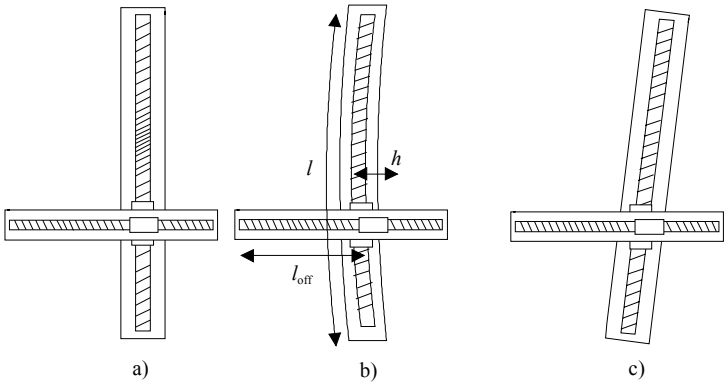

Fig. 2.4. Sources of the belt drive error; a) pitch error, b) yaw error, and c) misalignment error.

Table 2.1. Effect of an angular error on the position table accuracy.

Angular error	Offset axis	Error caused to	ε_{max} (mm)
x (roll)	x	-	-
y (pitch)	x	z	0.2
z (yaw)	x	y	0.6
x	y	z	0.3
y	y	-	-
z	y	x	0.1
x	z	y	0.1
y	z	x	0.1
z	z	-	-

2.2 Test system

Considering the characteristics of a typical pick and place system, the main requirements are fast movement, high acceleration, high deceleration, and strength to carry the working load. In our case, the objects to be moved weigh up to 5 kg. The accuracy during the movement and the contour error will probably not belong to the main interests in pick and place applications, but in cutting or printing applications, they are important for the customer, and should be taken into account when designing the system and determining its maximum performance.

In the design stage of the test system, the acceleration and deceleration requirements of the system were adjusted to 50 m/s^2, the cart velocity was set to 5 m/s, and the linear movements of the carts were 1600 mm and 1200 mm in the *x*- and *y*-direction, respectively. In the *z*-direction, requirements were less demanding than in the *x*- and *y*-directions; 20 m/s^2 acceleration and deceleration, 2 m/s cart velocity, and 300 mm cart linear movement.

The machinery meeting the performance values set for the test system was delivered by Festo Oy. The final choice for the test system was a three-degrees-of-freedom linear portal robot, which is a combination of Festo's linear tooth belt axis driven by permanent magnet synchronous motors manufactured by Electric Service and Repair (ESR). The motors were equipped with high-resolution SinCos absolute position encoders, and the linear movement was measured with a linear magnetic encoder. For the tool head, a pneumatic gripper was chosen as the primary tool for picking up the objects, but it can be easily replaced for example by a cutting device, if the target is to study a cutting application. A conveyor belt is assembled below the portal robot, which enables the study of synchronization features between the linear drives

and the assembly line. Permanent magnet servo motors are driven by ABB ACSM1 frequency converters, and the motion control references and the position and speed control are calculated in the Beckhoff embedded PC. The references and actual values between the controller and drives are transmitted via the SERCOS II fieldbus. The main principle of the test system is shown in Fig. 2.5.

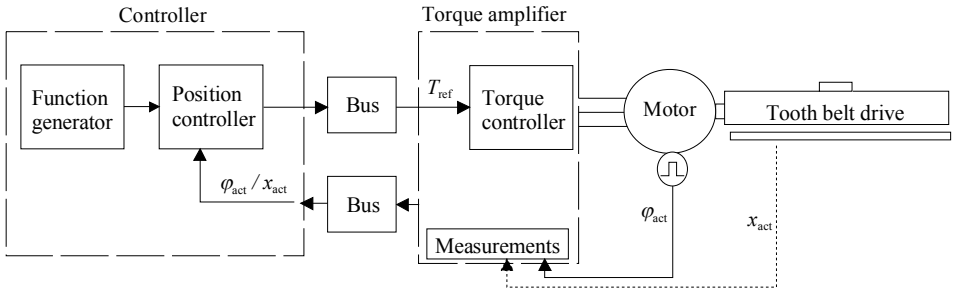

Fig. 2.5. Control system of the tooth belt test drive.

2.2.1 Mechanics and measurements

The test system is illustrated in Fig. 2.6. In both *x*- and *y*-directions, there are two tooth belt guides side by side connected by a connection shaft. This solution provides a double moving force, and faster acceleration and deceleration than a normal one-axis solution. The *z*-direction has only one axis. Each of the tooth belt linear axes is driven by a permanent magnet synchronous motor. The *x*- and *y*-directions are direct driven, but in the *z*-direction, there is a 1:3 gearbox to guarantee enough torque to pull the mass up. The axis position is measured both with absolute encoders connected to the motor shaft and with linear magnetic band encoders, which measure the movements of the carts.

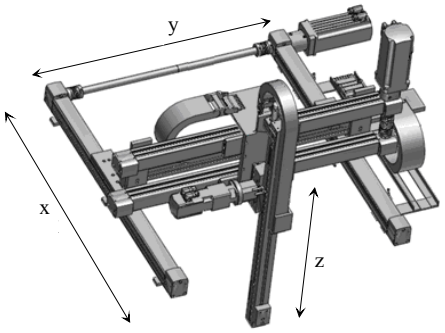

Fig. 2.6. Test system mechanical layout shown with the most essential components. The *x*- and *y*-axes are directly driven by servomotors. The *z*-axis is driven by a gear servomotor.

Table 2.2 lists the key parameters of the system. The repetition accuracy of the tooth belt drives is high enough for pick and place applications. These tooth belt drives are in practice backlash free, which means that the bidirectional approach does not result in considerable errors. The high accuracy provided by the tooth belt drives also requires an accurate assembly and solid foundation for the test system. When designing the assembly of the system, the accuracy requirements and error sources given in Section 2.1 should be taken into account. The inertia ratio of the *x*-axis is 14.9.

Table 2.2. Parameters of the test system.

	X-direction	Y-direction	Z-direction
Guide type	DGE-ZR-RF-40	DGE-ZR-RF-25	DGEA-ZE-18
Number of guides	2	2	1
Gear ratio	1:1	1:1	1:3
Stroke length (mm)	1600	1200	300
Max working load (kg)	60	30	6
Max force (N)	1220	520	230
Max speed (m/s)	10	10	3
Max driving torque (Nm)	24.2	7.4	1.4
No-load torque (Nm)	2	1	0.3
Max acceleration (m/s^2)	50	50	50
Repetition accuracy (mm)	±0.1	±0.1	< ±0.05
Moving weight (kg)	50.37	13.03	6.0
Axis pinion diameter (mm)	39.79	28.65	25.78
Inertia J_L (kgm^2)	0.0235	0.0031	0.00015
Motors			
Manufacturer	ESR	ESR	ESR
Motor Type	MR 7454-U5-N030	MR 7442-U5-N030	MR 7412-U5-N060
Rated Power (W)	4080	1250	430
Rated speed (min^{-1})	3000	3000	6000
Torque at rated speed (Nm)	13	4.0	0.7
Peak torque (Nm)	52.0	20	3.6
Inertia ($10^{-3}kgm^2$)	1.58	0.28	0.0196
Inertia ratio (J_L/J_M)	14.9	11.0	6.73

The structure of the test setup can be seen in Fig. 2.6. The *x*-axis guides carry both the y-axis and z-axis mechanical structures, and the *y*-axis guides carry the *z*-axis mechanical structure. This is one of the main problems of the portal robot structure; the total mass to be moved is very high compared with the payload. For example, the *x*-axis guides have to move 50.37 kg, while the payload is only 1 kg. Because of the mechanical structure, the performance of the test setup will be lower than the single-axis performance, which is determined only by the inertia of the single axis structure and the payload.

We can calculate the maximum performance of the test system, when the parameters of the system are given and we know the total moving weight of the axes. Let us consider two different cases. In the first case, the reference velocity trajectory is triangular, which means that the system is accelerated and decelerated with the maximum force, and no constant velocity range is used. In the second case, the velocity reference has a trapezoidal profile. Now, the system is accelerated with the maximum force to the given constant velocity and then driven

with this velocity until the system is decelerated with the maximum force. The latter one is perhaps the most widely used ramp type in industry, but the maximum forces are seldom used.

The point-to-point time can be calculated, when the boundary values of the system are known. The total point-to-point time $t_{\text{p-to-p}}$ consists of the acceleration time t_{acc}, constant speed time t_{const}, and the deceleration time t_{dec}

$$t_{\text{p-to-p}} = t_{\text{acc}} + t_{\text{const}} + t_{\text{dec}}, \tag{2.5}$$

where

$$t_{\text{acc}} = t_{\text{dec}} = \frac{\frac{v}{R} J_{\text{tot}}}{T_{\text{max}}} \tag{2.6}$$

v is the used constant cart velocity, R the radius of the pulley, and J the total inertia of the system. The constant velocity time can be calculated

$$t_{\text{const}} = \frac{L - 0.5vt_{\text{acc}} - 0.5vt_{\text{dec}}}{v}, \tag{2.7}$$

where L is the length of the movement.

In Table 2.3, the maximum performance values of the system are presented for the triangular (tri) and trapezoidal (tra) velocity profiles, respectively. The mass of the moving part is 1 kg, and the effects of friction or additional disturbances are not taken into account. Also the inertia of the system is assumed to be exactly the same as given in Table 2.2. The maximum production rate for an ideal case is 51 products per minute. This does not include settling time or the time that the vacuum gripper needs to pick the object up or place it down. If the gripper needs 0.1 second to operate, this will decrease the maximum production rate to 44 products per minute. Further, if the system needs time to settle to the position, the production rate decreases again; this means that the reference tracking capability of the system is a significant factor. As it can be seen, the movement of the x-axis will be the most critical factor for the production rate, and therefore, this thesis concentrates mainly on the performance of the x-axis. However, if we take a closer look at the single axis performance of the x- and y-axes (the axes move only the payload), the production rate is increased by over 50 %. This shows clearly that the axes of a portal robot should be as light as possible, and additional mechanical components should be avoided. When the structure is made lighter, the system may become more flexible and also more expensive.

Table 2.3. Point-to-point times with triangular (Tri) and trapezoidal (Tra) velocity profiles.

	X-direction		Y-direction		Z-direction	
Ramp type	Tri	Tra	Tri	Tra	Tri	Tra
Ramp up time (s)	0.285	0.209	0.197	0.129	0.125	0.1
Constant time (s)	--	0.191	--	0.171	--	0.1
Ramp down time (s)	0.285	0.209	0.197	0.129	0.125	0.1
Maximum velocity (m/s)	5.55	4.0	6.1	4.0	2.45	2.0
Linear movement (mm)	1600	1600	1200	1200	300	300
Point-to-point time (s)	0.579	0.609	0.394	0.429	0.25	0.3
Production rate (1/min)	51	49	76	69	120	100
Point-to-point time (s) Single axis	0.358 (9m/s)	0.48 (4m/s)	0.32 (10m/s)	0.38 (4m/s)		
Production rate (1/min) Single axis	83	62	93	78		

The RMS torque of the *x*-axis corresponding to the movement of the motion profiles calculated in Table 2.3 can be calculated by using Eq. (1.4). First, we assume that the settling time is zero, the torque needed in the constant velocity part of the profile is 3 Nm, the gripper needs 0.2 seconds to operate, and the motor is effectively cooled. Then, the RMS torque is 17.5 Nm, which is much higher than the nominal torque of the motor.

Point-to-point values calculated above assume that the mass is divided evenly on both guides. As described above, the *x*- and *y*-axes consist of two guides connected by a connection shaft to guarantee the double moving force. When the *y*-axis structure is considered, we may assume that the mass is evenly distributed because of the short connection shaft, which means that if the connection between the guides can be assumed rigid, the mass is distributed almost evenly on both guides. This is not the case in the *x*-axis structure. Figure 2.7 shows that the mass that is distributed on both *x*-guides depends on the position of the *y*-axis. When the mass is in the centre of *x*-axis point, the weight will be distributed evenly on both guides, but in other cases, one of the *x*-guides has to move more mass than the other axis, and needs more force for that. This should be taken into account when the maximum accelerations of the *x*-axes are calculated.

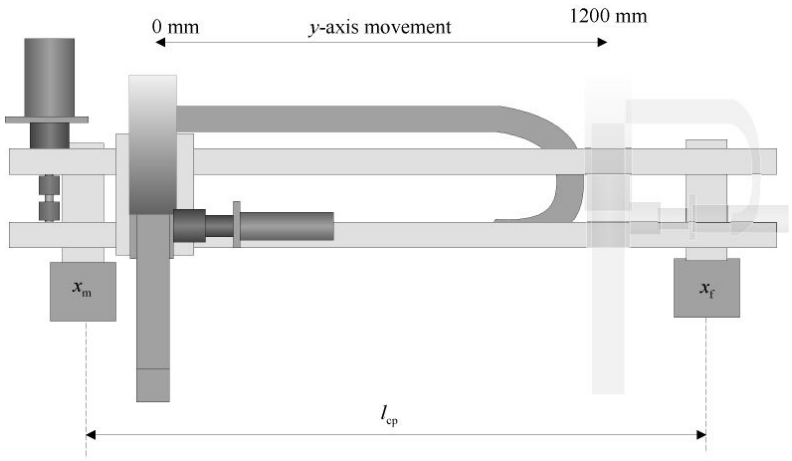

Fig. 2.7. *y*-axis structure to illustrate the weight change of both *x*-guides, when the *y*-axis is moved from the start point to the end point of the linear movement range.

We can calculate how the mass varies. First, we have to define which part of the weight moves, which part is distributed evenly on both guides, and which part is distributed only on one guide. Then, we can calculate the masses distributed on both *x*-guides with the position of the *y*-axis. The *x*-guides are denoted x_f and x_m

$$x_\mathrm{f} = m_\mathrm{fix} + \frac{y(x)}{L_\mathrm{cp}} \cdot m_\mathrm{fm} + \frac{L - \left(L - \frac{L_\mathrm{ener} - y(x)}{2} \right)}{L} \cdot m_\mathrm{ufm} \tag{2.8}$$

$$x_\mathrm{m} = m_\mathrm{fix} + m_\mathrm{my} + \left(1 - \frac{y(x)}{L_\mathrm{cp}} \right) \cdot m_\mathrm{fm} + \left(1 - \frac{L - \left(L - \frac{L_\mathrm{ener} - y(x)}{2} \right)}{L} \right) \cdot m_\mathrm{ufm}, \tag{2.9}$$

where m_fix is the mass that is evenly distributed on both guides, m_fm is the mass that moves, and m_ufm is the mass that moves but is not evenly distributed (energy carriage). $y(x)$ is the position of the *y*-axis cart, L is the length of the *y*-axis movement, L_ener is the length of the energy carriage, and L_cp is the distance of the centre point of the *x*-guides. By Eqs. (2.8) and (2.9), we obtain Fig. 2.8; we can see that the mass is evenly distributed when the *y*-axis position is around 900 mm.

This is mainly caused by the mass of the *y*-axis motor, which is assembled directly above the x_m-guide, and the motor is quite heavy compared with the other masses of the *y*-axis structure.

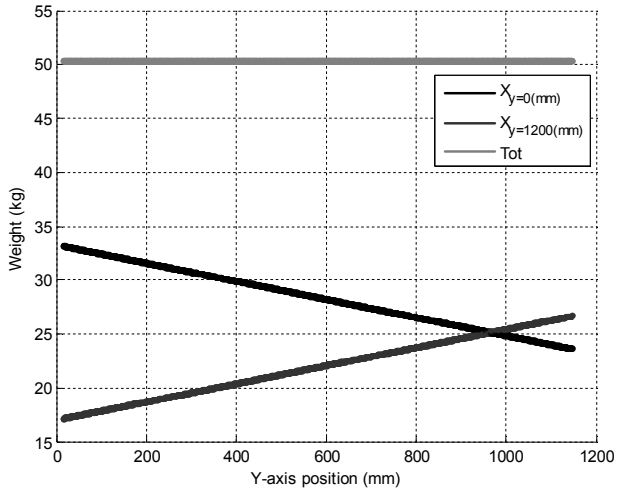

Fig. 2.8. Dependency of the *x*-axis mass on the position of the *y*-axis cart.

The total weight of the mechanical structure that the *x*-axis moves, calculated using the values given by the manufacturer of the tooth belt axis, is 50.36 kg. We also weighed the movable mass; the result was 52 kg, which is only 1.6 kg more than the calculated weight. The total inertia of the system can be calculated by using measurement results

$$J_{\text{meas}} = T_{\text{acc}} \frac{\Delta t}{\Delta \omega}, \tag{2.10}$$

where $T_{\text{acc}}=T_{\text{ref}}-T_{\text{fric}}$ is the torque used in acceleration, T_{ref} is the torque reference, T_{fric} is the estimated torque needed to overcome the static friction (stiction) of the system, Δt is the acceleration time, and $\Delta\omega$ is the angular velocity difference. Figure 2.9 shows two cases: in the first case, only one *x*-guide is accelerated without a load, and in the second case, two *x*-guides connected by a connection shaft are accelerated without a load. Here, 'without load' means that the *y*- and *z*-axis mechanical structures are removed from the system and only the inertia of the mechanical structure of the *x*-axis remains. We can see that even though the torque reference is constant, the acceleration of the motor changes during motion. This phenomenon can be explained with the non-linear friction of the test system. According to the measurements, the one-guide solution needed 1.5 Nm torque and the two-guide solution 2.4 Nm torque to overcome the stiction of the system. Using Eq. (2.10) and assuming that T_{fric} is 1.5 Nm and 2.4 Nm for one-guide and two-guides solutions, respectively, we can calculate the inertia of the *x*-axis structure J_{meas}. The value of J_{meas} varies significantly depending on the selected time instant Δt, and can get values between 52 and 145 kgcm^2. Adding the mass of the *y*-axis and *z*-axis to the inertia of the *x*-axis, we get that the total inertia of the *x*-axis varies between 240 kgcm^2 and 330 kgcm^2, when the nominal value of the system (calculated based on the datasheet values) was 250 kgcm^2.

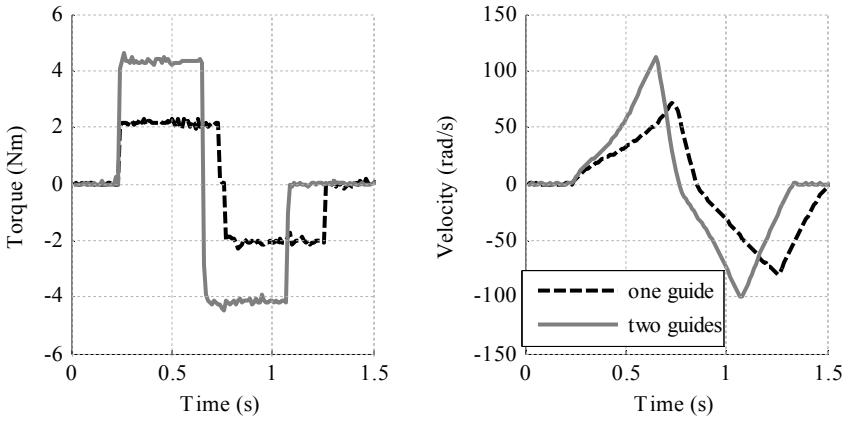

Fig 2.9. a) Torque command and b) velocity of the motor. The inertia of the system can be calculated by using a constant torque reference. The figure illustrates a case where only one x-guide is connected to the motor shaft and a case with both *x*-guides connected to the shaft in no-load situation.

When the variation of the mass is taken into account, new maximum accelerations can be calculated so that the maximum forces of either of the *x*-axis guides are not exceeded. Figure 2.10 shows the maximum accelerations given by the manufacturer (line A = 50 m/s^2 and D = 19.5 m/s^2; A is the single axis performance and D is the designed value including the *y*- and *z*-axis structure, the mass variation not included), the maximum forces given by the manufacturer (lines E and F, with the mass variation included), and thirdly, the maximum acceleration when the maximum tooth belt force is calculated according to SKS (1999) (lines B and C). When applying this method, the maximum force is 1297 N, which is over two times as high as the value given by the drive manufacturer. This implies that Festo uses quite large safety margins. The large safety margins can be needed, if the accuracy between the given inertia and the real inertia of the system is poor. For example if the "real" inertia were 320 kgcm^2, but the given inertia were 250 kgcm^2, the maximum acceleration and deceleration would decrease substantially.

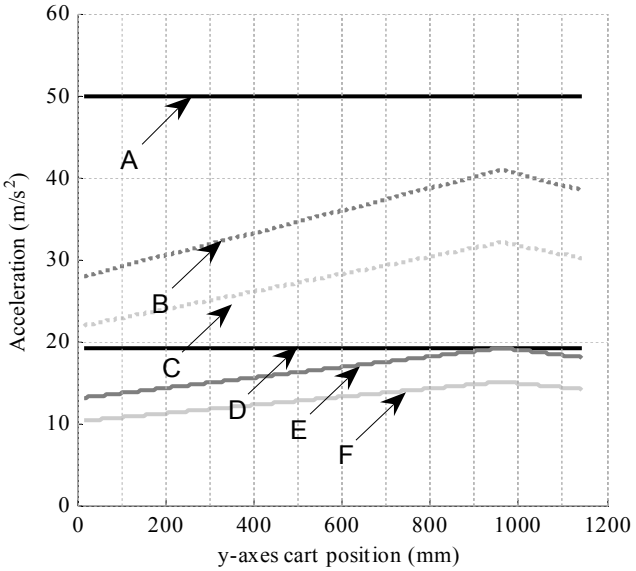

Fig. 2.10. Dependency of the axis maximum acceleration on the y axis cart position with different calculation guidelines. A) single-axis method, B) SKS method when the inertia is 251 kgcm^2, C) SKS method when the inertia is 320 kgcm^2, D) Festo design value, E) Festo method when the inertia is 251 kgcm^2, and F) Festo method when the inertia is 320 kgcm^2.

Yet another reduction of the performance, which was not taken into account in the design values given by Festo, was that the maximum velocity of the cart is reduced when the connection shaft is used in two-axis systems. The reduction depends on the dimensions of the connection shaft, length, and diameter. In our test setup, a connection shaft, KSK-40, is used between the *x*-guides and the length of the shaft is 1430 mm, which means that with the values presented in Fig. 2.11 we have to reduce the *x*-axis velocity to 1.8 m/s, which is significantly less than the ordered 5.0 m/s. This would not be a problem, if both *x*-guides were driven by motors of their own. However, this arrangement is quite complex to implement because of the accurate synchronizing requirement of both the *x*-guide movements. If there were some synchronizing error, the whole mechanism might twist. The connection shaft used in the *y*-axis structure is KSK-25, but it is only 200 mm long, and it does not reduce the maximum velocity of the *y*-axis cart.

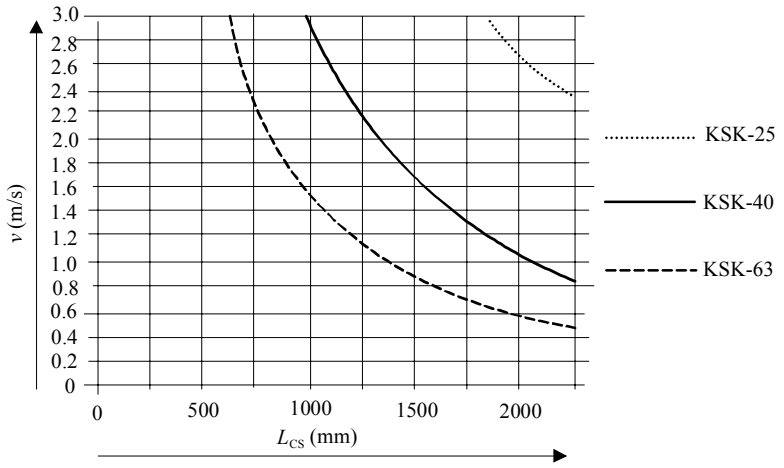

Fig. 2.11. Maximum cart velocities when a connection shaft is used. We can see that the connection shaft KSK-40 reduces the maximum allowable velocity to 1.8 m/s with the 1430 mm shaft length, bearing in mind that the initial requirement was 5 m/s (Festo 2006).

The reductions shown in Fig. 2.10 and 2.11 have a great effect on the performance of the system. Figure 2.12 shows the point-to-point motion profiles compared with the maximum single axis performance (Fig. 2.10, line A). First, only the maximum force of the tooth belts is reduced to the worst-case scenario and calculated based on the SKS method (Fig. 2.10, line C), which is almost the same as the design value of Festo, showing that the large safety margins of Festo are reasonable. Second, the maximum force is reduced to the worst-case scenario, calculated based on the Festo method (Fig. 2.10, line F), the velocity of the cart is limited to 1.8 m/s. If both the force and velocity limitations are taken into account, the point-to-point time is increased to 1.069 seconds, which is almost three times as high as the corresponding single-axis performance and 1.85 times the design value (Table 2.3).

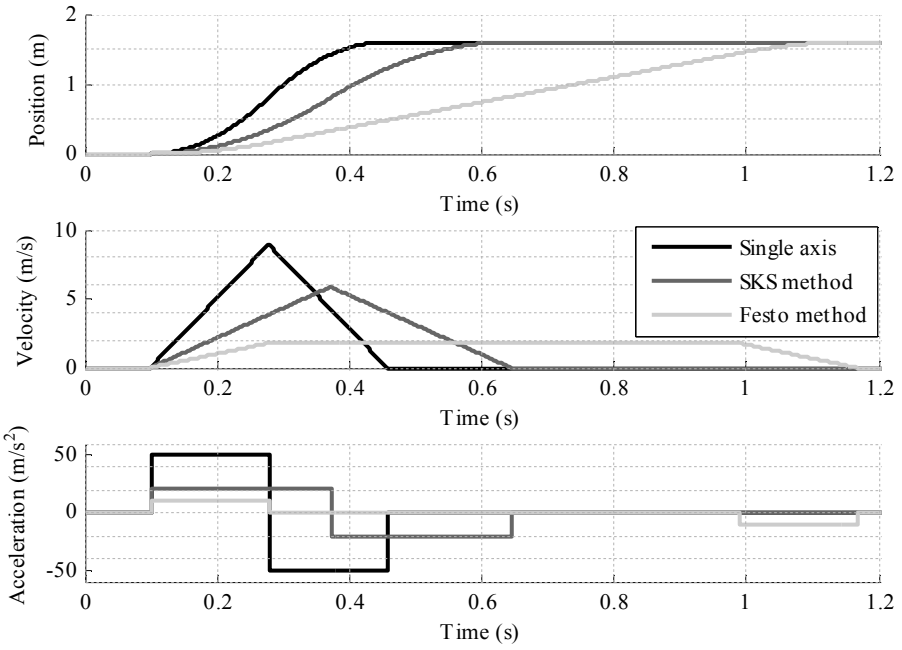

Fig. 2.12. Motion profiles; single-axis performance, force of the belt limited based on the SKS method, force of the belt limited based on the Festo method, in which the cart velocity is limited because of the connection shaft.

2.2.2 Motion control and frequency controller

The frequency converters of the test system, shown in Fig. 2.13, are ACSM1 series drives manufactured by ABB. It should be observed that these drives are not servo drives but high-performance frequency converters. As was shown in Section 1.1, the difference in performance between servo drives and high-performance frequency converters has decreased dramatically during the past few years. It will be of interest to see how these frequency converters will perform in motion control applications. ABB offers the ACSM1 series as high-performance machinery drives, which provide torque, speed, and motion control for demanding applications. The ACSM1 torque control is based on ABB's own direct torque control (DTC) and it drives both asynchronous and synchronous motors with various feedback devices. The ACSM1 supports different kinds of fieldbus topologies as well as a drive-to-drive link, which can be used for synchronized peer-to-peer communication. For analog and digital messages there are plug-in I/Os, and also extensions are available, if the standard number of I/Os does not suffice. It is also possible to modify or extend the drive functionality by using a Solution Program Composer (SPC). The most important parameters of the frequency converters are collected in Table 2.4.

Table 2.4. Parameters of the frequency converter used in the test system.

	x-direction	*y*-direction	*z*-direction	Conveyor
Frequency converter	ACSM1-04AM	ACSM1-04AM	ACSM1-04AM	ACSM1-04AM
Output current (A)	24	7	2.5	2.5
Max output current (A)	42	14.7	5.3	5.3
Output voltage (V)	0-*U*in	0-*U*in	0-*U*in	0-*U*in
Output frequency (Hz)	0-500	0-500	0-500	0-500
Output power (kW)	11	3	0.75	0.75
Options				
SERCOS interface	X	X	X	X
FEN-11 ABS	X	X	X	X
Input filter	X	-	-	-
Brake resistor	X	X	-	-

The FEN-11 ABS option module provides two inputs (SinCos absolute, TTL incremental encoder), and one output. The output can be used for encoder emulation. The SERCOS interface provides a SERCOS II standard interface with torque, speed, position, or synchronized operations with the minimum cycle time of 250 µs.

Fig. 2.13. ACSM1 high-performance frequency converter.

Even though the ACSM1 is capable of position and speed control, in this study it is used only as a torque amplifier, and the references are given via the SERCOS II fieldbus. The main controller is the Beckhoff embedded PC CX1030, shown in Fig. 2.14, which uses a 1.8 MGHz Intel® Pentium® M processor. The internal memory of the Beckhoff controller is expanded from 258 Mbytes to 1 GB. The operating system is Windows CE with TwinCAT automation software, which provides a powerful programmable logic controller (PLC). With the TwinCAT NC I option, CX1030 constitutes an advanced Motion Control system, and it can also be used to interpolate axis movements. A SERCOS Master Interface Module CX1500-M750 is needed for SERCOS communication, and four KL5101 incremental encoder modules are used to read the measurements of the linear magnetic band encoders that are used to calculate cart movements in the *x*-, *y*- and z-directions. One additional module is for the pulse encoder of the conveyor belt. Furthermore, different kinds of digital and analog input and output connections are needed as well as a relay output for the mechanical brake of the z-axis motor.

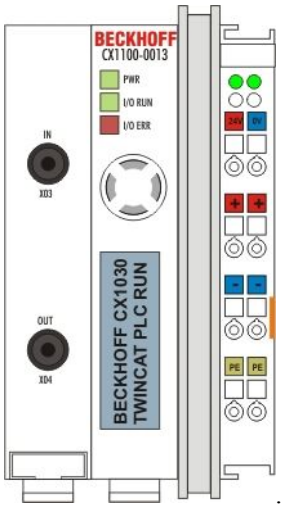

Fig. 2.14. Master controller, Beckhoff CX1030.

2.2.3 SERCOS interface

Communication between the embedded PC and the frequency converters is carried out by a SERCOS II interface, which is designed for motion control applications as was described in Section 1.5. For the control designer, it is important to know the limitations of the fieldbus interface, because wrong assumptions of the performance of the fieldbus may lead to problems. One of the typical problems is that the controller has not enough time to calculate the references for the slave drives.

Figure 2.15 shows one SERCOS data transfer cycle. MST stands for Master Synchronization Telegram from the master. It acts as a time mark for all slaves to determine when to talk on the bus and when to acquire the feedback signals. $t_{1,1}$ is the predetermined time after which the first drive in the system places its data on the bus in the Drive (Amplifier) Telegram (AT). The same applies to all drives. The drives are instructed during a SERCOS initialization phase when to transmit their message compared with the MST. When the last drive has placed its data on the bus, the master controller calculates new references, using the actual values of the slave drives. Next, the new references are sent to the slaves in the Master Data Telegram (MDT). The MDT is one long message with space set aside for each drive in the ring. The drives have been previously instructed on where their data is located within the MDT. As the MDT is received by a drive, it “fast forwards” to the start location for its information and retrieves it (Kynast 2005).

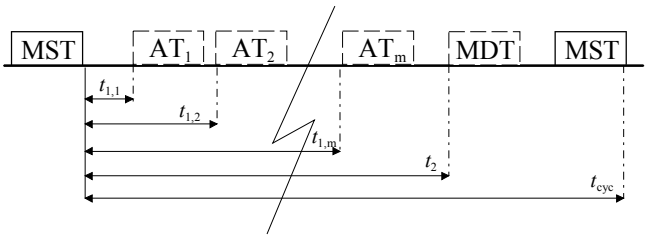

Fig. 2.15. Sercos cycle, Master Synchronization Telegram (MST), Drive Telegram (AT), and Master Data Telegram (MDT).

A MST sequence is six bytes long. It consists of Beginning of Frame (BOF), Drive Address (ADR), INFO, Frame Check Sequence (FCS), and End of Frame (EOF). The MST is sent with a broadcast target address, that is, all connected drives will receive the telegram. For this purpose, all slaves have received a synchronization marker according to which every connected drive coordinates its functional synchronization and its transmitting timeslot.

The structure of the Drive Telegram (AT) is shown in Fig. 2.16. The AT consists of BOF, ADR, Data record, and FCS and EOF sequences. The Data record sequence includes both fixed and variable data. The fixed part contains drive status information; for example, whether the drive is ready to operate. Non-cyclic information can be included in the AT message in the drive service info sequence. This part can be 2, 4, 6, or 8 bytes long. The variable data contains the values of one or more idents. In our test system, the actual velocity and position values are sent in this sequence, both being 32 bits long. This part can be up to 16 bytes long.

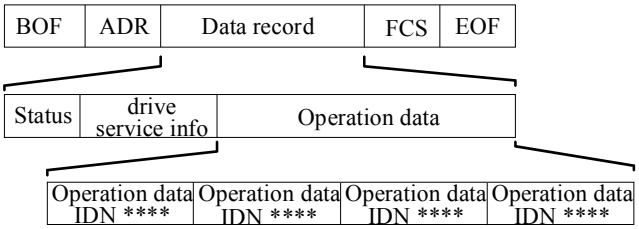

Fig. 2.16. Drive telegram (AT) sequence.

In the Master Data Telegram (MDT), shown in Fig. 2.17, the Data record includes a record for each drive in the ring, otherwise it is like an AT sequence. The fixed part of the MDT consists of commands to the drive, such as enable, disable, or halt commands. The Master servo info is needed to transmit the non-cyclic commands to the slave drives and can be 2, 4, 6, or 8 bytes long. The variable part of the MDT sequence consists of reference values to the drives chosen according to the application. In our test system, the references are 16 bits long torque commands.

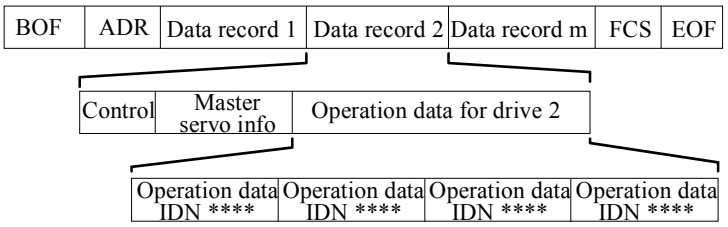

Fig. 2.17. Master Data Telegram (MDT) sequence.

The total delay of the loop consists of several independent time delays. When the process operates with a SERCOS interface, the delay of the closed-loop control, shown in Fig. 2.18, consists of the controller delay t_c, the delay from the controller to the amplifier t_{ca} (transmitting delay), the amplifier delay t_a, the sensor delay t_s, and the delay from the sensor to the controller t_{sc} (receiving delay). The controller delay t_c is typically small compared with the other delays, and it is usually ignored in the delay analysis. The transmitting delay t_{ca} and the receiving delay t_{sc} depend on the cycle time of the SERCOS loop. The amplifier t_a and the sensor t_s time delays depend on the features of the slave drives, that is, whether they are optimized for small reaction times for the references given via the fieldbus or not.

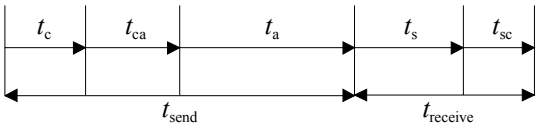

Fig. 2.18. Time delays in the system. Transmitting delay t_{ca}, receiving delay t_{sc}, amplifier delay t_a, and sensor delay t_s.

Figure 2.19 illustrates one SERCOS cycle of the test system. The time $t_{1,1}$ is the time when the first slave inserts its AT data into the bus; this time depends on the configuration of the SERCOS interface of the system, and it is 2 µs in our test system. The time delay between the AT sequences is 2 µs. The transmitting time of the AT sequences depends on the bus bandwidth and the length of the AT messages. In the test system, the transmitting times are 16 µs for the conveyor belt and 20 µs for other slaves. The AT messages include the actual values of the speed and position measured from the motor shafts. When the last slave drive has inserted its AT data into the bus $t_{1,end}$, the master starts to calculate new references for the slaves after a waiting time of 20 µs. This waiting time guarantees that every AT sequence from the slaves has arrived and is ready to be used in the control loops in the master controller. 20 µs is the minimum time recommended by Beckhoff (manufacturer of the master controller). $t_{1,end}$ is 84 µs in the test system, and thus the master controller can start to calculate the control loop at the time instant of 104 µs. The references are inserted into the bus in the MDT sequence at the time t_2, which is t_{cyc}-59 µs, where t_{cyc} is the cycle time of the fieldbus. Transmitting of the MDT message will take 35 µs. Adding t_{MDT} to the time between t_2 and $t_{1,end}$ gives the control delay t_c plus the SERCOS transmitting delay t_{ca}

$$t_2 + t_{MDT} - t_{1,end} = t_c + t_{ca} . \tag{2.11}$$

At the time t_3 the new references are available for the slave drives, and the torque controls of the slave drives start their own cycles. Torque controller needs time t_{tc} to increase or decrease the

current depending on the reference. The value of t_3 depends on the parameters of the drive. In our test system t_3 is t_{cycle}-3 µs. Thus, the total amplifier delay t_a consists of

$$t_a = (t_3 - t_2 + t_{MDT}) + t_{tc} . \tag{2.12}$$

When the motor current changes, it has an effect on the motor angular position. The motor angular position is measured using an encoder connected to the motor shaft. The output of the encoder is read by the torque amplifier, and it calculates the position in a form that can be used in the slave drive control sequences. This calculation brings the time delay t_c. At the time t_4, the feedback information is acquired from the sensor (the data is delayed by the time of t_s). The exact time of t_4 depends on the configuration of the system SERCOS interface, and it is t_{cyc}-26 µs in the test system. Thus, the time delay from the sensor to the controller (SERCOS receiving delay) consists of

$$t_{sc} = (t_{cyc} - t_4) + t_{1,end} . \tag{2.13}$$

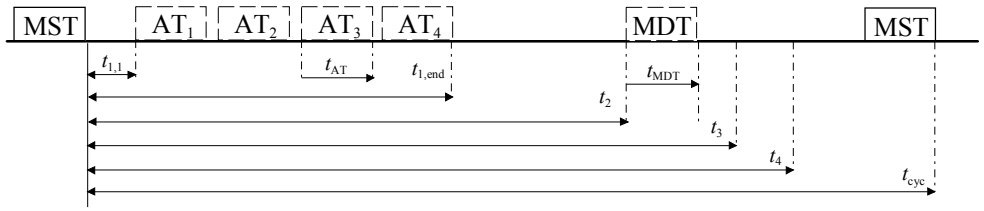

Fig. 2.19. SERCOS timing in the test system.

Table 2.5 presents the delays of the SERCOS loop calculated with different cycle times, and shows also how far the cart moves during this delay period at the velocity of 4 m/s. As can be seen in Table 2.5, the time delays of the amplifier t_a and the sensor t_s, respectively, are the main delays when the cycle time is reduced to 250 µs. The cycle time 250 µs may provide problems because of the small t_c+t_{ca} time. The controller may not have enough time to calculate the new references and to put them on the bus. This, of course, depends on the control structure and computation power of the master controller.

Table 2.5. Time delays of the sercos loop with different cycle times

Cycle time t_{cyc}	$t_c + t_{ca}$	t_a	t_s	t_{sc}	t_{tot}	e (4 m/s)
1000 µs	857	280	300	110	1547	6.2 mm
500 µs	357	280	300	110	1047	4.2 mm
250 µs	107	280	300	110	797	3.2 mm

Because the total loop delay is larger than the cycle time of the system, it may be difficult to perceive the length of the delay. Figure 2.20 shows the formation of the loop delay. At the time instant t_4 the feedback information is acquired from the sensor, but it is delayed by the time of t_s (300 µs). The feedback information is transmitted to the master controller in time of t_{sc} (110 µs), the controller calculates new references and transmits them to the slave drive in the time of t_c+t_{ca} (107 µs). The current of the motor is changing according to the new reference after the time of t_a (280 µs). This will be take place in every cycle time of the fieldbus.

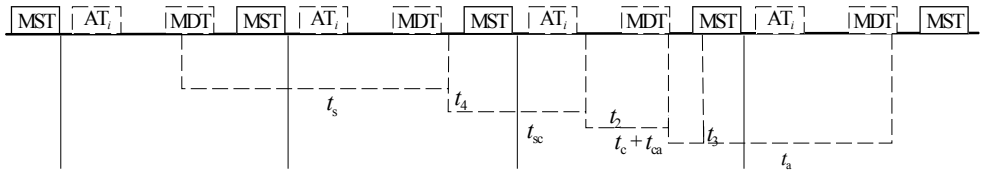

Fig. 2.20. Development of the loop delay with a cycle time of 250 µs.

By using these standard telegram types given above and assuming that the control of the slave needs a calculation time of 20 µs per slave from the master, we can calculate how many slave drives can be included in the ring with different cycle times of the SERCOS ring. Figure 2.21 shows that by using 8 Mbit/s transmitting bound rate and 250 µs cycle time, we can insert four slave drives into the ring. If the bound rate is increased to 16 Mbit/s, there can be six slave drives in the ring. The SERCOS standard promises a far higher number of slave drives to be added to the ring, but this will not include any delays or calculation times of the master drive. The number describes only how many bits can be transmitted with the maximum bound rate, and it assumed that MDT and AT messages are of the maximum length.

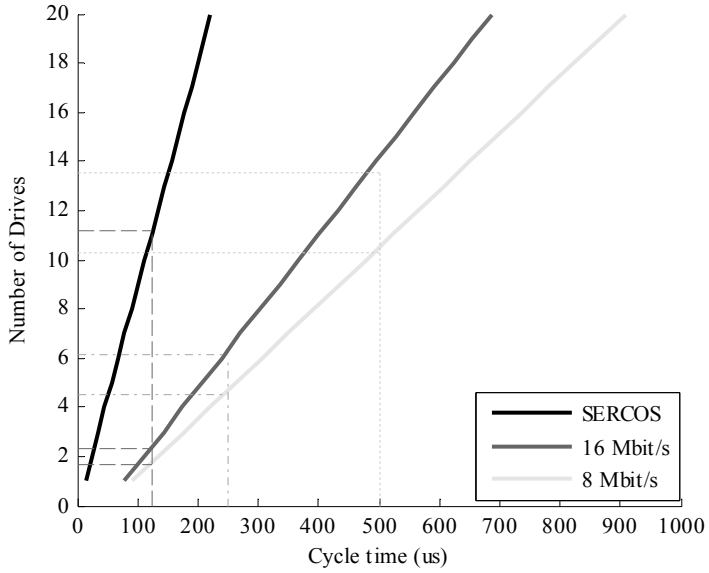

Fig. 2.21. SERCOS cycle time versus number of slaves on the ring. SERCOS is the maximum bandwidth of the bus, with no other calculations included. 16 Mbit/s contains the calculation delays and other delays. 8 Mbit/s is similar to 16 Mbit/s, but the transmission rate is reduced to 8 Mbit/s instead of 16 Mbit/s.

2.3 Modeling of the tooth belt linear drive

2.3.1 Mathematical model of the tooth belt drive

A mathematical model of the tooth belt linear axes is introduced in (Hace et al. 2004). It consists of a timing belt, two pulleys, a gearbox, and a load. The model is quite complex and non-linear. It assumes that the motor is connected rigidly to the driving pulley and there is no backlash in the system. Frictions are considered as unknown disturbances. The model of the tooth belt linear axes that Hace et al. (2004) proposed is

$$\begin{aligned}
&\left(J_1 + k_g{}^2\left(J_g + J_m\right)\right)\cdot \ddot{\varphi}_1 + f_{f1} = k_g T_{ref} - R\left[K_1(x)\left(R\varphi_1 - x\right) - K_3(x)\left(R\varphi_2 - R\varphi_1\right)\right] \\
&J_2\ddot{\varphi}_2 + f_{f2} = R\left[K_2(x)\left(x - R\varphi_2\right) - K_3(x)\left(R\varphi_2 - R\varphi_1\right)\right] \\
&m_L\ddot{x} + f_f = K_1(x)\left(R\varphi_1 - x\right) - K_2(x)\left(x - R\varphi_2\right),
\end{aligned} \tag{2.14}$$

where J_1 and J_2 are the inertia moments of the pulleys, J_G and J_m are the inertias of the reducer and the motor, respectively, m_L is the mass of the load, R the radius of pulleys, k_g is the gear ratio of the reducer, K_1, K_2, and K_3 are the position-dependent elasticity coefficients of the belt, φ_1 and φ_2 are the angular positions of pulleys, x is the cart position, T_{ref} is the torque reference to the system, and f_{f1}, f_{f2}, and f_f are the disturbances to the pulleys and the cart. The basic principle of the mechanical model of the flexible axes is shown in Fig. 2.22.

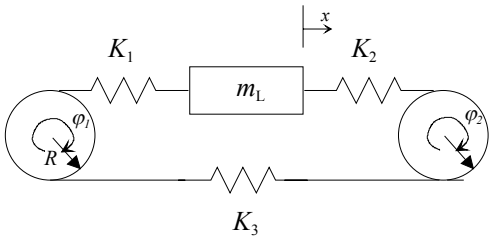

Fig. 2.22. Model of the linear tooth belt axis. R is the pulley radius, φ_1 and φ_2 are the angular positions of pulleys, K_i is the spring constant at different parts of the belt, m_L is the load mass, and x is the position of the mass.

Because there is no gearbox in the test system (x- and y-directions), and the inertias of the pulleys are small compared with the inertia of the motor and the load, the system can be simplified to a two-mass model. This can be rearranged as follows

$$\begin{aligned}
&J_m \cdot \ddot{\varphi}_m + f_{f1} = T_{ref} - RK_{eff}\left(R\varphi_m - x\right) \\
&m_L\ddot{x} + f_f = K_{eff}\left(R\varphi_m - x\right),
\end{aligned} \tag{2.15}$$

where K_{eff} is the equivalent spring constant of the system. Figure 2.23 shows the block diagram of Eq. (2.15).

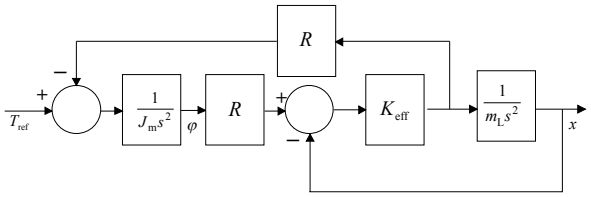

Fig. 2.23. Simplified block model of the linear tooth belt axis. Damping and frictions are not included.

The transfer function from a torque reference T_{ref} to an angular position of the motor φ_{m} based on Eq. (2.15) is given in the form

$$\frac{\varphi_{\mathrm{m}}}{T_{\mathrm{ref}}} = \underbrace{\frac{1}{\left(J_{\mathrm{m}}+m_{\mathrm{L}}R^2\right)s^2}}_{\textit{Rigid Part}} \underbrace{\frac{m_{\mathrm{L}}s^2 + K_{\mathrm{eff}}}{\frac{J_{\mathrm{m}} \cdot m_{\mathrm{L}}}{J_{\mathrm{m}} + m_{\mathrm{L}}R^2}s^2 + K_{\mathrm{eff}}}}_{\textit{Flexible Part}} . \tag{2.16}$$

The transfer function can be assumed to consist of two parts, a rigid part and a flexible part. In some cases, the whole system is analyzed and modeled using only the rigid part, which gives too optimistic estimate of the behavior of the system and more optimistic performance than a system where the flexible part is modeled. Weakness of Eqs. (2.14)–(2.16) above is that they do not include any damping, and models give constant vibration after a transient situation. In real systems vibrations will be damped at some time constant. The transfer functions from the torque reference T_{ref} to the motor angular position φ_{m} should be written as

$$\frac{\varphi_{\mathrm{m}}}{T_{\mathrm{ref}}} = \underbrace{\frac{1}{\left(J_{\mathrm{m}}+m_{\mathrm{L}}R^2\right)s^2 + b_{\mathrm{l}}s}}_{\textit{Rigid Part}} \underbrace{\frac{m_{\mathrm{L}}s^2 + b_{\mathrm{s}}s + K_{\mathrm{eff}}}{\frac{J_{\mathrm{m}} \cdot m_{\mathrm{L}}}{J_{\mathrm{m}} + m_{\mathrm{L}}R^2}s^2 + b_{\mathrm{s}}s + K_{\mathrm{eff}}}}_{\textit{Flexible Part}} , \tag{2.17}$$

where b_{l} is the viscous friction of the system and b_{s} the damping constant of the belt. The transfer function from the torque reference to the angular velocity of the motor ω_{m} is

$$\frac{\omega_{\mathrm{m}}}{T_{\mathrm{ref}}} = \frac{1}{\left(J_{\mathrm{m}}+m_{\mathrm{L}}R^2\right)s + b_{\mathrm{l}}} \frac{m_{\mathrm{L}}s^2 + b_{\mathrm{s}}s + K_{\mathrm{eff}}}{\frac{J_{\mathrm{m}} \cdot m_{\mathrm{L}}}{J_{\mathrm{m}} + m_{\mathrm{L}}R^2}s^2 + b_{\mathrm{s}}s + K_{\mathrm{eff}}} . \tag{2.18}$$

The damping constant of the tooth belt drive can be approximated by (Graham 1996)

$$b_{\mathrm{s}} = 2\xi J_{\mathrm{i}}\omega_{\mathrm{i}} , \tag{2.19}$$

where ξ is the approximated damping of the system, J_{i} is the inertia of the system in the studied case, and ω_{i} is the resonant angular frequency in the studied resonance case. Another way of calculating the damping can be found in (Niiranen 2009)

$$b_{\mathrm{s}} = \frac{\xi}{\pi \cdot f_{\mathrm{res\_min}}} k_i \ , \tag{2.20}$$

where $f_{\mathrm{res\_min}}$ is the approximated minimum resonance frequency of the system and k_{i} is the spring constant of the system in the studied frequency point. According to Niiranen (2009), the approximated damping of the system varies between 0.005 and 0.05, where the higher value is for a flexible coupling and the lower for rigid couplings.

Assuming that the resonant frequency is 56 Hz, the spring constant k_{i} is $7.5 \cdot 10^5$ N/m, the inertia of the motor 0.00158 kgm^2, and the load referred to the motor shaft is $J_{\mathrm{L}} = m_{\mathrm{L}} \cdot R^2$. The approximated damping of the system varies between 0 and 0.05, which gives the damping constants $b_{\mathrm{s}} \in [0, 20, 50, 150]$ Ns/m. The effect of the damping constant b_{s} of the belt is shown in Fig. 2.24. We can see from the figure that when b_{s} is 150 Ns/m, the resonance of the system is damped already after 8–10 cycles. With other damping constants, the belt will oscillate quite strongly for a long time before damping.

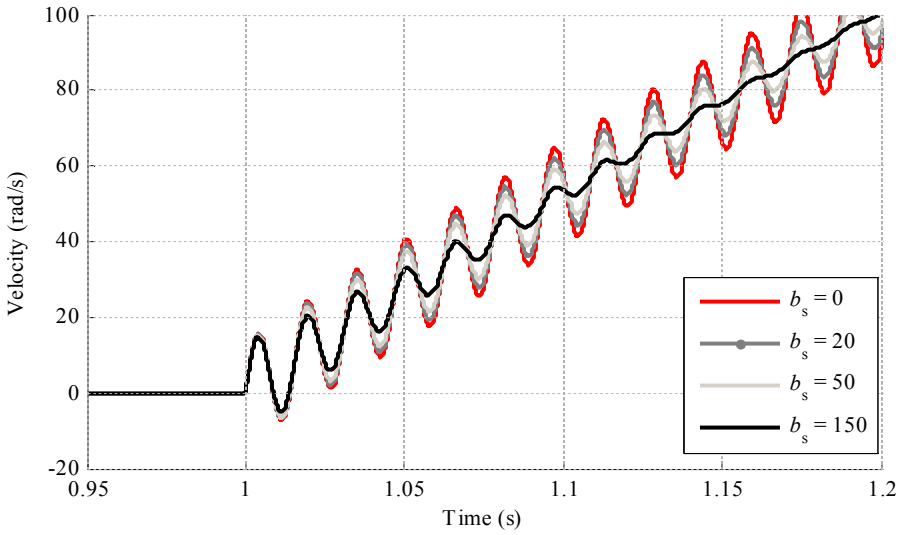

Fig. 2.24. Response of the system when the damping constant of the tooth belt drive is varied.

The transfer function from the torque reference T_{ref} to the cart position x can be given as

$$\frac{x}{T_{\mathrm{ref}}} = \frac{1}{\left(J_{\mathrm{m}} + m_{\mathrm{L}} R^2\right) s^2 + b_1 s} \frac{b_{\mathrm{s}} s + K_{\mathrm{eff}}}{\frac{J_{\mathrm{m}} \cdot m_{\mathrm{L}}}{J_{\mathrm{m}} + m_{\mathrm{L}} R^2} s^2 + b_{\mathrm{s}} s + K_{\mathrm{eff}}}, \tag{2.21}$$

and for the velocity of the cart

$$\frac{\dot{x}}{T_{\text{ref}}} = \frac{1}{\left(J_{\text{m}}+m_{\text{L}}R^2\right)s + b_{\text{l}}} \frac{b_{\text{s}}s + K_{\text{eff}}}{\dfrac{J_{\text{m}} \cdot m_{\text{L}}}{J_{\text{m}} + m_{\text{L}}R^2} s^2 + b_{\text{s}}s + K_{\text{eff}}} . \tag{2.22}$$

Then main differences between the two transfer functions presented by Eqs. (2.17) and (2.21) for the motor shaft and the cart position, respectively, are shown in Fig. 2.25. When the transfer function is from the torque reference to the position of the motor shaft, there is an anti-resonant frequency in the system. This can be seen also in the second order in the numerator of the flexible part of Eq. 2.17.

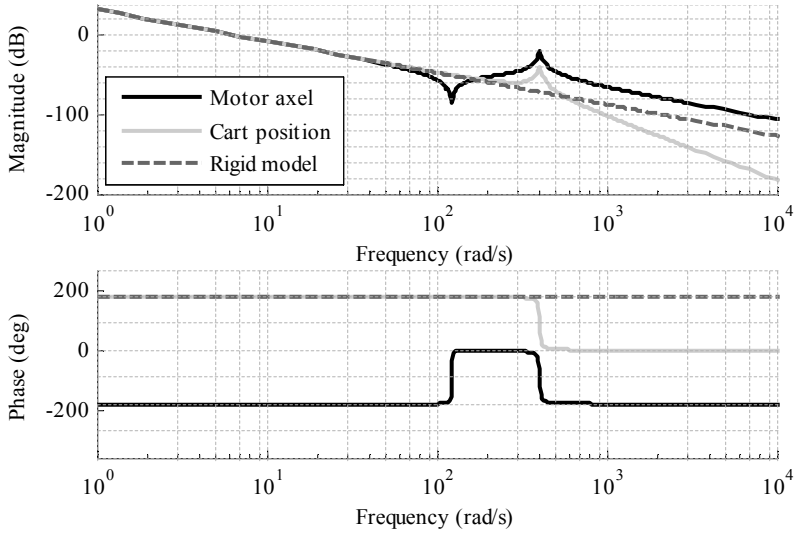

Fig. 2.25. Magnitudes and phases from the torque reference to the motor shaft and the cart position, respectively. These are compared with the rigid body model.

The spring constant K_{eff} is typically assumed to be constant with all possible positions of the cart; see for instance (Hace et al. 2001; Hace et al. 2004). In a real system, K_{eff} varies with the positions of the cart, which makes the resonant frequency vary as a function of cart position; this will be shown in Section 2.3.2. The equivalent spring constant $K_{\text{eff}}(x)$ can be derived by considering the system as a two-mass system with three springs connecting the masses together, where the two serial springs ($K_2(x)$ and $K_3(x)$) are first connected together, and then the result is connected in parallel with the spring $K_1(x)$ (Graham 1996)

$$K_{\text{eff}}(x) = K_1(x) + \frac{1}{\dfrac{1}{K_2(x)} + \dfrac{1}{K_3(x)}} = K_1(x) + \frac{K_2(x) \cdot K_3(x)}{K_2(x) + K_3(x)} . \tag{2.23}$$

However, in a tooth belt linear axes, the spring constant $K_3(x)$ can be fixed to a constant value K_3 independent of the cart position x, without making a big mistake while the other two spring constants inevitably must be handled as functions of cart position. Equations for spring

constants can be derived from Hooke's law if the belt stretching characteristics are known. Tensile strain can be written as follows

$$\varepsilon = \frac{\delta}{l_0}, \tag{2.24}$$

where δ is the stretched part of the particle, when stretching with the force F, and l_0 is the initial length of the particle. The value of the tensile strain is typically given by the manufacturer of the tooth belt axes, and it is a function of the tension force of the tooth belt as we will see in Fig. 2.26. The red dots are the initial belt tension forces recommended by Festo. This means that the belt is already strained 0.11 % of its nominal length. If the tension force of the belt is not accurate, there will be some uncertainties in the value of the spring constant. This should be taken into account when the parameter variation of the system is determined.

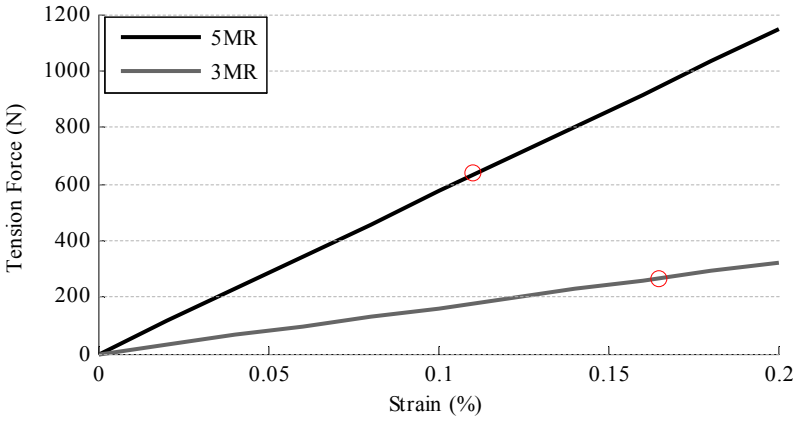

Fig. 2.26. Strain % of the test system, 5 MR is the belt of the x-axis and 3 MR is the belt of the y-axis.

An equation for the spring constants can then be derived from Hooke's law

$$\begin{aligned} F_{\text{init}} &= K \cdot x = K \cdot \delta = K \cdot \varepsilon \cdot l_0 \\ \Rightarrow K &= \frac{F_{\text{init}}}{\varepsilon} \cdot \frac{1}{l_0}, \end{aligned} \tag{2.25}$$

where F_{init} is the initial tension of the belt and l_0 is the initial length of the belt. With Eq. (2.25), functions for the position-dependent spring constants $K_1(x)$ and $K_2(x)$ can be found, and the value for the fixed spring constant K_3 can be calculated

$$\begin{aligned} K_1(x) &= \frac{F_{\text{init}}}{\varepsilon} \cdot \frac{1}{l_1 + x} \\ K_2(x) &= \frac{F_{\text{init}}}{\varepsilon} \cdot \frac{1}{l_2 - x} \end{aligned} \tag{2.26}$$

$$K_3 = \frac{F_{\text{init}}}{\varepsilon} \cdot \frac{1}{l_3} = 2.64 \cdot 10^5 \, \frac{\text{N}}{\text{m}},$$

where l_1, l_2, and l_3 are the lengths of the belts. In Fig. 2.27, the x-axis spring constants K_1, K_2, K_3, and K_{eff} are shown as a function of cart position.

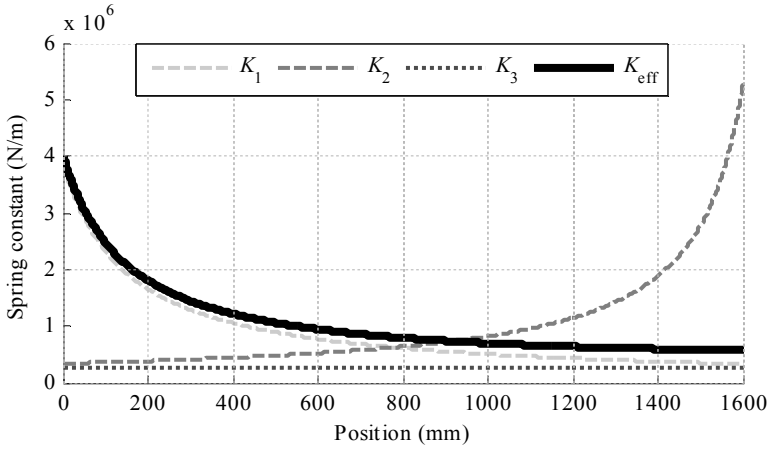

Fig. 2.27. *X*-axis spring constants as functions of cart position.

It can be seen in Fig. 2.27 that the spring constant K_1 mostly affects the equivalent spring constant. When moving away from the motor, the equivalent spring constant differs increasingly from the spring constant K_1. When considering the spring constants K_1 and K_2, the initial length l_0 varies when the cart is moving. The initial length of the belt together with the driving force F_{driven} is the main parameter that determines how much the belt will stretch during the operation. The stretch is calculated with

$$\delta = \varepsilon \frac{F_{\text{driven}} l_0}{F_{\text{init}}}. \tag{2.27}$$

It should be mentioned that if the position of the cart is measured with the linear band encoder, the stretched part of the belt does not have any effect on the accuracy of the system. Nevertheless, if the position is measured with the motor shaft encoder, the stretched part cannot be observed, which will have some effect on the accuracy of the system. According to the repair instructions of the electrical linear axis, Festo (2003), the initial tension of the x-axis belt is 640 Nm, the tensile strain ε is 0.11 %, the maximum driven force F_{driven} is 610 Nm, and the initial length of the belt varies between 0.15 m and 1.75 m. Thus, the stretch of the x-axis can be varied from 0.16 mm to 1.8 mm. Correspondingly, the y-axis initial tension F_{init} is 267 Nm, F_{driven} is 260 Nm, ε is 0.16 %, and the initial length of the belt varies between 0.15 m and 1.35 m. The stretch of the y-axis varies between 0.2 mm and 2.1 mm.

The analysis and the equations above hold for a situation in which we have only one tooth belt axis in the test system. As was described in Section 2.2, we have two axes side by side connected by a connection shaft. The x-axis has a 1434 mm and the y-axis a 200 mm long connection shaft. The connection shaft will add one more spring constant to the system as we

can see in Fig. 2.28, where the left-hand side is a schematic diagram of the two-axis system and the right-hand side is a block diagram of the spring constants.

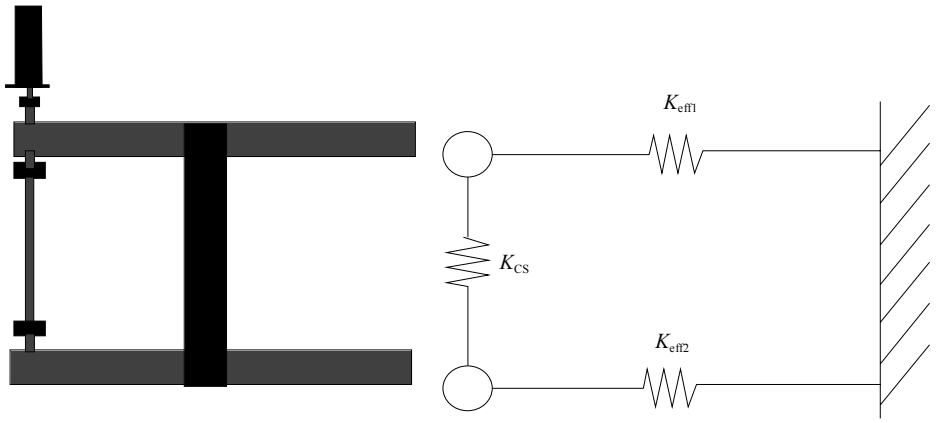

Fig. 2.28. Two belt drives and the equivalent spring constant.

The spring constant of the connection shaft can be calculated using the torsion modulus (Graham 1996)

$$I_{\text{V}} = f_{\text{i}} \frac{\pi\left(D^4 - d^4\right)}{32}, \tag{2.28}$$

where I_{V} is the torsion modulus of the cross-section, f_{i} is the shape factor of the connection shaft, D the outer diameter, and d is the inner diameter of the connection shaft. The spring constant is

$$K_{\text{CS}} = \frac{G \cdot I_{\text{V}}}{L_{\text{CS}}}, \tag{2.29}$$

where G is the shear modulus of the material and L_{CS} is the length of the connection shaft. Using the equations above, we can calculate the bend angle φ_{CS} and the same angle converted to the linear motion x_{CS}

$$\varphi_{\text{CS}} = \frac{T \cdot L_{\text{CS}}}{G \cdot I_{\text{V}}} = 0.0115 \text{ rad} \tag{2.30}$$

$$x_{\text{CS}} = \frac{\varphi_{\text{CS}}}{2\pi} \cdot 0.125 \cdot 1000 \text{mm} = 0.23 \text{mm}, \tag{2.31}$$

where T is the torque of the connection shaft. This means that the position difference between the x-axis carts can be 0.23 mm, which may be a critical difference in applications requiring high accuracy.

2.3.2 Resonances of the belt

In the previous sections, when discussing the performance of the system, it was assumed that the system was rigid and there were no harmful vibrations present. This is seldom true. Actually, vibration is often a limiting factor in a practical performance. The physical explanation of the vibration phenomena lies in the interplay between potential energy and kinetic energy. One target of the vibration analysis is to predict the response of a vibrating system. The main vibration sources in our test system were the belt of the linear tooth belt drive and also the connection shaft between the two belt drives. In some cases, the foundation of the mechanical structures can be a source of vibration, but in our case, the foundation can be assumed stiff. A simple way to calculate belt resonances is

$$f_{\text{resBELT}} = \frac{1}{2\pi}\sqrt{\frac{K_{\text{eff}}\left(J_{\text{m}} + m_{\text{L}}R^2\right)}{J_{\text{m}}m_{\text{L}}}} \tag{2.32}$$

or

$$f_{\text{resBELT}} = f_{\text{anti-resBELT}}\sqrt{1 + R_{\text{mL}}}\ , \tag{2.33}$$

where R_{mL} is the inertia ratio of the load and the motor $R_{\text{mL}} = J_{\text{l}}/J_{\text{m}}$, and the anti-resonance is calculated as

$$f_{\text{anti-resBELT}} = \frac{1}{2\pi}\sqrt{\frac{K_{\text{eff}}}{m_{\text{L}}}}\ . \tag{2.34}$$

Actually, Eqs (2.32)-(2.34) give undamped natural frequency of the system, because damping is assumed zero. Unfortunately, the resonance calculation of the multi-inertia tooth belt linear drive system is not so straightforward, because the inertias and the belt spring constants can vary as a function of cart position. Figure 2.29a shows how sensitive Eq. (2.32) is to parameter uncertainties. The resonance frequency is calculated varying one parameter at a time keeping the other parameters constant: J_{m} is varied between 0.002 and 0.01 kgm^2, m_{L} between 35 and 65 kg, and K_{eff} between $4.0\cdot10^5$ and $5.0\cdot10^6$ N/m, and every variation range is divided into 50 parts. Figure 2.29b shows the minimum, maximum, and nominal resonance frequencies of the system when the parameters are varied within the described ranges. The maximum resonance frequency is obtained when $J_{\text{m}} = 0.002$ kgm^2, $m_{\text{L}} = 35$ kg and $K_{\text{eff}} = 5.0\cdot10^6$ N/m, the minimum when $J_{\text{m}} = 0.01$ kgm^2, $m_{\text{L}} = 65$ kg and $K_{\text{eff}} = 4.0\cdot10^5$ N/m, and the nominal resonance frequency when $J_{\text{m}} = 0.053$ kgm^2, $m_{\text{L}} = 50$ kg and $K_{\text{eff}} = 7.5\cdot10^5$ N/m. These resonances are compared with the measured resonances in different cart positions. We measured the resonance frequencies of the system by adding a pseudo random binary sequence (PRBS) signal to a constant torque reference, measured the motor velocity and angle, and calculated the resonance frequency from the motor velocity. We can clearly see from the measured resonances that the resonance frequency depends on the cart position. This is quite an obvious result, as Fig. 2.27 shows how significantly the equivalent spring constant varies as a function of cart position.

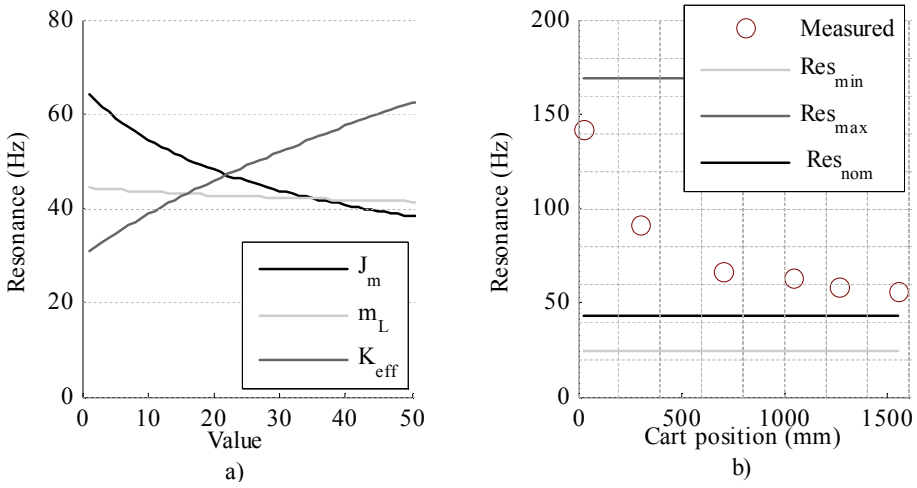

Fig. 2.29. Resonance frequency as a) a function of parameter variation. J_m is varied between 0.002 and 0.01 kgm^2, m_L between 35 and 65 kg, and K_{eff} $4.0 \cdot 10^5$ and $5.0 \cdot 10^5$ N/m keeping other parameters at nominal values; b) the measured resonances compared with the minimum, maximum, and nominal model resonances.

Figure 2.29 shows that the resonance frequency will increase as the motor inertia and the load inertia decrease, and a higher spring constant will increase the resonance frequency. We can see that the measured resonances will change significantly as a function of cart position. This is mainly caused by the change in the spring constant K_1, which has the most significant effect on the equivalent spring constant of the belt drive K_{eff}; see Fig. 2.27.

Now, we can calculate the magnitudes and phases of the system from the torque reference to the motor angular position, Eq. (2.17), using the worst-case scenarios compared with the nominal model of the system, Fig. 2.30. Figure shows also the response of the rigid body model. The rigid body model is accurate up to the anti-resonance frequency of the system, after which the rigid body model gives wrong phases and magnitudes.

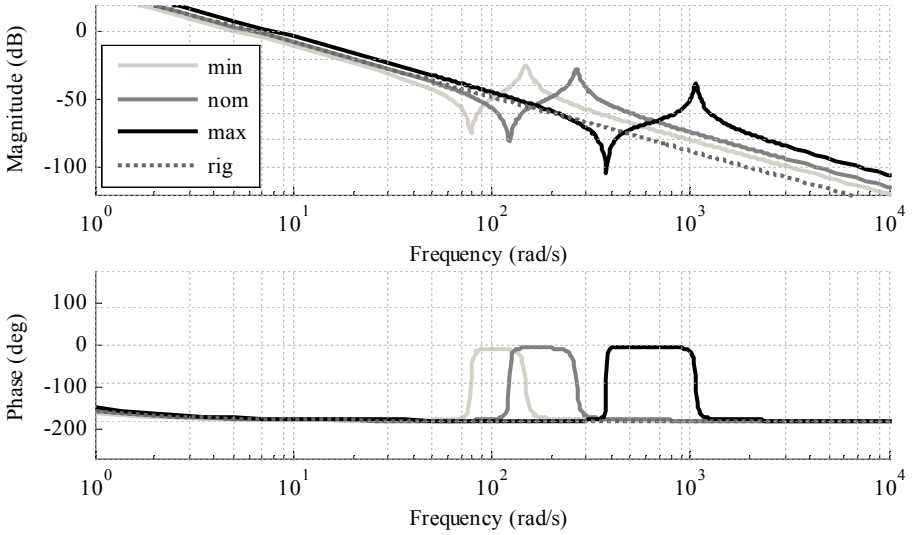

Fig. 2.30. Magnitudes and phases of the system from the torque reference to the motor angular position.

The initial tension of the belt is critical to the operation capability of the tooth belt drive. The tension can be measured using the method described in the *Repair instructions* manual (Festo 2003), where the initial tension F_{init} is measured using a known length of the belt l_{belt} that is capable of vibration, the known resonance range f, and the weight per meter of the belt m_{belt}

$$f = \frac{1}{2 \cdot l_{\text{belt}}} \sqrt{\frac{F_{\text{init}}}{m_{\text{belt}}}} . \tag{2.35}$$

The resonance of the connection shaft is given by

$$f_{\text{resCS}} = \frac{1}{2\pi} \sqrt{\frac{K_{\text{CS}} \left(J_{\text{belt1}} + J_{\text{belt2}} \right)}{J_{\text{belt1}} J_{\text{belt2}}}} , \tag{2.36}$$

where J_{belt1} and J_{belt2} are the total inertia of the belt drive axis.

The resonances of the systems that have multi inertia and multiple spring constants for example the x-axis structure of the test system, shown in Fig. 2.28, can be calculated by (Graham 1996)

$$\begin{aligned}
& m_{\text{L1}} \ddot{x}_1 + K_{\text{eff}\,1} x_1 - R^2 K_{\text{eff}\,1} \varphi_1 = 0 \\
& J_{\text{m}} \ddot{\varphi}_1 + \left(K_{\text{eff}\,1} \cdot R^2 + K_{\text{CS}} \right) \varphi_1 - K_{\text{eff}\,1} x_1 - K_{\text{CS}} \varphi_2 = 0 \\
& J_2 \ddot{\varphi}_2 + \left(K_{\text{CS}} + K_{\text{eff}\,2} \cdot R^2 \right) \varphi_2 - K_{\text{CS}} \varphi_1 - K_{\text{eff}\,2} x_2 = 0 , \\
& m_{\text{L2}} \ddot{x}_2 + K_{\text{eff}\,2} x_2 - R^2 K_{\text{eff}\,2} \varphi_2 = 0
\end{aligned} \tag{2.37}$$

where m_{L1} is the mass of the axis 1, m_{L2} is the mass of the second axis, K_{eff1} is the equivalent spring constant of the axis 1, K_{eff2} is the spring constant of the second axis, x_1 is the position of the axis 1, x_2 is the position of the second axis, φ_1 is the angular position of the driven pulley of the axis 1, and φ_2 is the angular position of the driven pulley of the second axis.

The mass normalized stiffness can be calculated as (Graham 1996)

$$\widetilde{K} = M^{-0.5}\left(K \cdot M^{-0.5}\right), \tag{2.38}$$

by which the eiqenvalues of the system can be obtained. When the eigenvalues of the x-axis drive system of the test setup are calculated, Eq. (2.37), the mass matrix of system is

$$M = \begin{bmatrix} m_{L1} & 0 & 0 & 0 \\ 0 & J_m & 0 & 0 \\ 0 & 0 & J_2 & 0 \\ 0 & 0 & 0 & m_{L2} \end{bmatrix} \tag{2.39}$$

and the spring constant matrix of the same system is

$$K = \begin{bmatrix} K_{eff1} & -R^2 K_{eff1} & 0 & 0 \\ -K_{eff1} & \left(R^2 K_{eff1} + K_{CS}\right) & -K_{CS} & 0 \\ 0 & -K_{CS} & \left(K_{CS} + R^2 K_{eff2}\right) & -K_{eff2} \\ 0 & 0 & -R^2 K_{eff2} & K_{eff2} \end{bmatrix}. \tag{2.40}$$

According to Ellis and Lorenz (2000), if the inertia of the transmission components is small compared with the motor and the load, the stiffness of the components can be treated as a single, composite, equivalent spring constant that interconnects the motor and the load. With this assumption, the inertia of the second axis pulley can be neglected and the stiffness between the motor and the second axis can be treated as a single spring constant ($1/K_{CSeff} = 1/K_{CS}+1/K_{eff2}$).

The results are shown in Fig. 2.31, where the belt resonance and anti-resonance are shown together with the resonance of the connection shaft as a function of cart position. This result shows that the dynamics of the connection shaft can be neglected in the transfer function used in the control design, because it will be almost at the same frequency as the anti-resonance of the belt.

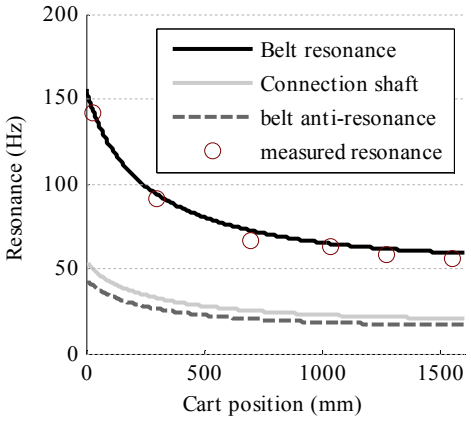

Fig. 2.31. Belt resonance, anti-resonance, and resonance of the connection shaft.

2.3.3 Friction and backlash

Friction is present in all mechanical systems. Friction occurs when the surfaces of two pieces contact each other. Friction is widely studied especially in classical mechanical engineering. The control engineer must understand the friction phenomena, especially if high-precision control is required. For example, the performance of the system may decrease and the steady-state error or limit cycles may occur because of friction. Friction can be divided into three different components: Coulomb friction, static friction (stiction), and viscous damping. Figure 2.32 illustrates influences of friction and backlash to the whole system. As can be seen, Coulomb friction, also called sliding friction, has a constant value, which changes only when the direction of the motion is changed. Stiction, also known as break-away friction, has a value other than zero only when the motor speed is zero, and elsewhere the value of stiction is zero. The force required to overcome the static friction is called the break-away force. If the sliding friction is smaller than the static stiction, a Stribeck effect will occur. The viscous damping is changing as a function of motor speed. Rolling friction is less significant than the sliding friction. In mechanics, backlash is also quite common especially when a gearbox is used. Backlash means that the motor turns briefly before the load moves. Together, these forces make a system nonlinear. (Olsson et al. 1997), (Chen et al. 2006)

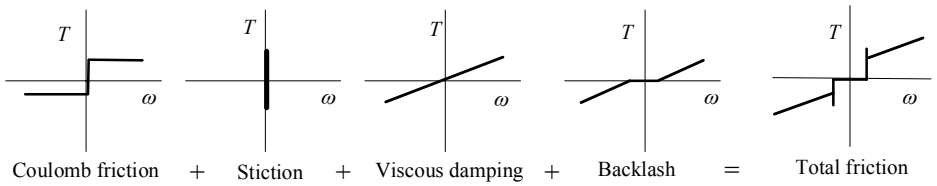

Fig. 2.32. Total effect of friction phenomena in a system.

Modeling of different types of friction has always been a challenge for a controller designer, who would prefer that the frictions are linear and that only a viscous damping factor has to be modeled. However, in linear tooth belt drives, the friction is non-linear, the Coulomb friction is high, and viscous damping is small, which makes it impossible to use only one viscous damping factor to illustrate the process friction and damping dynamics in the whole velocity range. A

high value of a viscous damping factor describes the frictions with a reasonable accuracy at low speeds, but at high velocities, friction will be described as too large compared with a real system. Correspondingly, a low value of viscous damping describes frictions quite accurately at high speeds, but it does not provide satisfactory attenuation at a low frequency. Typically, some kind of a compromise is found or the designed controller is analyzed with both a low and high value of viscous friction.

Figure 2.33 shows the measured friction at the cart velocities of 0.1 m/s, 0.2 m/s, 0.3 m/s, 0.4 m/s, and 0.5 m/s as a function of x-axis cart position. We can see that the break-away friction is large compared with the viscous friction. Friction is also position dependent. Figure 2.34 shows the friction at the cart velocity of 0.3 m/s in both directions of motion.

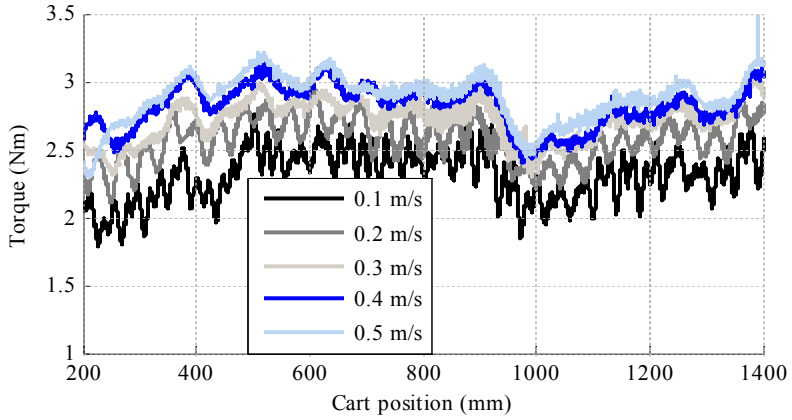

Fig. 2.33. Friction torque at different velocities of the cart.

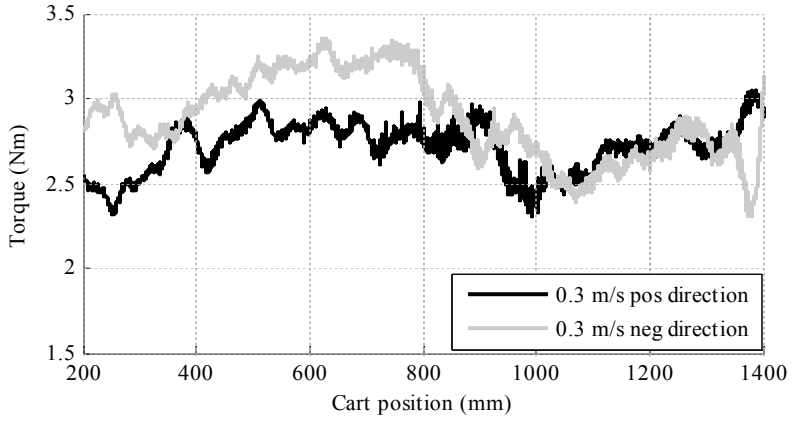

Fig. 2.34. Friction torques when the cart moves in the positive and negative direction, respectively.

Figures 2.33 and 2.34 show that a dynamic friction model should be used for accurate motion control applications both in simulations and in friction compensation of an actual machine control structure.

There are many different methods to compensate the friction. According to Olsson et. al (1997), in motion control systems, friction compensation should be applied in the inner loop (current loop); however, it is difficult to modify commercial products. Effective friction compensation requires accurate measurement or estimation of the velocity of the system. Moreover, the compensation becomes challenging if there are some dynamics between the control signal and the friction, for example a non-linear torque amplifier or a significant delay. In tracking applications, the friction can be compensated with a feedforward, because the velocity of the system is known in advance. Even though friction compensation is a very efficient way to reduce the error of the system, it is not discussed in detail in this thesis, as the focus of the work is not on the friction compensation methods. Friction compensation methods are developed and tested for example in (Olsson et. al 1997), where the LuGre friction model is used. Chen, Tan, and Huang (2006) propose a dual-relay approach to the estimation of friction parameters in servomechanical systems. Tao, Changhou, and Zhuyan (2006) analyze the friction characteristics in two regimes, pre-sliding and dynamic, which significantly improves the tracking performance.

3 VIBRATION REJECTION

Tooth belt drives are flexible systems, and the resonances of the system occur at low frequencies. Flexibility can be the major challenge for the control system, and cause difficulties to the desired trajectory tracking. The vibration caused by the resonance of the system can degrade the position accuracy during motion and also in the setpoint position. Solutions to the problem of mechanical vibration include stiffening of the mechanical structure, adding damping to the system, using additional vibration sensors and vibration controllers, making the closed-loop controller more sophisticated and complex, or using the references that do not excite resonances. This chapter shows how to design proper references for flexible mechanisms, and what kinds of problems a wrong reference may cause. First, some passive methods to prevent the vibrations are introduced; position reference generation and filtering of the torque reference. After that, active methods such as a traditionally designed PID-based control structure, a cascaded control structure, and a reference tracking feedforward are discussed.

3.1 Passive methods

3.1.1 Position reference

There are two methods for positioning; a point-to-point method and a contour method. The point-to-point method is used when the object needs to be moved from the starting point to the desired end position. This method is typically used with pick and place applications. Sometimes the motion has to be specified in more detail than only by the starting and end point. When the axis has to move along a desired path, the contour method is used. The path is then divided into more specified sections, and the trajectory generator will produce a continuous curve. In both methods, the trajectory generator gives the position, velocity, and acceleration references and these references can then be used in the control loop of the machine. Even though the motion has more than one degree of freedom, the trajectory is divided into each axis, and the trajectory generation simplifies into one-axis movement.

In many applications, the positioning requirements are the following: an object of weight m_L has to travel a distance s in time t, the starting and end velocity is zero, and the position accuracy is Δs. In material handling processes, the accuracy Δs is typically from 0.1 mm to 1 mm (Kiel 2008). The time t should be minimized, because it is typically non-productive time. The positioning sequence can be divided into three parts: accelerating from zero to the desired velocity, motion at a constant velocity, and decelerating to zero velocity. The distance s and the mass of the object m can vary. Any type of motion requires a force

$$F = m \cdot a \,. \tag{3.1}$$

where F is the force, m is the mass to be moved, and a is the acceleration of the mass. Integrating the acceleration a yields a velocity v, and integrating the velocity gives a position.

$$v(t) = \int a(t)dt \tag{3.2}$$

$$s(t) = \int v(t)dt \,. \tag{3.3}$$

The equations above are for linear motion. In many industrial applications, linear displacement Δs is produced by converting rotational displacement into linear

$$\Delta s = r \cdot \Delta\varphi \ , \tag{3.4}$$

where r is the radius that is used to convert the rotational angle φ into the linear position s. Using the same radius, we can also convert the variables F, m, a, v, and s to T, J, α, ω, and φ, that is, torque, mass of inertia, angular acceleration, angular velocity and angle, respectively. This yields

$$T = J \cdot \alpha \tag{3.5}$$

$$\omega(t) = \int \alpha(t) dt \tag{3.6}$$

$$\varphi(t) = \int \omega(t) dt \ . \tag{3.7}$$

To avoid exciting mechanical resonances and in order to maintain high accuracy, the generated trajectories should have smooth profiles. A smooth profile means that both the motion function and the first derivative are continuous. To create a smooth path with a continuous position and velocity, we start with the linear function but add a parabolic blend region to each path point (Kiel 2008). During the blend portion of the trajectory, constant acceleration is used. Sometimes also the accelerations and decelerations have to be smooth, and this can be obtained by adding limits to the first and second derivative of the velocity. The second derivate of the velocity is known as jerk. In order to have a smooth movement, the acceleration and deceleration have to be controlled. This yields trapezoidal acceleration and deceleration profiles, which decreases the jerk of the system as shown in Fig 3.1

Jerky motion increases mechanical faults and causes mechanical vibrations of the system, which also decreases the accuracy of the system and increases the contouring error. Acceleration and deceleration can be controlled either after or before interpolation. If acceleration and deceleration are controlled after the interpolation, there will be some phase lag, and consequently, error during the motion. Research has been made on function generation in machining processes; for example Olabi et al. (2010) described a method for feedrate planning for six-axis industrial robots; the paper shows how important it is to avoid jerky motion profiles.

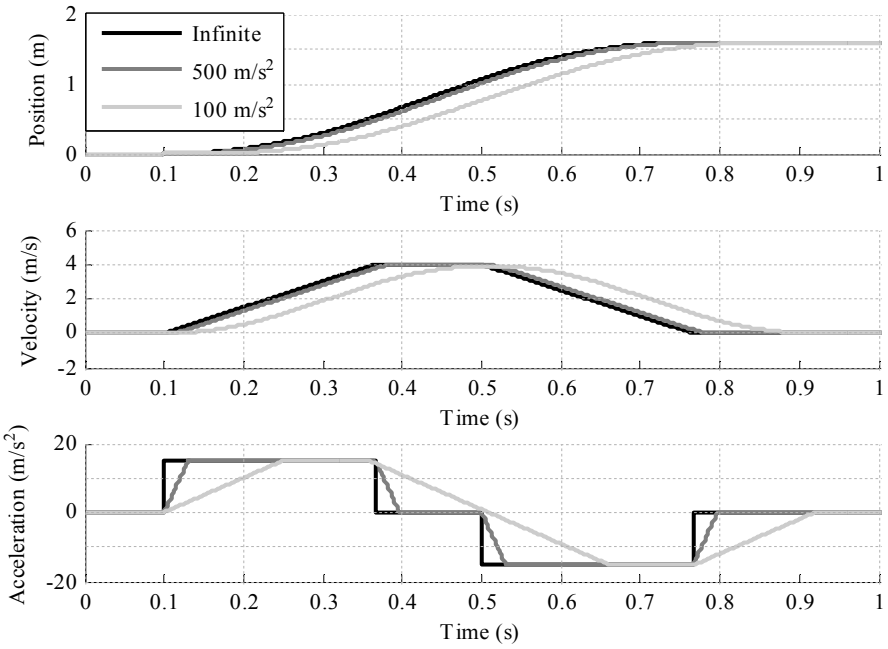

Fig. 3.1. Trajectories with different jerks. Jerk is "infinite", 500 m/s^2 or 100 m/s^2.

The method applied in this thesis for vibration rejection is based on ensuring that the reference is smooth enough for the system by reducing the bandwidth of the acceleration and deceleration profiles below the lowest resonance of the system. Section 2.3.2 shows that the lowest resonance of the belt can be 23 Hz. According to Ott (1988), the maximum frequency of a unit pulse is related to its rise time

$$f_{\max} = \frac{1}{\pi \cdot t_{\mathrm{r}}}, \tag{3.8}$$

where t_{r} is the rise time of the pulse. Another rule of thumb is that the time in which the maximum acceleration is reached should be at least twice as long as the period of the resonant frequency (Kiel 2008). This assumption yields a 0.087 s rise time for the torque reference. Figure 3.2 illustrates how important it is to reduce the rise time of the torque reference.

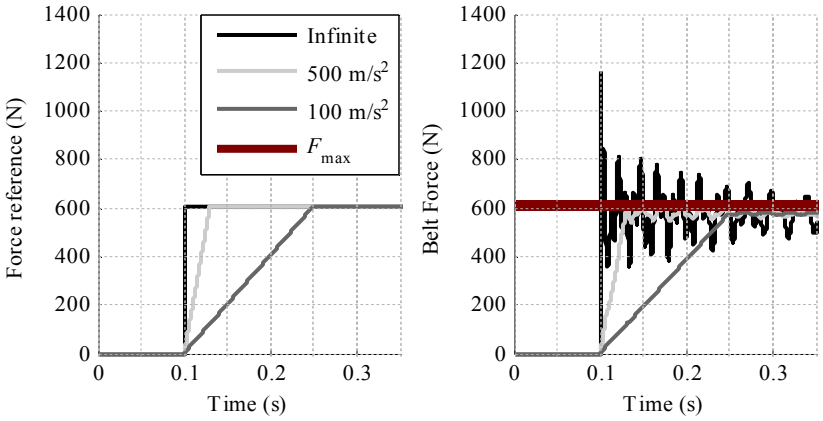

Fig. 3.2. Forces of the belt when the rise time of the reference force is varied.

The cost of the reduced vibration is an increase in the rise time. All three reference commands produce the desired motion, that is, a rapid change in position, but the commands produce vastly different amounts of residual vibration. Of course, this can significantly reduce the point-to-point time. To avoid or address these problems, a lot of effort has been put into research on developing new and more sophisticated trajectory generator algorithms. Erkorkmaz & Altintas (2000) proposed a quintic spline trajectory generation algorithm that produces continuous position, velocity, and acceleration profiles. The new trajectory generation method was tested in a three-axis milling machine, and the results showed that the jerk of the profile has to be minimized, if high-accuracy products are desired. Kataoka et al. (2008) suggested a position reference filtering method to avoid resonances of the system. A notch filter was tuned to damp the resonance frequency, and a lead filter was used to compensate the phase lag of the notch filter. An accurate and low-vibration movement could be achieved with this method. The drawback, however, was that the higher frequencies were amplified compared with the original reference. Yet another method for design command generators for flexible systems is presented in (Singhose 1997), where the commands are generated for instance to limit the transient deflection to a desired level.

The second problem is related to calculating how the mechanism will move under application of a set of joint torques. The dynamic equations for path generation do not take into account all the effects acting on the machine. These include only those forces that arise from rigid body mechanics. For example, friction is not included. In machines where significant gearing is present, the forces resulting from friction can actually be 25% of the torque required to move the manipulator.

3.1.2 Torque reference filtering

Section 3.1.1 showed how to avoid vibrations by limiting the jerk of the reference commands. In some cases there are high-amplitude load disturbances, which may excite resonances to the system. Because of the load disturbances, also the control system must be designed to damp the resonance frequencies. Schmidt & Rehm (1999) list several techniques to reduce the resonance effects in a system; these include for instance lowering the gain of the velocity controller,

stiffening the mechanics, filtering the reference or the feedback, measuring the load position and closing the additional feedback loop, adding observers to estimate the load velocity, and damping the closed loop control using this signal.

One of the most widely applied methods for damping the resonances is low-pass filtering of the torque reference. The filter can be of the first, second, or higher order. This is not effective when there are low-resonance frequencies in the system, and therefore, low-pass filtering is mainly used to filter the measurement noise or other high-frequency disturbances. If the resonance frequency is exactly known and it is constant during motion, a notch filter or a standard second-order filter can be used. There are multiple studies available concentrating on torque reference filtering techniques (Ellis 2000; Ellis & Lorenz 2000; Younkin 2004; Ellis and Gao 2001; Schmidt & Rehm 1999), just to mention a few. Most of the papers listed above concentrate also on different kinds of observers or on an acceleration feedback technique; nevertheless, these techniques are quite sensitive to parameter variation and are therefore left out of this thesis. However, the author has studied a rigid body observer in (Jokinen et al. 2006; Jokinen et al. 2007). The latter publication concentrates on the sensitivity to estimation error of the loop delay. This section provides an outline of the theory behind the filtering methods and shows how these methods can be implemented, what benefits can be achieved, and what are the possible drawbacks in the case of linear tooth belt drives.

The easiest solution to damp the resonance frequency is to use a low-pass filter, which is tuned to achieve the desired attenuation. The transfer function of the first-order low-pass filter is

$$H_{1\mathrm{st}}(s) = \frac{\omega_0}{s + \omega_0}, \tag{3.9}$$

where ω_0 is the cut-off frequency (-3dB) of the filter. We can calculate the attenuation of the filter at the desired frequencies by replacing $s = j\omega$ where ω is the studied frequency and ω_0 is the cut-off frequency of the filter

$$A_{1\mathrm{st}} = 20 \cdot \log\left|\frac{\omega_0}{j\omega + \omega_0}\right|. \tag{3.10}$$

When the resonant frequency and the desired attenuation at this frequency are known, the cut-off frequency ω_0 can be calculated as

$$\omega_{0,1\mathrm{st}} = \sqrt{\frac{{\omega_{\mathrm{res}}}^2}{\frac{1}{\left(10^{-\frac{A}{20}}\right)^2} - 1}}, \tag{3.11}$$

where ω_{res} is the resonance frequency and A the desired damping (dB). However, when we use the first-order low-pass filter, the attenuation is 20 dB/decade, which may not be enough. If more attenuation is needed, we can use a second-order filter

$$H_{2\mathrm{nd}}(s) = \frac{{\omega_0}^2}{s^2 + 2 \cdot \xi \cdot \omega_0 s + {\omega_0}^2}, \tag{3.12}$$

where ξ is the damping factor of the filter. By using a second-order filter we get 40 dB/decade attenuation. The attenuation at different frequencies of the second-order filter can be calculated

$$A_{\mathrm{lst}} = 20 \cdot \log \left| \frac{{\omega_0}^2}{(j\omega)^2 + 2 \cdot \xi \cdot \omega_0 j\omega + {\omega_0}^2} \right|. \tag{3.13}$$

When the resonant frequency and the desired attenuation at this frequency are known, the cut-off frequency ω_0 for the second-order filter can be calculated by using the damping factor ξ = 0.707

$$\omega_{0,2\mathrm{nd}} = \sqrt[4]{\frac{{\omega_{\mathrm{res}}}^4}{\frac{1}{\left(10^{-\frac{A}{20}}\right)^2} - 1}}. \tag{3.14}$$

The price of using the low-pass filter is the phase lag. The phase starts to roll off a decade before the cut-off frequency. This is the main reason why the low-pass filter is not very effective when the resonance frequency is near the bandwidth of the velocity loop. The best results can be obtained when the filters are used to reduce high-frequency noise while generating minimal phase lag at the gain crossover frequency (Ellis 2000).

The second and very widely used method is notch filtering of the resonance frequency. The notch filter is a standard function in the high-performance servo drives and it is a standard function in the PLC function libraries. While a low-pass filter attenuates all frequencies above the cut-off frequency, the notch filter removes only a narrow band. Because the notch filter passes high frequencies, they usually cause only some phase lag at the gain crossover frequency, assuming that the notch frequency is well above that. Both notch and low-pass filters can compensate resonance. The transfer function of the standard notch filter is written as

$$H_{\mathrm{notch}}(s) = \frac{s^2 + 2\frac{d}{c}\omega_0 s + {\omega_0}^2}{s^2 + 2\frac{1}{c}\omega_0 s + {\omega_0}^2}, \tag{3.15}$$

where the parameters d and c set the attenuation and width of the filtered bandwidth, respectively, and ω_0 is the cut-off frequency. The notch filter increases the gain margin and causes less phase distortion at lower frequencies than a low-pass filter. It also passes the frequencies above the resonance. The main problem of the notch filter is that it is very sensitive to the parameter variation of the system. If the resonance frequency changes, the notch filter will be ineffective.

Yet another filter type is a bi-quadratic filter. It has two poles and two zeros, which can be adjusted independently. The transfer function of a bi-quad filter is

$$H_{\text{bi-quad}}(s) = \frac{s^2 + 2\xi_z\omega_z s + {\omega_z}^2}{s^2 + 2\xi_P\omega_P s + {\omega_P}^2}, \tag{3.16}$$

where ξ_z and ξ_P are the damping factors of the zero and the pole, respectively. ω_z and ω_P are the frequencies of the zero and the pole, respectively.

Figure 3.3 shows a simulated situation where the reference is filtered using a first-order low-pass filter, which is tuned to damp the 45 Hz belt resonance using different attenuations compared with the step response. The filtered reference is used as an input for the system described in Eq. (2.14). These simulations are open-loop responses, and the reference is only filtered using these designed reference filters. As can be seen, the torque reference to the system is smoothed, but a resonance is still excited and the velocity of the motor is oscillating.

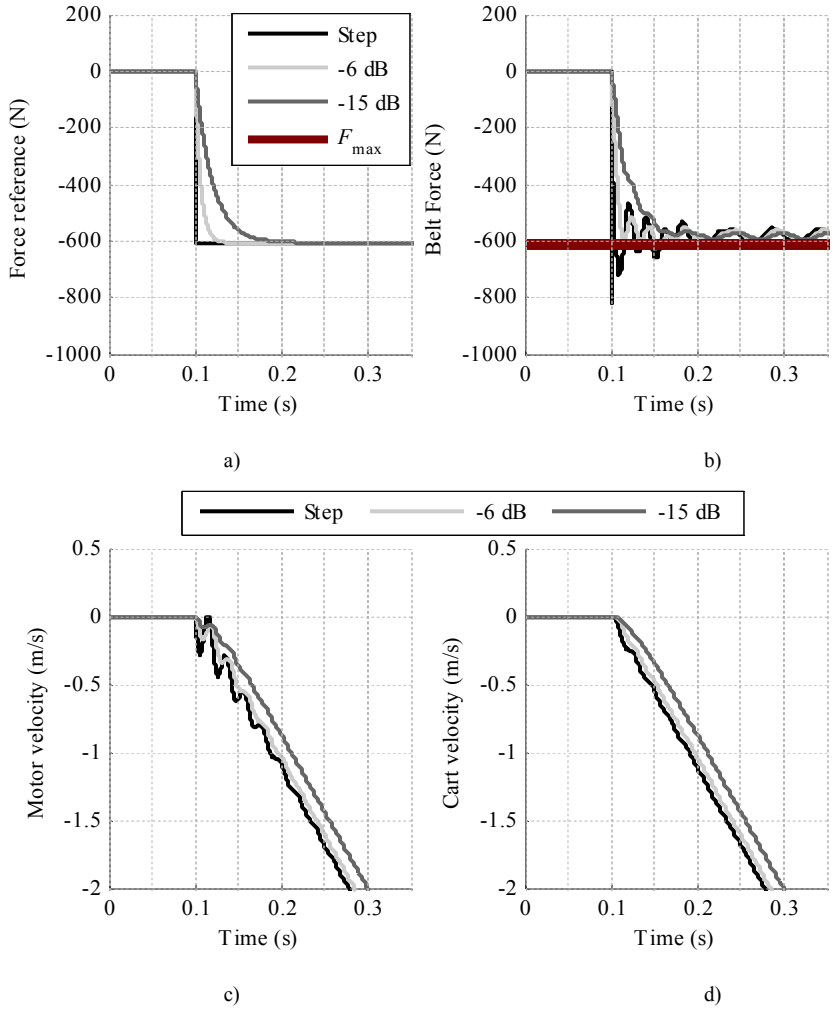

Fig. 3.3. Simulation results with different attenuations of the first-order low-pass filter; a) force reference, b) force of the belt, and c) velocity of the motor d) velocity of cart.

If the torque reference is ramped as proposed in Eq. (3.8), the resonance frequency has not so large amplitude as when the low-pass filters were used. Figure 3.4 compares the results when a notch filter is used to damp the belt resonance to the ramped reference and to the step response. The figure shows that the notch filter attenuates the belt resonance frequency effectively, but because the system consists of several resonance frequencies, the force of the belt overshoots the maximum force that can be used.

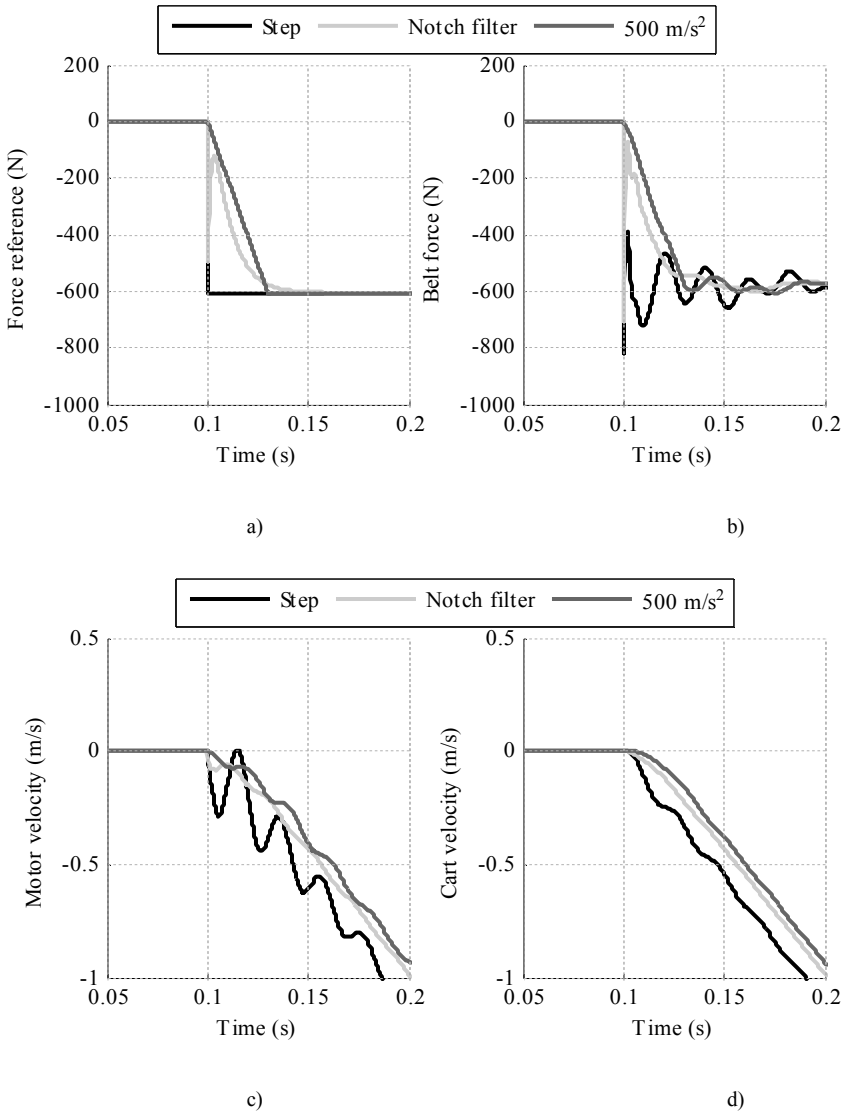

Fig. 3.4. Simulation results with the notch filter and ramped response are compared with the step response. a) Force reference, b) force of the belt, and c) velocity of the motor d) velocity of the cart.

If the resonance frequency is constant, the notch filter can be tuned to attenuate the resonance frequency. Figure 3.5 shows how a properly tuned notch filter attenuates the resonance frequency of the system.

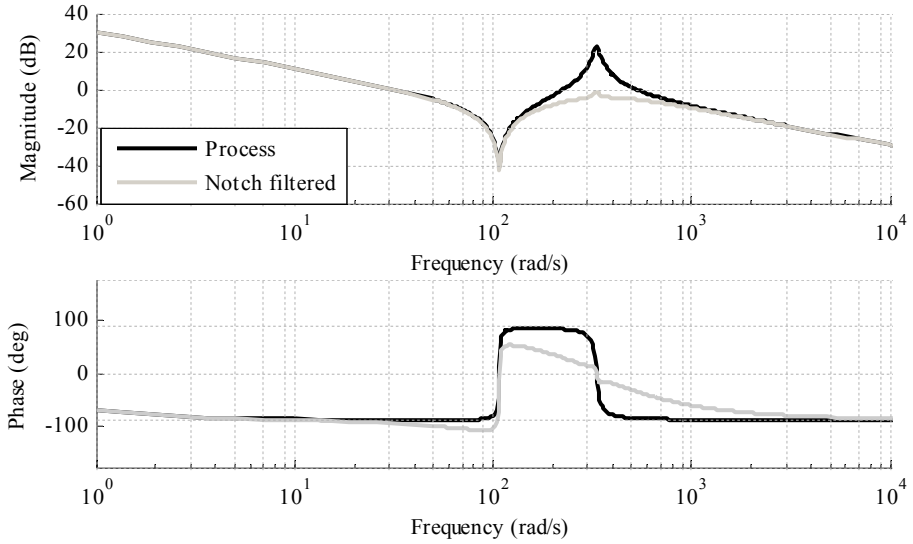

Fig. 3.5. Magnitudes and phases from the torque reference to the motor velocity of the open-loop system without torque reference filtering and filtered with a notch filter.

However, because the values of the system parameters vary during operation as is the case with the linear tooth belt drive, the use of a fixed-gain notch filter is not an effective solution. The reason for this is that if the mechanical resonance varies between 50 and 150 Hz, the notch filter cannot attenuate the whole resonance frequency range, as can be seen in Fig. 3.6.

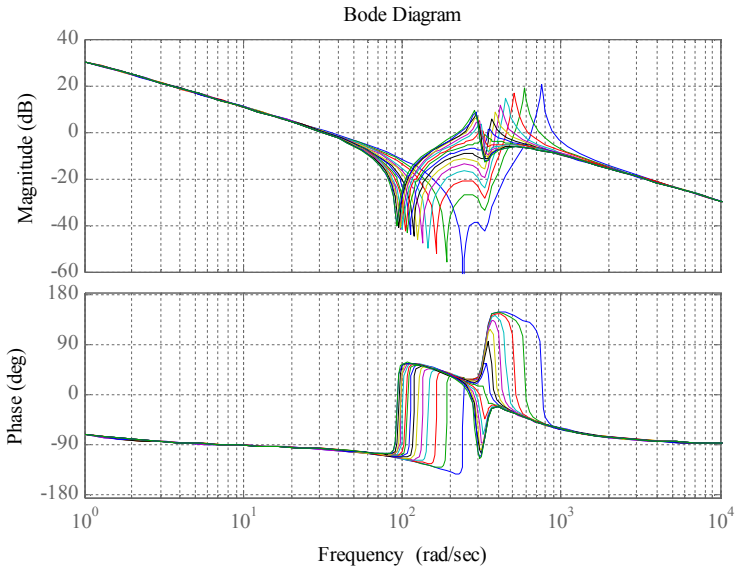

Fig. 3.6. Magnitudes and phases from the torque reference to the motor velocity of the open-loop system when the notch filter is fixed, but the mechanical resonance of the system varies.

Figures 3.3–3.6 show that the passive methods are not very effective in reducing the mechanical resonances of the system, if there are parameter uncertainties involved. Some more powerful methods, such as active ones, have to be used; alternatives are for example a properly tuned feedback controller or an adaptive notch filter.

3.2 Feedback controller

As was presented in Section 1.4, the control structure of a motion control device can be either a cascaded structure, where the typical construction is that the velocity controller is a PID controller and the position controller is a P controller or a PID position controller based structure. Both structures have their advantages and disadvantages, which should be known when the control structure is chosen.

3.2.1 Advantages of the feedback controller

The need for the control and the feedback can be analyzed as follows. Assume that a process $P(s)$ has disturbances $V(s)$ and $D(s)$. To provide the desired response $T(s) = Y(s)/R(s)$ from the reference to the output, a filter $C(s) = T(s)/P(s)$ has to be implemented, as shown in Fig. 3.7a. This filter is capable of guaranteeing the desired response as long as the process is constant, stable, and realizable, there are no uncertainties in the process model, and there are no disturbances $V(s)$ or $D(s)$ present. In order to compensate the uncertainties and disturbances, a feedback has to be implemented, Fig. 3.7b.

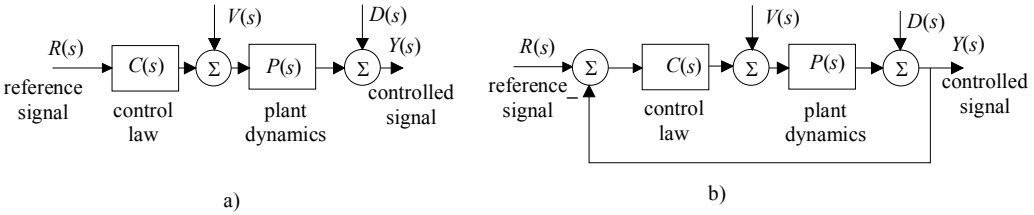

Fig. 3.7. a) Open-loop control, b) closed-loop control.

The system has to track the reference, and the external disturbance $V(s)$ should be attenuated in such a way that it has a minimal effect on the process output $Y(s)$. Assuming that the nominal model of the process is $P_{\mathrm{nom}}(s)$, the transfer functions from the reference and disturbance of the process when the feedback controller is used can be written as

$$T_{\mathrm{R}}(s) = \frac{C(s)\cdot P_{\mathrm{nom}}(s)}{1 + C(s)\cdot P_{\mathrm{nom}}(s)} = \frac{L_{\mathrm{nom}}(s)}{1 + L_{\mathrm{nom}}(s)} \tag{3.17}$$

$$T_{\mathrm{V}}(s) = \frac{P_{\mathrm{nom}}(s)}{1 + C(s)\cdot P_{\mathrm{nom}}(s)} = \frac{P_{\mathrm{nom}}(s)}{1 + L_{\mathrm{nom}}(s)}, \tag{3.18}$$

where $L_{\mathrm{nom}}(s) \equiv C(s)\cdot P_{\mathrm{nom}}(s)$ and it is defined as the nominal loop transfer function, $T_{\mathrm{R}}(s)$ is the transfer function from the reference to the output of the plant, and $T_{\mathrm{V}}(s)$ is the transfer function from the disturbance $V(s)$ to the output of the plant. The sensitivity function of the closed loop system is

$$S(s) = \frac{1}{1 + C(s) \cdot P_{\text{nom}}(s)} = \frac{1}{1 + L_{\text{nom}}(s)}. \tag{3.19}$$

The sensitivity function is from the output disturbance $D(s)$ to the output of the process $Y(s)$ and also from the reference $R(s)$ to the control error. If the feedback and the controller are not used, the open-loop non-compensated system is written in the form

$$T_{\text{R}}(\text{s}) = P_{\text{nom}}(\text{s}) \tag{3.20}$$

$$T_{\text{V}}(\text{s}) = P_{\text{nom}}(\text{s}) \tag{3.21}$$

and the sensitivity function is

$$S(\text{s}) = 1. \tag{3.22}$$

When comparing the sensitivity functions of Eqs. (3.19) and (3.22), we see that the effect of the $P(s)$ on the output $Y(s)$ is reduced by the factor $1/(1+C(s) \cdot P_{\text{nom}}(s))$ compared with the open-loop system. This is one of the main reasons to use a feedback controller.

3.2.2 Structure of PID-based controllers

The most simple robot controllers do not use a model-based approach. Consequently, a PID control scheme is often used. A proportional-integral-derivative (PID) controller or its variations are the most common control structures in industrial applications. According to Ellis (2000), almost 95 % of industrial processes are controlled with some kind of a PID controller. The transfer function of the PID controller can be described as

$$C_{\text{PID}}(s) = K_{\text{P}}\left(1 + \frac{1}{T_{\text{i}} s} + T_{\text{d}} s\right), \tag{3.23}$$

where K_{P} is the gain, T_{i} is the integrator time constant, and T_{d} is the derivation time constant. A high gain increases the response of the system but at the same time decreases the stability margin. The integral term increases the stiffness at low frequencies, ensures that there is no static error, and reduces the phase margin. The derivative term predicts the process output and thus improves the closed-loop stability. A pure derivative gain is not typically used in industry, because it amplifies high frequencies such as measurement noise. Hence, the PID controller is typically modified for practical applications as (Åström & Hägglund 1995)

$$C_{\text{PID}}(s) = K_{\text{P}}\left(1 + \frac{1}{T_{\text{i}} s} + \frac{T_{\text{d}} s}{\frac{T_{\text{d}}}{N} s + 1}\right), \tag{3.24}$$

where T_{d}/N is the first-order filter time constant. The D part increases the phase lead by 90º, which is beneficial from the viewpoint of the phase margin (PM), but at the same time, it decreases the gain margin (GM) by increasing the gain at high frequencies. A larger PM means less overshoot, and a lower GM more high-frequency oscillations. A good principle is that the

GM should be 10–25 dB and the PM 30–80º. A decreased GM can be a problem, if the gain of the process increases during operation. In a motion control system, a reduction in the inertia increases the gain. This is a reason why the D-part is not often used in industry. Then, the controller is just a PI controller. According to Ellis (2000), a PI controller may require 55º PM to achieve 20 % overshoot, whereas a PID controller might eliminate all overshoot with just 40º PM. The PID or the PI controller provides a good reference tracking and good enough disturbance regulation performance for most applications. It is also easy to tune and simple to use, if the problems with the D-term are not taken into account, which makes it the primary choice when the control structure is chosen. Perhaps the best-known tuning method for the PID controller is the Ziegler-Nichols method (Ziegler & Nichols 1942). There are also plenty of different rules of thumbs for tuning of the PID controller. For example, the bandwidth of the control system should be 1/3, 1/5, or 1/10 of the resonance frequency of the system, T_i/T_d should be 4, and N should be between 8 to 20 (Åström & Hägglund 1995). If the process consists of oscillatory modes, the PID controller may not be the most sufficient controller, but it is nevertheless used in most of the cases. According to Åström and Hägglund (1995), for a system with oscillatory modes, the normal situation is that T_i is much smaller than T_d and the value of the parameter N is critical. But if the process requires all the performance that the controller can give or the system consists of time delays, these tuning rules cannot be used.

For applications where the disturbance regulation is the most critical criterion, there are better controllers than the traditional PID controller. Often, the problem is modified into a two-degrees-of-freedom (TDOF) problem where the feedback controller $C(s)$ is designed for disturbance rejection, and the reference tracking performance is taken care of by a pre-filter $F(s)$. The block diagram of the TDOF control structure is shown in Fig. 3.8.

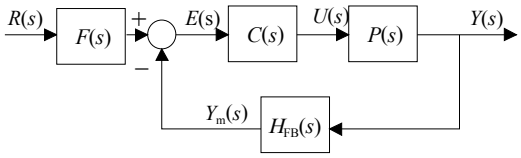

Fig. 3.8. Two-degrees-of-freedom control structure.

There are studies (Ellis 2000; Younkin 2004; Ellis & Lorenz 1999) where different kinds of TDOF controllers are used as motion control systems. Ellis (2000) proposed that the pre-filter $F(s)$ is modeled as

$$F(s) = K_{pf} + (1 - K_{pf})\left(\frac{1}{T_i s + 1}\right), \tag{3.25}$$

where K_{pf} is from zero to one and the control system forms the PID+ structure. When K_{pf} is one, the structure is a traditional PID controller, but when K_{pf} is reduced, the controller becomes a TDOF controller. The PID+ structure allows a smaller integral time constant compared with the PID controller, which improves the DC stiffness. The input filter cancels peaking caused by the small integral time constant. If the derivative part of the controller is not used, the control structure can also be called a pseudo-derivative feedback controller (PDF) when K_{pf} is zero, and when $0<K_{pf}<1$, it can be called a pseudo-derivative feedback with feed-forward controller or

PID+ controller (Ellis 2000). Control structures can be compared, if the tuning method is the same for all controllers. Ellis (2000) proposes a five-step experimental tuning method:

1. Select K_{pf} to 1
2. Use large amplitude square wave command, but avoid saturation. Raise K_p for 10% overshoot
3. Raise T_d to eliminate most overshoot
4. Select K_{pf} from zero to one
5. Decrease T_i for 10% overshoot

The tuning method described above is not directly usable for flexible systems because of the mechanical resonance, see Section 3.1. To analyze the performance of the PID and the PID+ controller with different values of K_{pf}, we use the rigid part of the transfer function of the test system, Eq. (2.18). The transfer function is from the torque reference to the velocity of the motor. Assume that the inertia of the motor and the mass of the load are nominal values, J_m = 0.0047 kgm^2, m_L = 51.2 kg, b_l = 0.005 Nms/rad, and the loop delay τ_d = 850 µs. To simplify the control system, we assume that the derivative part is not used. Table 3.1 gathers the performance differences of the controllers. The bandwidth of the system (BW) is the -3 dB point. The integrated absolute errors were calculated according to (Åström & Hägglund 1995)

$$IAE = \int_0^\infty |e(t)| dt , \tag{3.26}$$

where $e(t)$ is the error between the actual speed and the reference value. The time range used to calculate the value for IAE was from zero to two seconds, and the sampling time used was 100 µs.

Table 3.1. PID+ controller parameters using different values of K_{pf}.

K_{pf}	1.0	0.75	0.5	0.25	0.0
K_p (Nms/rad)	16	16	16	16	16
T_i (ms)	40	6.5	3.6	3.0	2.8
T_d (ms)	0	0	0	0	0
BW (rad/s)	1420	1140	967	827	797
IAE	0.0747	0.0121	0.0069	0.0065	0.0065

Figure 3.9 shows the closed-loop bandwidth of the system and the load sensitivity (stiffness), T_V, with the PI, PI+ (K_{pf} = 0.75), and PDF controllers (K_{pf} = 0). The bandwidth of the PDF controller is 56 % of the bandwidth of the PI controller, but the load sensitivity is about 25 dB better than with the PI controller. The reason for the improved low-frequency stiffness is that the time constant of the integral part of the controller is reduced. The inertia of the system and the derivative time constant (if used) will produce the high-frequency stiffness, and the controller gain will be the main parameter for the medium-frequency stiffness.

The simulation results for the tracking error and the load disturbance error are shown in Figs. 3.10 and 3.11, respectively. The parameters of the system are described above, and the gains of

the controller are listed in Table 3.1. The system is first accelerated to 200 rad/s with the maximum force, and after that a 26 Nm load is added. We see that only the PI controller can integrate the acceleration error, but the response to the load disturbance is the slowest one. To the contrary, the PDF gives the largest error during acceleration but the response to the load disturbance is the fastest. This means that the PDF controller is significantly better than a PI controller for applications with large load disturbances. Furthermore, the PI controller is better for tracking.

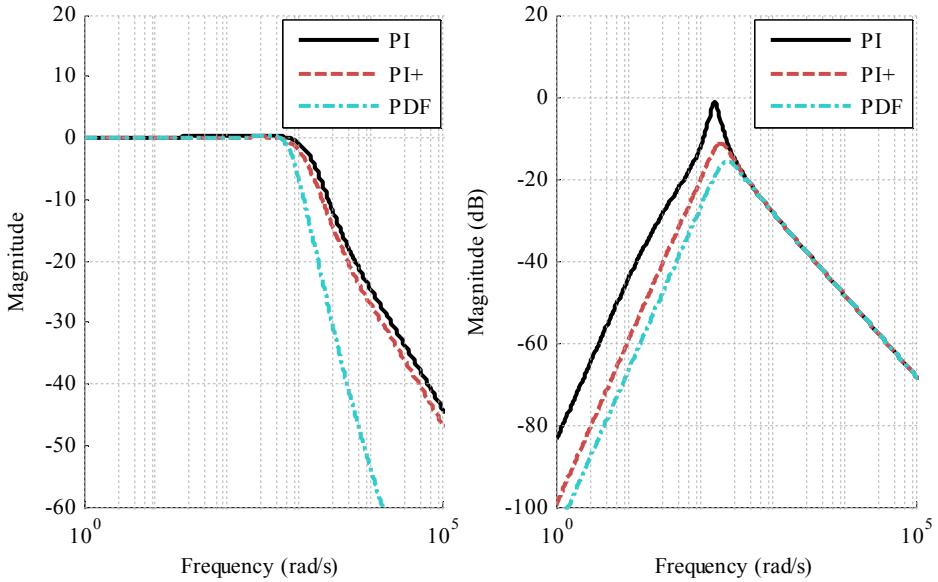

Fig. 3.9. PI controller, PI+ controller (K_{pf} = 0.75), and PDF controller (K_{pf} = 0); the closed-loop bandwidth of the system (left) and the stiffness for loads (right).

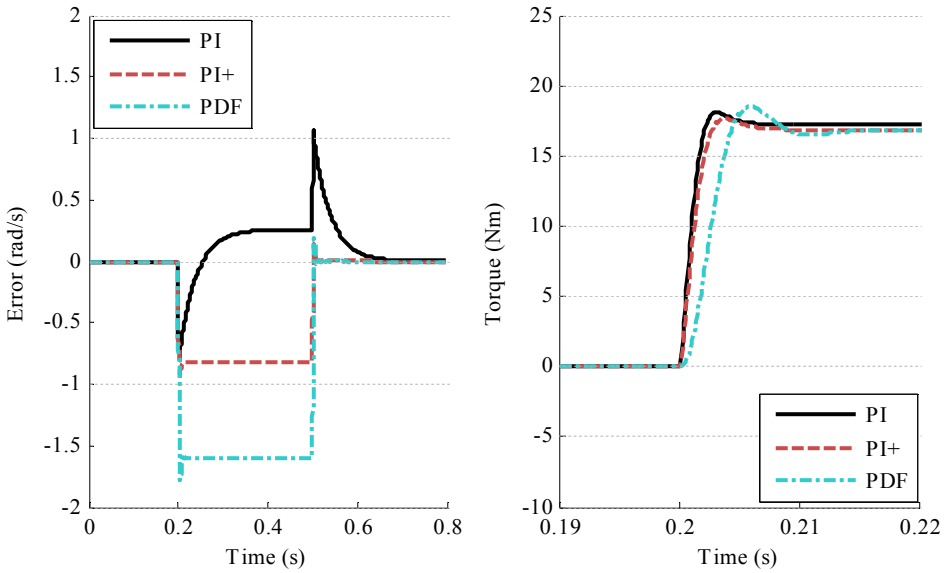

Fig. 3.10. System is accelerated from zero to 200 rad/s. The error figure shows that the PI controller can integrate the error almost to zero, but there is some overshoot. The torque figure shows only the time when the torque reference of the velocity controller is increased, because at that time we can see the main difference between the controllers, which is the torque reference rise time.

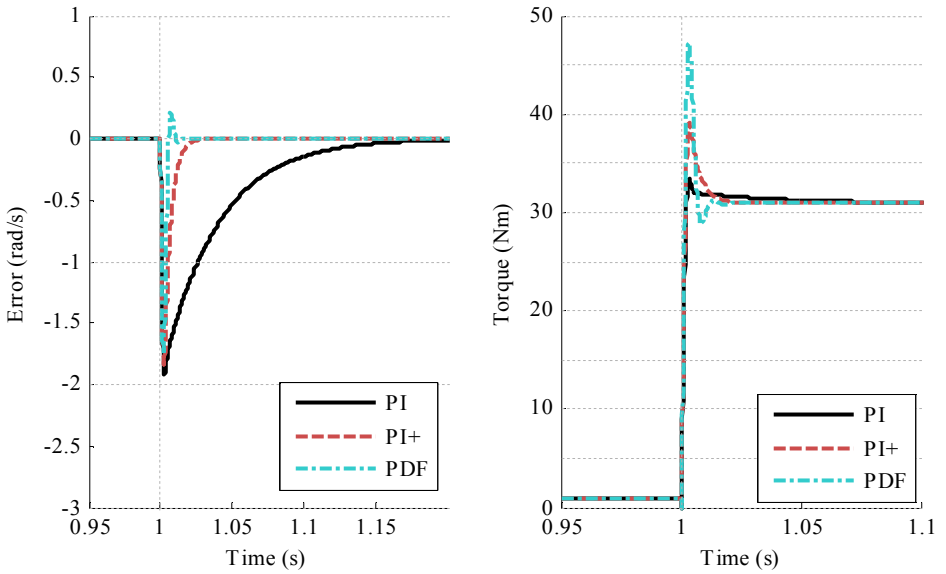

Fig. 3.11. Two times the nominal load is added to the system. We can see that when the velocity controller is of the PDF type, the error is fast integrated to zero, but the amplitude of the torque reference is about 1.5 times the required torque. This may lead to saturation of the output of the controller.

It should be noticed that a PID position controller can not be compared directly with a normal PID controller, because of the second integrator in the process. Still, the same phenomenon seen

in Figs. 3.10 and 3.11 is present when these PID-based control structures are used in the position control. When the PID position controller is used, there is no separate velocity loop. The output of the PID position controller is a torque command. The derivative part of the PID position controller act as a proportional term to the velocity error and the proportional term of the PID position controller act as an integral term to the velocity error. The derivative part of the PID controller was not typically used; however, the PD type position controller is very common in industry. If low-frequency stiffness is required, the integral term will be added to the PD position controller; however, an integral part of the controller can cause instability, which can be seen in high-acceleration movements. According to Åström and Hägglund (1995), for systems that are of a higher order than two, a more sophisticated controller than the PID controller can improve the performance of the control. The drawback of the PID position controller is also that if the inertia of the system changes, every parameter of the PID position controller must be retuned.

3.2.3 Cascaded control structure

The previous section focused on PID-based control structures and a PID-based position controller. In motion control systems, a cascaded structure with separate velocity and position controllers is also very common. Typically, both a position and velocity controller are PID-based structures. There are numerous of cases where a cascaded structure can be used. The limitation is that there must be several feedback signals but only one control variable. In a cascaded structure there are an inner loop and an outer loop, as illustrated in Fig 3.12. The inner loop is called a secondary loop and the outer loop a primary loop. The outer loop controls the primary signal of the process. Typically, the secondary loop has a faster response than the outer loop, and thus a large part of the disturbances are compensated by the inner loop, and the remaining error is compensated at the slower rate in the outer loop. Improvements in the performance of the system can be expected when the cascaded structure is used.

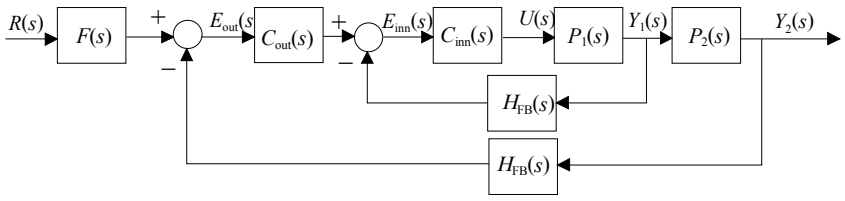

Fig. 3.12. Cascaded control structure.

A position-controlled process where $P_1(s)$ consists of the process dynamics, and $P_2(s)$ is only an integrator is the special case of the cascaded structure, because the integral action in the inner loop is equivalent to the proportional control in the outer loop. If the integral action is used in the inner loop, the proportional action in the outer loop must be reduced (Åström & Hägglund 1995). This is a significant disadvantage for the performance of the system. On the other hand, if the velocity is measured from the motor shaft but the position from the load, the performance may increase; however, an additional feedback will be required. A cascaded structure consists of two different controllers. The choice of the controller structure is based on the dynamics of the process and the nature of the disturbances. Typically, in motion control applications, a P position controller and a PID-based velocity controller are chosen. Tuning of the cascaded structure may be difficult. First, the inner loop must be tuned, and after that the outer loop. This means that the tuning procedure may require more time.

3.2.4 Feedforward

In motion control systems, accurate reference tracking capability is required. A normal feedback controller may not fulfill the performance requirements. This leads to the need for a feedforward function. It is very common that the feedforward controller is used together with the feedback controller, and typically, velocity and acceleration feedforward functions are integrated into the standard servo frequency converters. When a PID position controller is used, both feedforward functions are also integrated into the controller. The block diagrams of the servo drive controllers are shown in Section 1.4.

An "ideal" reference tracking feedforward controller $FF(s)$ is an inverted model of the nominal system $P(s)$. To analyze the effect of the reference tracking feedforward controller, we assume that the feedback controller is $C(s)$, feedback dynamics is $H(s)$, and we do not have any disturbances. Now, the control signal is

$$U(s) = C(s)(R(s) - Y_{\mathrm{m}}(s)) + FF(s)R(s), \tag{3.27}$$

where $Y_{\mathrm{m}}(s)$ is the measured value of the process output. The error to the reference change of the closed-loop control is given in the form

$$E(s) = R(s) - Y_{\mathrm{m}}(s) = -\frac{1 - P(s) \cdot FF(s) \cdot H(s)}{1 + P(s) \cdot C(s) \cdot H(s)} R(s) \ , \tag{3.28}$$

which shows that if the magnitude of the feedback controller $C(s)$ is high, the output follows the reference exactly without feedforward. If the feedforward $FF(s)$ is the inverse of the process $P(s)$, $FF(s) = P(s)^{-1}$, also the output tracks the reference exactly even tough the $C(s) = 0$. This is the reason why the inverted model of the nominal system is typically used as a feedforward. The error between the reference $R(s)$ and the output of the process $Y(s)$ of the reference feedforward, also named as feedforward sensitivity from the reference to the output is (Faanes & Skogestad 2003)

$$S_{\mathrm{FF}}(s) = 1 - P(s) \cdot FF(s). \tag{3.29}$$

The feedback sensitivity function will be

$$S_{\mathrm{FB}}(s) = \frac{1}{1 + P(s) \cdot C(s) \cdot H(s)} \ . \tag{3.30}$$

An ideal feedforward controller based on inverting the nominal process model removes the effect of the reference change such as $E(s) \equiv 0$, if there are no process uncertainties or disturbances. Also, if the gain of the feedback controller is high at the studied frequency, a pure feedback controller will reduce the error of the system to zero.

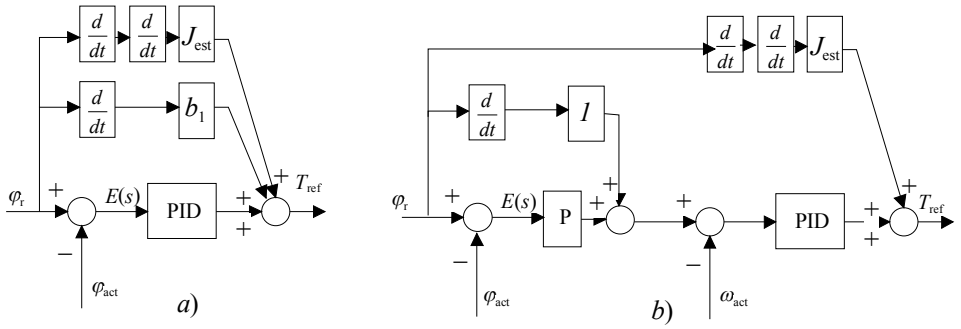

Fig. 3.13. Block diagram of the feedback plus a reference feedforward controller. a) PID position controlled and b) cascaded controlled.

A feedback controller is effective as long as the gain of the sensitivity function $|S_{FB}| < 1$. Also a feedforward improves the performance if $|S_{FF}| < 1$ (Skogestad & Postlethwaite 2005). Because there are always some parameter and model uncertainties present, we need to present the "actual" sensitivity

$$S^*(s) = S_{\text{nom}}(s)\frac{1}{1+E(s)T(s)}, \tag{3.31}$$

where $S_{\text{nom}}(s)$ is the nominal sensitivity of the process

$$S_{\text{nom}}(s) = \frac{1}{1+C(s)P_{\text{nom}}(s)H(s)}, \tag{3.32}$$

where $P_{\text{nom}}(s)$ is the nominal model of the process. E is the relative error of the process

$$E(s) = \frac{P_{\text{act}}(s)}{P_{\text{nom}}(s)} - 1, \tag{3.33}$$

where $P_{\text{act}}(s)$ is the actual process. T_{nom}(s) is the nominal complementary sensitivity of the process

$$T_{\text{nom}}(s) = 1 - S_{\text{nom}}(s). \tag{3.34}$$

The "ideal" reference feedforward controller will reduce the error when the relative modeling error is less than one (Faanes & Skogestad 2003)

$$\left|S_{\text{FF}}(s)\right| = \left|E(s)\right| = \left|1 - \frac{P_{\text{act}}(s)}{P_{\text{nom}}(s)}\right| < 1. \tag{3.35}$$

In modern frequency converters, feedforward functions are implemented in the control loop, Fig. 3.13, and an acceleration feedforward over a velocity controller can be written as

$$FF_{\text{acc}}(s) = J_{\text{est}}s^2, \tag{3.36}$$

where J_{est} is the estimated total inertia of the system. A velocity feedforward over a position controller is derived from the position reference φ_r

$$FF_{vel}(s) = s \, . \tag{3.37}$$

If a PID position controller is used, the velocity feedforward is used to compensate the viscous friction b_1 of the system

$$FF_{velPID}(s) = b_1 s \, , \tag{3.38}$$

and if both acceleration and velocity feedforwards are used with a PID position controller, the total feedforward is

$$FF_{acc+velPID}(s) = J_{est} s^2 + b_1 s \, . \tag{3.39}$$

These are also the most commonly used reference feedforward controllers, and they increase the reference tracking capability in most of the cases. All of them are for a "rigid" model without any other dynamics than just the total inertia and friction of the system. A more sophisticated feedforward controller structure can compensate the dynamics of the torque controller and the delay of the control loop. In such a case, the ideal feedforward controller is

$$FF_{ideal}(s) = \frac{\left(J_{est} s^2 + b_1 s\right)\left(\tau_e s + 1\right)\left(\frac{\tau_d}{2} s + 1\right)}{-\frac{\tau_d}{2} s + 1} \, , \tag{3.40}$$

where τ_e is the estimated time constant of the torque control of the frequency converter and τ_d is the estimated delay of the system.

A properly designed feedback controller is insensitive to uncertainties within the system bandwidth, but the feedforward controller is sensitive to the system model uncertainty, which may produce some problems especially in systems with flexibility. With feedback it is possible to reduce the effect of the disturbance with frequencies below the system bandwidth. By using the disturbance feedforward, we aim at reducing the effects of faster disturbances (Åström & Hägglund 1995), while by using the reference tracking feedforward, we want to track higher frequencies than what is possible with the normal feedback controller. In industrial applications it is typically simplified to compensate the time constant and damping of the rigid body model. Some textbooks present the basic principles of the model inverse based feedforward functions for both reference tracking and disturbance rejection (Åström & Hägglund 1995: Ellis 2000). Typically, the main problem of these textbook approaches is that they do not consider the model error possibility.

The controller may have been designed by adopting a robust approach to the flexible system, but the reference tracking feedforward instead has been designed by applying an inverse model of the rigid body of the system, and the robustness for parameter uncertainty has not received any attention in the design. A typical approach in industrial applications is also that the feedforward controller is used assuming the system to be rigid. The standard feedforward functions used in the servo drives do not even enable the use of an inverse model of the flexible system, and if the reference of the system is not band limited, problems may occur. Figure 3.14

shows the result of using "a rigid body" feedforward together with a robust feedback controller. Even though there is no parameter uncertainty in the system, the problems are quite clear. The usage of the acceleration feedforward significantly increases the amplification of the system starting from 23 Hz. If the reference of the control system consists of such frequencies, there will be a dramatic overshoot at these frequencies, which may lead to a mechanical damage of the system or the control system may saturate, and consequently, the motor may rush.

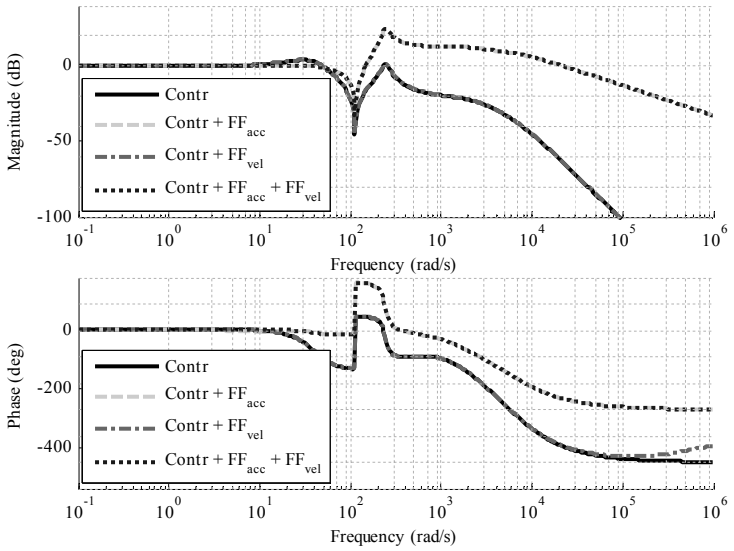

Fig. 3.14. Magnitudes and phases of the closed-loop control of a flexible system, when using only the feedback controller (Contr), the feedback controller and the acceleration feedforward (Contr + FF_{acc}), the controller and the velocity feedforward (Contr + FF_{vel}) and finally, the controller and both the acceleration and velocity feedforwards (Contr + FF_{acc} + FF_{vel}).

The main reason for the amplification of the frequencies above 23 Hz can be seen in Fig 3.15, where the sensitivity functions of the flexible system are shown. The acceleration feedforward will increase the performance of the system to the frequency of 17 Hz, but after that it will decrease the performance of the system $|S_{FF}| > 1$. Even though the feedback controller is robust, the control effort of the feedback controller will be insufficient to compensate the amplification of the acceleration feedforward, which can be seen in Fig. 3.16.

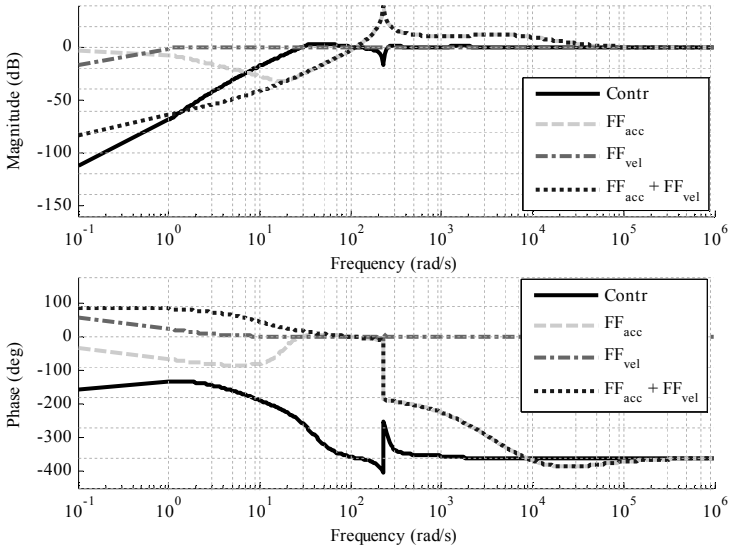

Fig. 3.15. Sensitivities of a flexible system, when using only the feedback controller (Contr), the acceleration feedforward (FF_{acc}), the velocity feedforward (FF_{vel}), and both the acceleration and velocity feedforwards ($FF_{acc} + FF_{vel}$).

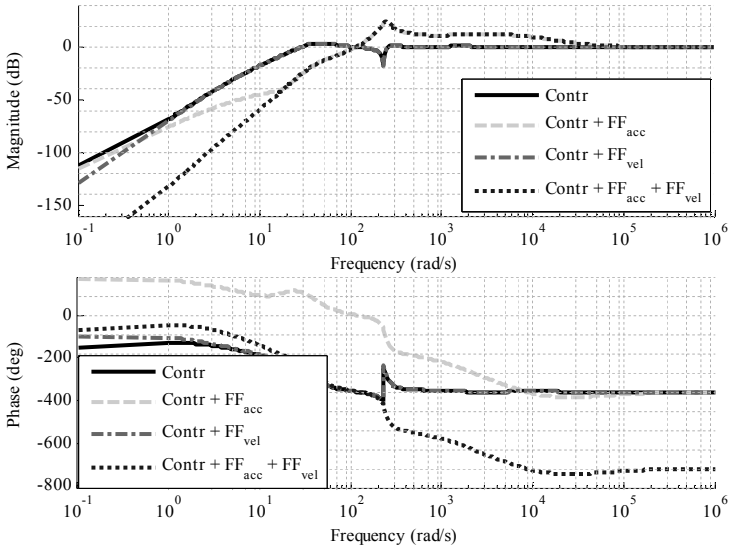

Fig. 3.16. Sensitivities of a flexible system, when using only the feedback controller (Contr), the feedback controller and the acceleration feedforward (Contr + FF_{acc}), the controller and the velocity feedforward (Contr + FF_{vel}) and the controller and both the acceleration and velocity feedforwards (Contr + FF_{acc} + FF_{vel}).

The results shown in Figs. 3.14–3.16 illustrate a case when there are no parameter uncertainties and the feedforward function is based on the inverse of the "rigid model".

3.2.5 Lead/lag filter

When the process includes resonances and time delay, the PID position controller may be difficult to tune for high-performance requirements because of the phase changes discussed in the previous sections. The easiest way to increase or decrease the phase is a lead/lag filter. The lead/lag filter is also a common function in standard frequency converters and motion controllers. The transfer function of the phase-lead/lag filter is

$$LL(s) = \frac{T_1 s + 1}{T_2 s + 1}, \tag{3.41}$$

where $T_1 > 0$, and in the case of phase-lead compensation $0 < T_2 < T_1$ or $T_2 > T_1$ for phase-lag compensation. One lead/lag filter cannot compensate more than 90º phase. If the application needs more compensation, more than one lead/lag filter can be used. Figure 3.17 shows the magnitudes and phases of both a lead and lag filter. The lead filter is tuned to give a 75º phase lead at the frequency of 350 rad/s, and the lag filter to decrease the phase by 45º at the frequency of 550 rad/s. The magnitude of the lead filter starts to increase over a decade before the frequency of 350 rad/s, and the phase begin to increase by two decades before this frequency. The high frequency magnitude is increased permanently by 35 dB. This may cause problems, if there is some measurement noise present.

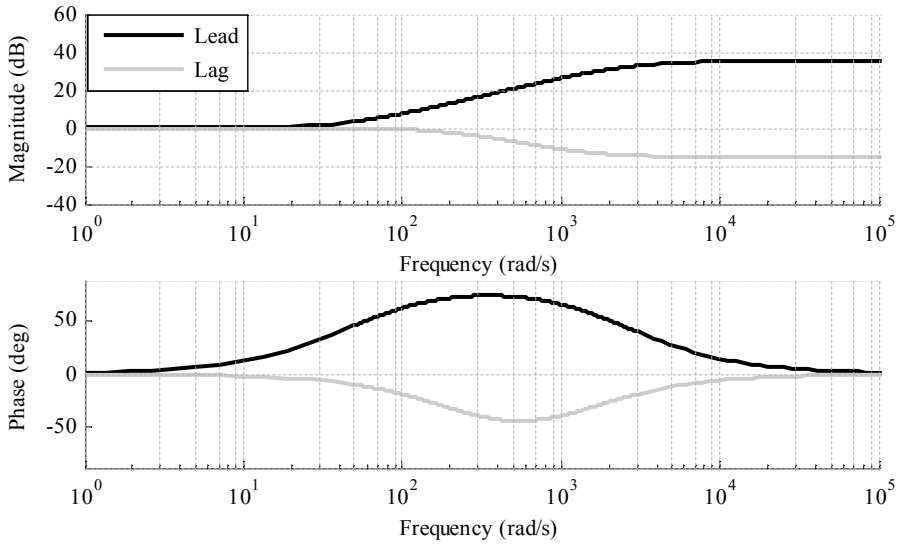

Fig. 3.17. Magnitudes and phases of lead and lag filters. The lead filter gives a 75º phase lead at the frequency of 350 rad/s and the lag filter decreases the phase by 45º at the frequency of 550 rad/s.

4 CONTROL SYSTEM DESIGN WITH QFT

The major challenge in the design of a controller for machinery applications is that the values of the parameters in the model are seldom known accurately in advance. The problem is known as parameter uncertainty. For example, the spring constant of the system varies, or the inertias of the motor and the load are not known accurately; see Fig. 2.29. The system model may also include non-parametric uncertainty, sometimes referred to as model uncertainty. The friction of the system, which is typically non-linear but is linearized for the model, or some of the process dynamics that are not modeled are examples of non-parametric uncertainties. In our case, the dynamics of the connection shaft and the highest resonance frequency of the belt drive are not included in the model, see Fig. 2.31. The problems of parameter uncertainty and non-parametric uncertainty are not related to tooth belt drives only, but are present in all control systems. Some of the variation in the process parameters can be estimated and compensated with different kinds of observers. Because of the problems with parameter uncertainty, it is not clear whether it makes sense to prepare a complicated model-based control law for the manipulator control. At the time of 1986, the robot manufacturers were of the opinion that it is not worthwhile to use a complete manipulator model in the controller (Craig 1986). However, today there are some studies available that apply a complete model of the manipulator in the controller (Neugebauer 2007).

A continuous-time uncertain transfer function can include both parameter uncertainty and non-parametric uncertainty. If parameter uncertainty is to be modeled, it requires some knowledge of the variation in the parameters of the transfer function. Non-parametric uncertainty instead is used when the exact nature of the uncertainty cannot be attained by varying the parameters of the model or when identification algorithms are used. When parameter uncertainty or system model variation is present, adaptive or robust control designs are often suggested in the literature to solve the problem. A good guideline is to use the simplest control algorithm that satisfies the specification of the system; however, adaptive control algorithms are typically quite complex. The responses of adaptive systems are “better” over the full parameter range when the parameters are adapted, but it will take some time to adapt the parameters. Here, “better” means a lower overshoot, a faster rise time, and a larger bandwidth. A robust controller will have a better response when the parameters of the process are changing rapidly from one constant value to another, but the magnitude of the controller is higher than with adaptive controllers (Åström & Wittenmark 1995). A high-magnitude controller, however, makes the system more sensitive to the noise. Examples of robust control design methods are Linear-Quadratic-Gaussian (LQG), H_∞, and quantitative feedback theory (QFT).

This chapter concentrates on the QFT design method, and only parametric uncertainty is present in the system. A PID position controller and a P position controller cascaded with a PID velocity controller are designed for a tooth belt linear drive. The controllers are implemented to an embedded PC, and the torque references are given via the SERCOS fieldbus to the torque amplifier. The fieldbus brings some additional delays to the system, shown in Section 2.2.3, and thus, the effect of this delay on the performance of the controller is shown.

4.1 Introduction to the QFT design method

Quantitative Feedback Theory (QFT) is a frequency-domain design method (Horowitz 1982). It was introduced by Isaac Horowitz in the 1960s, and it is continuation of the work of Hendrik

Wade Bode. The QFT can be considered as an extension of the classical frequency-domain design developed for the practical design of feedback systems (Horowitz 2001). The designed feedback controller should accomplish all the performance specifications presented for the uncertainties of system parameters or load disturbances. Section 3.2.1 discusses the benefits of the feedback and why it should be used in motion control systems.

One of the main objectives of the quantitative feedback theory (QFT) is to design a simple, low-order, minimum-bandwidth controller, which meets the performance and stability requirements of the process. The minimum bandwidth controller is, however, inconsistent within the requirements of the motion control applications, which require a high-gain controller to guarantee the minimum tracking error. High-gain requirements can be taken into account in the performance specifications of the process. Performance specifications of the system, shown in Fig. 4.1, can be assumed to be time-domain performance criteria such as the maximum and minimum rise time of system, t_{rL} and t_{rU} respectively, the peak overshoot of the system M_p, and the settling time t_s. These time-domain criteria are then transformed into frequency domain specifications: B_U and B_L are the upper and lower boundaries, $L_m M_m$ is the peak overshoot, and ω_L and ω_U are the minimum and maximum bandwidth, respectively. The transformation methods can be found in (Yaniv 1999).

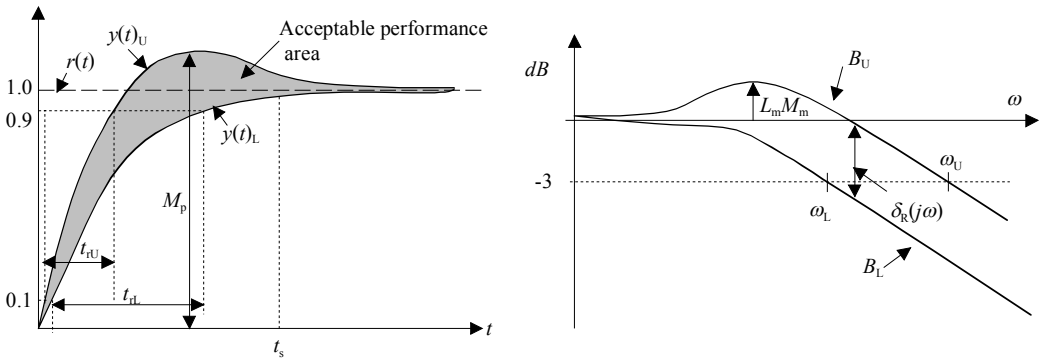

Fig. 4.1. System performance requirements; a) time domain response and b) frequency domain response (Houpis et al. 2006).

The philosophy of the QFT encompasses a wide range of applications. For example (Liu and Luo, 2005) applied the QFT method to design cascaded position and speed controllers for a XY position table of a linear permanent magnet synchronous motor (LPMSM) direct drive, which is used in automatic wire bonding machines. The process suffered from mechanical resonances at high acceleration/deceleration rates, and the resonance frequencies were dependent on the operation conditions and manufacturing tolerances of the machines. The authors used non-parametric uncertainty to model the system. The result was a 10^{th}-order velocity controller cascaded with the P position controller. The position controller was switched to the PI scheme at the end of the motion profile. Also an auto-tuning feedforward controller was implemented to increase the tracking performance.

Ahn and Chau (2007) designed a robust force controller for a low-cost hybrid (hydraulic and electric) actuator, and Karpenko and Sepehri (2006) a position controller for a pneumatic actuator. Hearns and Grimble (2002) used the QFT design method for rolling mills, where small parameter uncertainty was present; both a motor angle and a strip tension controller were designed in the work. Even though this was actually a MIMO system, the authors simplified it

into two separate SISO systems. Taghirad and Rahime (2005) designed a robust controller for a flexible joint robot, and Jinkun and Yuzhu (2007) a zero phase error compensation for a flight simulator. The latter one uses the QFT method to design a feedback controller, but the authors added a zero phase error (ZPE) feedforward controller to improve the tracking capability. Implementation of the ZPE feedforward controller requires accurate knowledge of the phase behavior of the system, which needs identification measurements of the system. García-Sanz et al. (2001) used the QFT method to select the robust parameters for a Smith Predictor in a pasteurization process in the food industry. The process was uncertain and consisted variable time delay.

Because the performance of the controller depends on how well the designer can "loop shape" the controller, an automatic procedure is developed to loop shape the controller to satisfy the QFT performance. For example Zolotas and Halikias (1999) described a method to calculate the optimum parameters for the PID position controller for a rigid system. The control structure did not include the filtering of the D-part. The D-part filtering was included to the design in (Yaniv and Nagurka 2004). Yaniv and Nagurka (2005) have also proposed an automatic loop shaping method for a mechanical servo system controller that consists of a lead element and a notch filter. The main problem of these automatic loop shaping methods is that the methods need a lot of computation power, if the system includes a large uncertainty.

When a robust control approach is chosen, the designer must be aware of the fact that every model of the system is only an approximation, and some uncertainties have to be taken into account. Here, the selection of the uncertainties plays an important role. If uncertainty boundaries are selected to be too small, meaning that every actual uncertainty is not included in the model, this will produce a high-performance design, but the actual system may be unstable. On the other hand, if too large uncertainty boundaries are chosen, the controller may be too conservative.

4.2 Closed-loop formulation

One of the main benefits of the QFT approach is that the designer can set performance requirements for the designed system. Performance requirements can be given as constant values or as transfer functions from the inputs to the outputs; for example a rise time and an overshoot of the reference step response can be determined to be within a known range, shown in Fig. 4.1, or the minimum magnitude and phase margins of the system can be given. All the supported inputs and outputs can be seen in Fig. 4.2, and the specifications of the performance requirements can be found from Borghesani et al. (2003). The performance requirements that are used in this study are listed in Table 4.1.

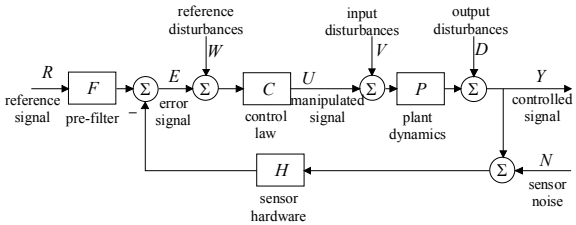

Fig. 4.2. Block diagram of the system.

Table 4.1. Performance specification types used in this study.

Specification	EXAMPLE OF APPLICATION	
$\left\lvert F\frac{PC}{1+PCH}\right\rvert \le W_1$	Gain and phase margins	*Y/R*
$\left\lvert \frac{1}{1+PCH}\right\rvert \le W_2$	Sensitivity reduction	*Y/D*
$\left\lvert \frac{CH}{1+PCH}\right\rvert \le W_5$	Control effort for sensor noise	*U/N*
$\left\lvert F\frac{PC}{1+PCH}\right\rvert \le W_6$	Tracking bandwidth	*Y/R*

Typically in motion control processes, robustness (W_1), sensitivity reduction (W_2, rejection of disturbances at the plant output), and tracking bandwidth (W_6) are the most interesting performance requirements. In applications where load disturbances are significant, disturbance rejection at the plant input should be taken into account when the control is designed. In this thesis, a control effort (W_5) is included to reduce the amplification of the high-frequency sampling noise. The tracking bandwidth can be left out of the considerations, if a pre-filter is not designed. The sensitivity reduction gives a better view of the performance of the feedback controller than the tracking bandwidth. In motion control applications, a reference feedforward is often used. The reference feedforward controller can be reduced to a pre-filter problem as will be shown, and reference tracking should then be analyzed together with sensitivity reduction.

4.3 Uncertainty model and plant templates

A conventional approach to the controller design is to linearize the system to one operation point. Horowitz introduced an idea to replace a nonlinear plant with a set of linear time-invariant plats (Borghesani et al. 2003).

$$\mathbf{P} = \left\{ P(s) = \frac{a_1 s^n + a_2 s^{n-1} + \ldots + a_{n-1}}{b_1 s^m + b_2 s^{m-1} + \ldots + b_{m-1}},\ a_n \in [c_n, d_n], b_n \in [e_n, f_n] \right\}, \tag{4.1}$$

where a_n and b_n, are the process parameters and c_n, d_n, e_n, and f_n are the maximum and minimum values of variation in the process parameters.

Quantitative feedback theory (QFT) is a frequency-domain-based method, which uses an open-loop transfer function of a plant over a specific range of the plant parameter uncertainty. Non-parametric uncertainty can also be taken into account in the design phase of the controller, but as stated previously, this thesis concentrates only on the parametric uncertainties. At each frequency, selected by the designer, the magnitudes and phases of the plants are collected together to form a magnitude and phase plane grid. This grid is called a template of the system. Figure 4.3 describes how the template is generated from three linear-time-invariant (LTI) models at the frequencies of ω_1, ω_2, ω_3, ω_4, and ω_5.

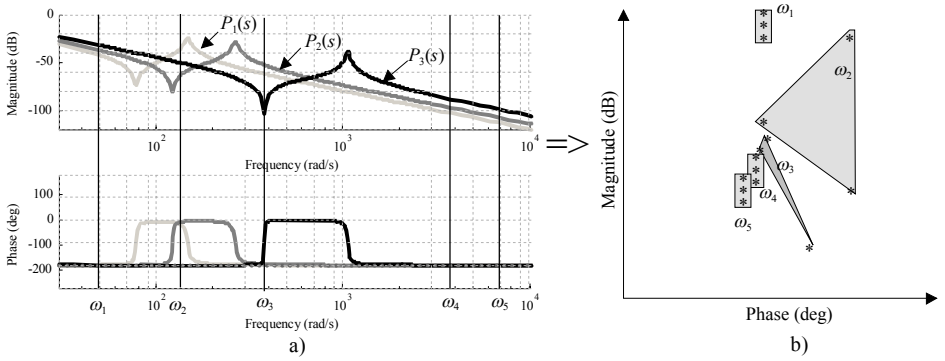

Fig. 4.3. a) Magnitudes and phases of three system models and b) Nichols chart plant templates.

The grid should be carefully assessed to ensure that it provides a "good" approximation of the process. Figure 4.4 depicts the difference between "good" and "bad" approximations. In the "good" approximation, the whole original template of the system is represented in the magnitude and phase plane, whereas a "bad" approximation does not represent every corner of the original template. Furthermore, some of the dynamics of the process will not be taken into account in the controller design phase, if this "bad" representation is used. For example, if the magnitude and phase of the process model $P_3(s)$ at the frequency of ω_3 in Fig. 4.3 is not included in the template, some of the process dynamics will be lost at this frequency, thereby resulting in a "bad" approximation. The template can also be obtained directly from frequency response measurements. If the measurements are made with several similar but not exactly the same machines, there can be sets of frequency responses.

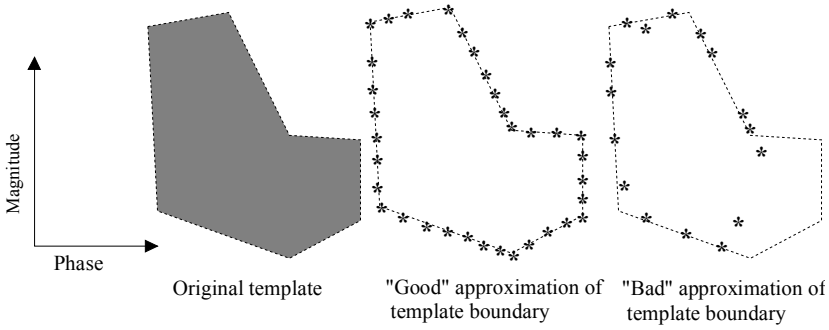

Fig. 4.4. Difference between "good" and "bad" approximations of the template boundaries (Borghesani et al. 2003). The "good" approximation represents the whole original template of the system, whereas the "bad" approximation leaves some process dynamics outside the controller design phase, which may lead to undesirable behavior of the system.

After selecting the variation of the parameters, we select the frequency points in rad/s, where the uncertain plant is computed. The frequency array must be chosen based on the knowledge of the process dynamics and performance. According to Borghesani et al. (2003), it is important to

compute the bounds up to the frequency where the shape of the template becomes invariant to frequency; the basic rule is to choose the frequencies at which the shape of the template shows significant variations compared with those at other frequencies. For example in the case of resonant plants with variation in the resonance frequency or the damping ratio, some of the selected frequencies may be quite close to each other. If we take a closer look at Fig. 4.3, we can see that an additional frequency between ω_1 and ω_2 should be selected to describe the anti-resonance frequency dynamics of $P_1(s)$. There should also be additional frequencies above ω_2 to estimate the shape and amplitude of the resonance frequencies of $P_1(s)$, $P_2(s)$, and $P_3(s)$. The frequency ω_5 is, however, unnecessary because it gives almost the same dynamics of the process as the frequency ω_4. This means that the selection of frequency array is based on a trial and error method.

4.4 Robust performance

To guarantee the robust stability, the Nichols envelope of the system should not intersect the critical point (–180º, 0 dB) in the Nichols chart. According to Skogestad and Postlethwaite (2005), robust stability can be determined as follows "The system is stable for all perturbed plants about the nominal model up to the worst-case model uncertainty." This condition is equivalent to limiting the magnitude constraint on the complementary sensitivity function. Assume that the templates of the system are simply connected and a loop transfer function $L(s) = C(s)P(s)H(s)$ has a fixed number of unstable poles. Now, it is sufficient to check the robust condition only over the boundary of the template, and we may assume that (Borghesani et al. 2003)

$$\left|\frac{L(j\omega)}{1+L(j\omega)}\right| < W_1(j\omega) > 1, \text{ for all } P \in \partial \boldsymbol{P},\ \omega \geq 0, \tag{4.2}$$

where W_1 is a safety factor or the robust margin of the system and $\partial \boldsymbol{P}$ denotes the boundary of the template. A similar margin can be given for the sensitivity reduction function.

$$\left|\frac{1}{1+L(j\omega)}\right| < W_2(j\omega), \text{ for all } P \in \partial \boldsymbol{P},\ \omega \geq 0. \tag{4.3}$$

Equation (4.3) forces the loop gain of the system to be small when the Nichols plot crosses the –180º line below 0 dB. In a conditional stable system, Eq. (4.2) forces the loop gain to be large when the Nichols plot crosses the 180º line above 0 dB. Figure 4.5a shows the robust margin bound of one frequency given by Eq. (4.2) in the complex plane and the same bound in the Nichols chart. The margin W_1 determines the size of the restricted area; a smaller W_1 gives a larger restricted area and larger margins. Correspondingly, Fig. 4.5b shows the sensitivity reduction bound given by Eq. (4.3). The frequencies before the sensitivity function plot cross the –180º line below 0 dB, and the bound forces the loop gain to be larger than the bound, but after –180º and 0 dB, the sensitivity reduction forces the loop gain to be smaller.

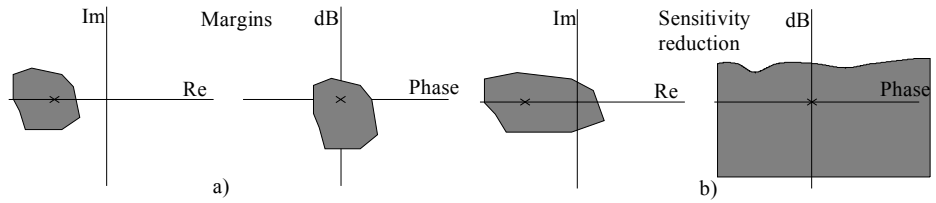

Fig. 4.5. QFT bounds in the complex plane, a) the Nichols chart margins, and b) sensitivity reduction. The specifications W_{s1} and W_{s2} constitute the restricted areas.

The safety factors W_1 and W_2 can be either constant values or functions. If constant values are used, W_1 and W_2 are denoted M_T and M_S, respectively. The minimum magnitude and phase margins can be given with the parameters M_T and M_S. M_T gives the margins for reference tracking and M_S for sensitivity. The gain margins can be calculated as (Skogestad & Postlethwaite 2005)

$$GM_T \geq 1 + \frac{1}{M_T} \tag{4.4}$$

$$GM_S \geq \frac{M_S}{M_S - 1} \tag{4.5}$$

and the phase margins

$$PM_T \geq 2\arcsin\left(\frac{1}{2 \cdot M_T}\right) \geq \frac{1}{M_T}[\text{rad}] \tag{4.6}$$

$$PM_S \geq 2\arcsin\left(\frac{1}{2 \cdot M_S}\right) \geq \frac{1}{M_S}[\text{rad}]. \tag{4.7}$$

For stable processes $M_S > M_T$ and typically $M_T < 1.25$ and $M_S < 2$, which gives a minimum 5.1 dB magnitude and 47º phase margins for tracking and a 6 dB magnitude and 29º phase margins for sensitivity.

However, if the maximum bandwidth has to be achieved, the safety margins can be reduced. Reducing the stability margins also affects the damping ξ and the overshoot of the system, which may decrease the accuracy of the motion control system. Table 4.2 gathers these values for a standard second-order system, and also the total variation of the system is given. The total variation (TV) describes the area of the total up and down movement (oscillation) of the signal, which should be as small as possible.

Table 4.2. Step response characteristics of the second-order system (Skogestad & Postlethwaite 2005).

ξ	Time domain, $y(t)$		Frequency domain	
	Overshoot	Total variation	M_T	M_S
2.0	1	1	1	1.05
1.5	1	1	1	1.08
1.0	1	1	1	1.15
0.8	1.02	1.03	1	1.22
0.6	1.09	1.21	1.04	1.35
0.4	1.25	1.68	1.36	1.66
0.2	1.53	3.22	2.55	2.73
0.1	1.73	6.39	5.03	5.12
0.01	1.97	63.7	50.0	50.0

If the safety margins are reduced, the designer must know the behavior and delay of the system more accurately. The designer must also be certain that the template of the system is accurate and there are no non-modeled dynamics involved in the process. The robust bounds given above are important for the quality of the response, but we must also discuss and analyze the speed of the response, which is related to the bandwidth of the system. Generally, a larger bandwidth gives a faster rise time for the system, but at the same time it will be more sensitive to the system and measurement noise. According to Skogestad & Postlethwaite (2005), the bandwidth of the system can be defined as a frequency range $[\omega_1,\omega_2]$ where the control is effective. When a tight control is required, we can assume that $\omega_1 = 0$ and $\omega_2 = \omega_b$, where ω_b is the needed closed-loop bandwidth. In this case, "effective" means that the use of the controller provides some benefits for the performance of the system; for example in the case of tracking, the error

$$e = r - y = -S \cdot r \tag{4.8}$$

and the control is effective if the relative error $|e|/|r| = |S|$ is small (S is the sensitivity function, r the reference, and y the output of the system). Typically, - 3dB is assumed, thus $|S| < 0.707$. Another definition for the term 'effective' is that the control is effective if it significantly changes the output response. For the tracking performance, the output

$$y = T \cdot r \tag{4.9}$$

and we can say that the control is effective as long as the magnitude of the complementary sensitivity function of the system T is reasonably large ($T > 0.707$). This bandwidth ω_{bT} is traditionally used as the definition of the bandwidth of a control system; however, according to Skogestad & Postlethwaite (2005), it is less useful for a feedback system than the definition based on the sensitivity $|S|$, because up to the frequency ω_b $|S|$ is less than 0.707 and the control improves the performance. Within the frequency range $[\omega_b, \omega_{bT}]$ the control still affects the output of the system, but it does not improve it anymore, and in some cases $|S| > 1$, which means that the control decreases the performance of the system. Finally, above the frequencies of ω_{bT} $|S| \approx 1$, and the control has no significant effect on the response of the system. The required sensitivity function can be described as

$$W_2(s) = \frac{\left(\frac{s}{M_s^{1/n}} + \omega_b\right)^n}{\left(s + \omega_b \cdot A^{1/n}\right)^n}, \tag{4.10}$$

where M_s gives the robust margin, ω_b is the desired bandwidth of the sensitivity function, and A is the attenuation at zero frequency. The order n of the sensitivity function is typically one, but if a high-gain controller is required, the order can be higher. Attenuation at the zero frequency should be zero, but for practical implementation reasons the value of A is greater than zero. Now only the frequency of ω_b has to be determined. A rule of thumb is that the controller bandwidth should be 1/3–1/10 of the resonance frequency, which can also be used as the bandwidth of the sensitivity function W_2 (Younkin 2003).

4.5 Pre-filter and feedforward design

When the main performance criterion of the system is the tracking of the reference signal, a reference tracking feedforward is needed to ensure the best possible tracking performance. Also the possibility to use a pre-filter should be considered. The benefits of a pre-filter were discussed in Section 3.2.1. When a pre-filter is used, the tracking specification is written in the form

$$\left| F(j\omega) \frac{C(j\omega)P(j\omega)}{1 + C(j\omega)P(j\omega)H(j\omega)} \right| \leq W_6(j\omega), \tag{4.11}$$

where W_6 represents the tracking criteria of the system. W_6 can be either a constant that limits the overshoot of the system or a frequency-weighted function that limits the tracking capability at different frequencies and gives the desired rise time to the system for step reference signals.

The reference tracking feedforward controller can be modified to represent a pre-filter design problem, if the controller block diagram is modified as shown in Fig. 4.6. The modification is needed, if the QFT toolbox of Matlab® is used for a feedback plus feedforward controller design, because the feedforward function cannot be directly implemented in the design procedure. Only a two-degrees-of-freedom design is supported. The modification gives a pre-filter plus a feedback controller structure, where the feedback controller can be designed to reject disturbances and the pre-filter is used for reference tracking. The first step is to design a feedback controller and assume $FF(s) = 1$. After the feedback controller has been designed, we can focus on the design of the feedforward $FF(s)$. To the best knowledge of the author, no QFT feedforward design has been published so far.

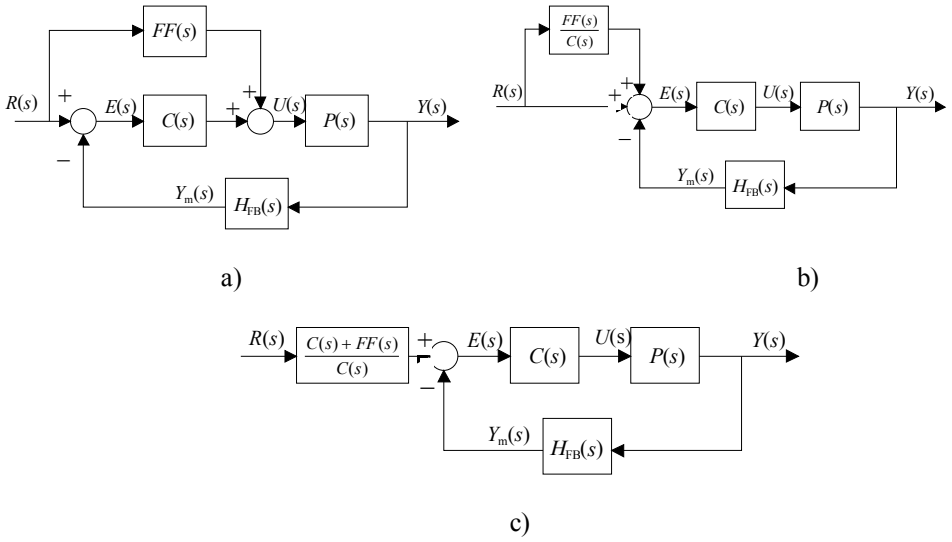

Fig. 4.6. Modified block diagram of the controlled system. The feedforward function is modified into a pre-filter design problem. a) Original circuit, b) development of the original circuit, and c) the final circuit showing the pre-filter design.

4.6 QFT design procedure

Design steps when the QFT toolbox is used in Matlab® are the following:

1. The template of the system is generated using the process transfer functions with parameter uncertainties in the selected frequency points. The generated template of the system must be a good approximation of the "original" template of the system. If the generated template does not accurately describe the whole original template (bad approximation), there are some unmodeled dynamics in the design, which may cause problems especially when low stability margins are used. The accuracy of the generated template results mainly from the knowledge of the system model and parameter variations of the system. The frequency points must be selected such that the shape of the template shows significant differences compared with the other frequencies nearby. In other words, these are frequency points in which the dynamics of the process changes significantly compared with the frequency nearby. For example in the case of the system resonance frequency, several frequencies in the low frequency range have to be chosen to describe the system accurately enough.

2. Formulating the closed-loop performance criteria for the system, that is, the stability margins, sensitivity, tracking, and disturbance rejection. If the process dynamics is not exactly known, the stability margins should be adjusted larger. The performance criteria for tracking and disturbance rejection depend on the required time-domain performance of the system. At this point, it is not possible to say whether the given performance criteria are valid. This is a drawback of the QFT design.

3. Computation of the QFT bounds. The bounds are calculated using the functions of the toolbox. If there are non-connected bounds at a single frequency, there may be large gaps between adjacent template points.

4. Loop shaping for the QFT feedback controller. This basically means that poles and zeros are added to the control system. It is possible to use a pre-determined control structure, for example a PID controller, or design a controller structure of its own. The loop shaping is made by using the nominal open-loop transfer function $L_{\text{nom}}(s)$ and the bounds calculated previously. The bounds are illustrated with a solid curve or with a dashed line. The solid curves indicate that the $L_{\text{nom}}(s)$ must lie above the bound at the frequency in question to satisfy the performance criteria, and on the other hand, the $L_{\text{nom}}(s)$ must lie below the dashed line at the frequency in question to satisfy the performance criteria. At this point we can see whether the performance criteria given in step 2 are attainable. If not, the performance criteria have to be reconsidered or the process must be redesigned.

5. Design of the pre-filters. After the feedback controller is designed, the pre-filter can be considered. The pre-filter design is needed if a two-degrees-of-freedom control structure is used or the reference feedforward is implemented.

6. Evaluating the performance criteria for the designed QFT controller. The performance is evaluated in the whole frequency range, not only at the frequencies that were used in the control design phase. If the criteria are violated in some frequency range, the designer may select this frequency for the frequency vector (go to step 1) or just fine-tune the designed controller (go to step 4).

4.7 QFT-based robust PID position controller design

In this section, a decentralized PID position controller for a tooth belt linear drive is designed by applying the QFT design method. The term ‘decentralized’ means that the controller is located in an additional control device such as a PLC, or in this case, an embedded PC, and the torque references are given via a fieldbus to the torque amplifier, which also calculates the actual values of the system using encoders. These actual values are then transmitted to the controller via the fieldbus. The detailed description of the test system is given in Section 2.2. The block diagram of the system is shown in Fig. 4.7, where the controller is $C(s)$, the pre-filter $F(s)$, the process $P(s)$, the fieldbus transmitting $\tau_{\text{TM}}(s)$, the fieldbus feedback $\tau_{\text{FB}}(s)$, $\varphi_{\text{meas}}(s)$ is the measured position of the process, $U(s)$ is the reference to the amplifier, and the $U^*(s)$ is the actual reference to the process affected by the fieldbus.

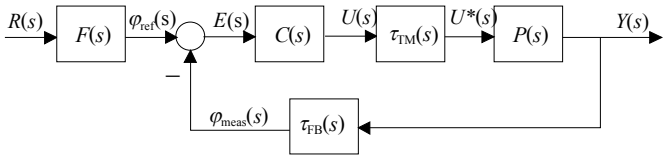

Fig. 4.7. Block diagram of the decentralized position-controlled system.

The transfer function from the torque reference to the actual motor angular position φ_m of the system is given and analyzed in detail in Section 2.3.1, but for the convenience of the reader, we recall it here:

$$P(s)=\frac{\varphi_m}{T_{ref}}=\frac{1}{\tau_e s+1}\frac{1}{\left(J_m+m_L R^2\right)s^2+b_1 s}\frac{m_L s^2+b_s s+K_{eff}}{\frac{J_m\cdot m_L}{J_m+m_L R^2}s^2+b_s s+K_{eff}}, \quad (4.12)$$

where τ_e is the time constant of the torque controller, J_m is the inertia moment of the motor plus additional inertias that are rigidly connected to the motor shaft, m_L is the mass of the load, R is the radius of pulleys, K_{eff} is the equivalent position-dependent elasticity coefficient of the belt, φ_m is the angular position of the motor, b_s is the damping constant of the belt, b_1 is the viscous friction of the system, and T_{ref} is the torque reference to the system. The nominal values and the variation of the system parameters are given in Table 4.3. The parameter variation range is based on the system behavior and on the known "uncertainties" of the system, which are determined in Section 2.3. The delay of the transmitting medium is modeled using the Padé approximation

$$\tau(s)\approx e^{-\tau_d s}\approx\frac{-\frac{\tau_d}{2}s+1}{\frac{\tau_d}{2}s+1}, \quad (4.13)$$

where τ_d is the delay. The designed PID controller is given in Eq. (3.24) and is of the form

$$C_{PID}(s)=K_P\left(1+\frac{1}{T_i s}+\frac{T_d s}{\frac{T_d}{N}s+1}\right), \quad (4.14)$$

where K_P is the gain, T_i is the integrator time constant, T_d is the derivation time constant, and T_d/N is the first-order filter time constant of the derivator. The lead/lag filters of Eq. (3.41) are used to compensate the phase shift of the delay. The design procedure of the QFT approach was shown in Sections 4.2–4.6.

Table 4.3. Nominal parameters of the system and variations of the parameters.

Parameter	Nominal value	Variation
J_m (kgm^2)	0.0053	0.002 – 0.01
K_{eff} (N/m)	$7.5\cdot10^5$	$4.0\cdot10^5$ – $5.0\cdot10^6$
m_L (kg)	50	35 – 65
b_s (Ns/m)	30	15 – 150
τ_e (s)	0.00018	0.00018

4.7.1 Designing the PID position feedback controller

The first step to design a controller by applying the QFT method is to generate a template of uncertain plants. The template of the system is generated by using Eqs. (4.12) and (4.13), the known parameter variation of the system and the fieldbus delays, which depend on the sampling time of the fieldbus as explained in Section 2.2.3. In this example, the fieldbus sampling time is 250 µs, which gives 387 µs and 410 µs ideal transmitting delays for the reference and feedback, respectively. Then, an additional delay of 50 µs is added to the system loop for certainty reasons, if there are some delays that are not included in the ideal loop delay. The template is calculated at discrete points. In this case ω = [1, 10, 50, 100, 400, 1000, 1500, 2000] rad/s. The reason for these discrete points is that the anti-resonance starts around 100 rad/s and the resonance frequency ends around 1500 rad/s. The frequency range between 100 rad/s and 1500 rad/s is the most interesting and important range when the stability of the system is analyzed. The other frequencies are mainly used for the examination of the performance requirements. Figure 4.8 shows clearly that the parameter variation mainly affects the frequencies between 100 rad/s and 1000 rad/s, which is the range where the anti-resonance and the resonance of the system occur. The magnitude and the phase can vary over 100 dB and 180 degrees, respectively. This kind of variation is so large that the conventional approach to linearize the system to one point certainly gives poor or even unstable results.

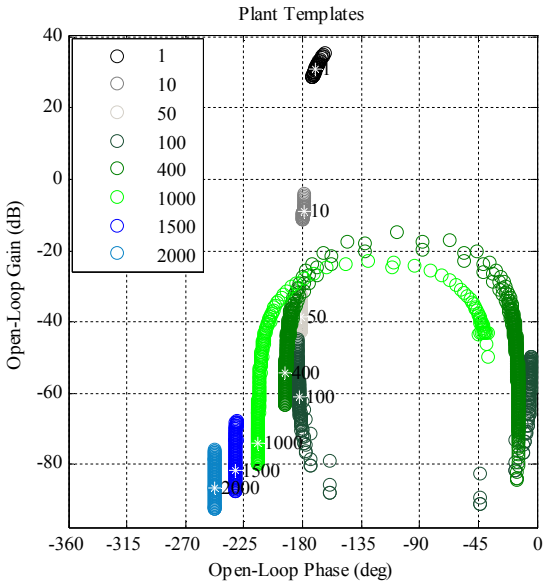

Fig. 4.8. Template of the system, when the fieldbus sampling time is 250 µs.

It is necessary to specify the robust performance requirements of the system that should be met with the designed controller. The main interests are

i) robust stability

ii) reference tracking

iii) sensitivity to measurement noise

The load disturbance rejection should also be considered if the process consists of active loads or significant load disturbances such as the cutting force in the crop shear applications. These are not major error sources in the case of the tooth belt drive, and the robust performance criteria for the load disturbances can be neglected. The specifications are used as guidelines for shaping the nominal loop transfer function $L_{\text{nom}}(s) = C(s) \cdot P_{\text{nom}}(s) \cdot \tau_{\text{nom}}(s)$, where $P_{\text{nom}}(s)$ is the nominal model of the process, $\tau_{\text{nom}}(s)$ is the nominal loop delay, and $C(s)$ is the designed controller.

i) Robust stability

To guarantee the robust stability of the system, the peak magnitude of the closed-loop frequency response is limited by

$$\left| \frac{L(j\omega)}{1 + L(j\omega)} \right| < W_1 = M_T = 1.7 , \tag{4.15}$$

which corresponds to the 4.0 dB minimum gain and the 34º phase margins used in Eqs. (4.4) and (4.6), respectively. These margins may sound quite small. However, although the response of the process will oscillate more than is typically the case in motion control systems, the minimum phase margin is still large enough for total unsynchronized communication between the embedded PC and the drive. The total unsynchronized communication can bring an additional delay of 250 µs to the system, which equals one communication cycle. The 250 µs additional delay decreases the phase margin by 21.5º at the frequency of 1500 rad/s, which is the highest frequency where the most critical stability issues are present, meaning that we can still guarantee the 12.5º minimum phase margin, if the communication between the embedded PC and the drive are delayed by one communication cycle.

In high-performance motion control systems, a properly designed reference is frequency band limited and smooth. If the control system is designed with such low margins as in this thesis, the need for smooth profiles is even more important. Smooth profiles guarantee that the system will not suffer from high-frequency reference inputs, which excites the resonance modes. A controller with low margins cannot damp the resonances efficiently enough for smooth and accurate movement. If the reference commands are not properly designed, or the system contains significant disturbances, the robust margins should be larger, which in turn increases the damping and decreases the overshoot and gives smoother and more accurate movement. Figure 4.9 shows the robust margin bounds of the system at the chosen discrete frequencies of ω.

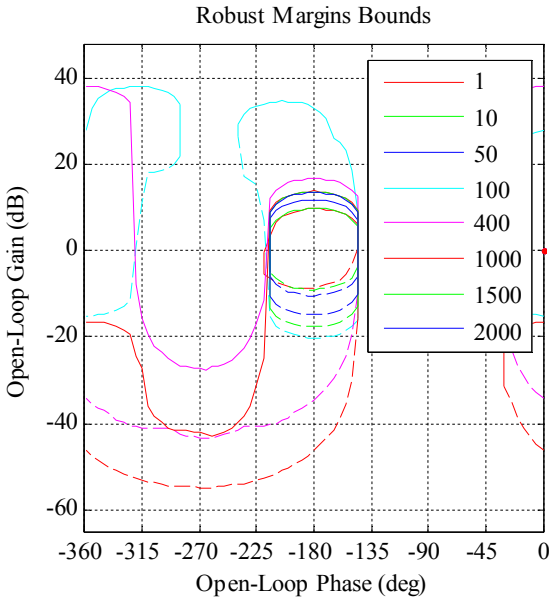

Fig. 4.9. Robust margin bounds of the system.

Figure 4.9 shows that the frequencies at 100 rad/s form two different bounds, one around the (-180º, 0 dB) point and the other around the (-360º, 0 dB) point. If there are two non-connected bounds at a single frequency, special attention has to be paid to the system design; the situation may result from too large gaps between adjacent template points, or from an originally non-connected plant. In this case the plant is originally non-connected, because both the anti-resonance and resonance of the system can be at the frequency of 100 rad/s. The anti-resonance frequency increases the phase by 180º and the resonance frequency decreases the phase by 180º, as was shown in Fig. 2.30. In Figures 4.9–4.15, the bounds are plotted either with solid or dashed lines; the solid lines imply that the $L_{\text{nom}}(s)$ must lie above the bound to satisfy the performance criteria and on the other hand, the $L_{\text{nom}}(s)$ must lie below the dashed line to satisfy the performance criteria.

***ii*) Reference tracking**

When the reference tracking capability is studied, it can be divided into two parts, namely the sensitivity function S and the complementary sensitivity function T. As was stated in (Skogestaad & Postlethwaite 2005) and discussed in Section 3.2, the sensitivity function S of the system is more important for the feedback controller designer than the complementary sensitivity function T. But when the reference tracking feedforward controller is used to increase the reference tracking capability, the complementary sensitivity function T will also be of interest. When a high-performance system is designed, the controller should be able to ensure zero error at zero frequency and small errors during output disturbances of the process, and follow the reference signal with a small error. Based on these requirements, the robust margin of the sensitivity function Eq. (4.3) has to be in the form (Skogestad & Postlethwaite 2005)

$$\left|\frac{1}{1+L(j\omega)}\right| < W_2(j\omega) = \left|\frac{\left(\frac{j\omega}{M_S^{1/n}} + \omega_b\right)^n}{\left(j\omega + \omega_b \cdot A^{1/n}\right)^n}\right|. \tag{4.16}$$

In this study n = 2, which gives 40 dB/decade roll-off rate at low frequencies. The structure of the PID position controller ensures that 40 dB/decade is possible to achieve. Attenuation at the zero frequency should be zero. We use A = 0.0001. Now only the frequency of ω_b has to be determined. In our case when the parameter variation is taken into account, the lowest resonance frequency of the tooth belt can be 23 Hz. In Fig. 4.10 ω_b is chosen to be 6 Hz, which corresponds to one-fourth of the minimum resonance frequency. The minimum resonance frequency can be calculated using the parameter uncertainties defined in the design phase, see Section 2.3. Figure 4.10 shows that the parameter uncertainty changes the dynamics of the system most at the frequencies between 100 and 1500 rad/s, where the robust template of the system varies most.

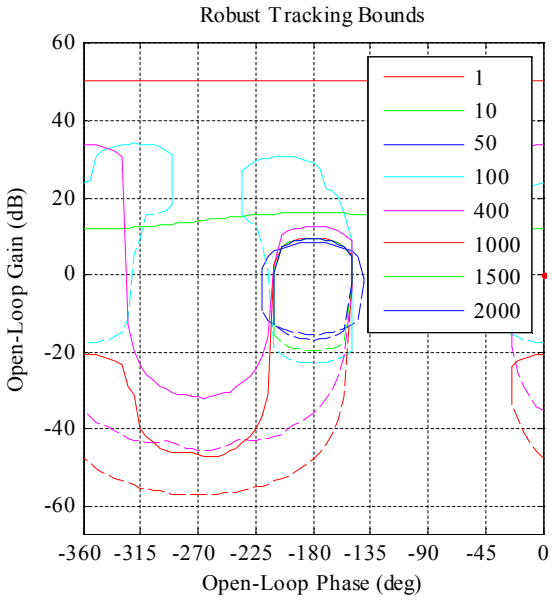

Fig. 4.10. Sensitivity bounds

Because of the usage of the reference feedforward controller, the reference tracking should also be analyzed and the performance criteria determined. The reference tracking bandwidth should be limited to one-third of the lowest resonance frequency of the system (Younkin 2003), which gives a maximum bandwidth f_{max}= 7.7 Hz for the tracking, thus,

$$\left| F(j\omega)\frac{L(j\omega)}{1+L(j\omega)} \right| < W_6(j\omega) = \left| \left(\frac{2\pi f_{\max}}{j\omega + 2\pi f_{\max}} \right)^n \right|. \tag{4.17}$$

If the maximum performance would like to achieve, it is not be practical to design a controller that would satisfy this maximum bandwidth criteria given in Eq. (4.17) with such a large variation of process parameters as in our test system. The maximum reference tracking requirement may become too difficult to meet, if the time delay of the system increases and the difference between the inertia of the motor J_m and the load inertia J_l becomes too large (>1:10). The reason for this is explained in Section 2.3, where the parameter variation of the system is introduced and the dynamic variation of the system is explained. Figure 4.11 shows the tracking bounds when the maximum bandwidth of the system f_{max} = 7.7 Hz. The magnitude of the open-loop transfer function of the system at the frequency of 1 rad/s, including the controller, can be varied between 32 dB and 68 dB depending on the open-loop phase at this frequency.

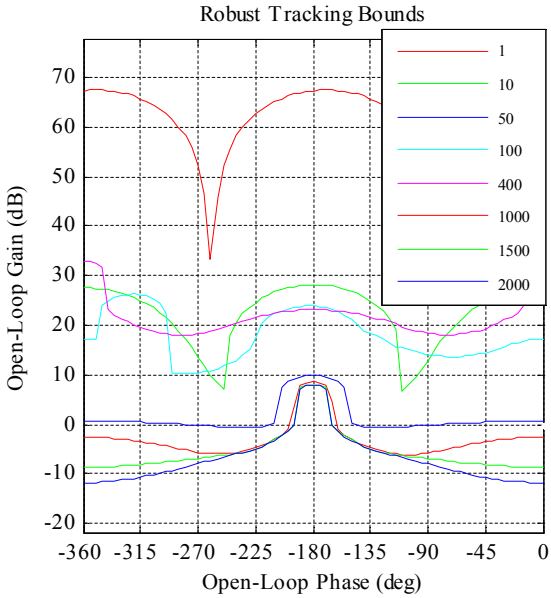

Fig. 4.11. Tracking bounds

iii) Sensitivity to measurement noise

It is quite typical in industrial applications that the measured position value is low-pass filtered in a 1–5 ms filter time. This reduces the measurement noise of the feedback signal, but at the same time decreases the phase margin of the system, which is seldom taken into account. In our case the motor angle measurement is made by using an absolute encoder, which provides highly accurate and large-resolution motor angle information. The measurement is then calculated in the frequency converter, and the actual motor angle and motor velocity is sent via the SERCOS II fieldbus to the controller, and the feedback signal is not filtered. The medium of the fieldbus is optic, and it can be assumed that there are no disturbances in the medium. However, the resolution of the measurement signal is limited, which is a question that has to be addressed in the study.

The resolution of the feedback information obtained via fieldbus is limited to 0.000025 rad. However, because of the fieldbus delay and the lead/lag filters, which are used to compensate the delay, the resolution may be too low. At least the high-frequency gain of the controller should be limited. The usage of the lead/lag filters increases the high-frequency gain, which was shown in Section 3.2.5. Let us assume that the maximum noise of the torque reference can be 2 % of the nominal value of the motor, which corresponds to 1 % of the maximum force of the tooth belt linear drive. Consequently, the high-frequency gain must be limited to 80 dB to ensure that when the system is varied with the minimum resolution, the torque reference will not reach 1% of the maximum tooth belt force. This limitation can be included in the QFT design phase, which gives the bounds shown in Fig. 4.12. We can see in Fig. 4.12 that the magnitude of the open-loop transfer function of the system should be less than -5 dB at the frequency of the 2000 rad/s.

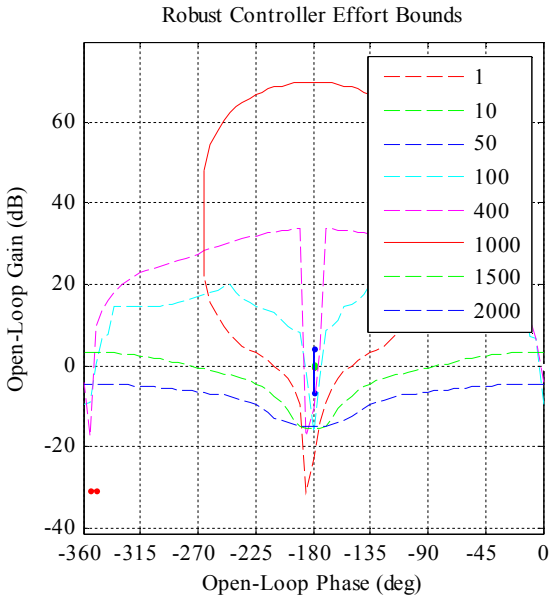

Fig. 4.12. Measurement noise limitation

When all the performance bounds are gathered together, and bounds that are overlapping each other are removed, we obtain a compilation of bounds presented in Fig. 4.13.

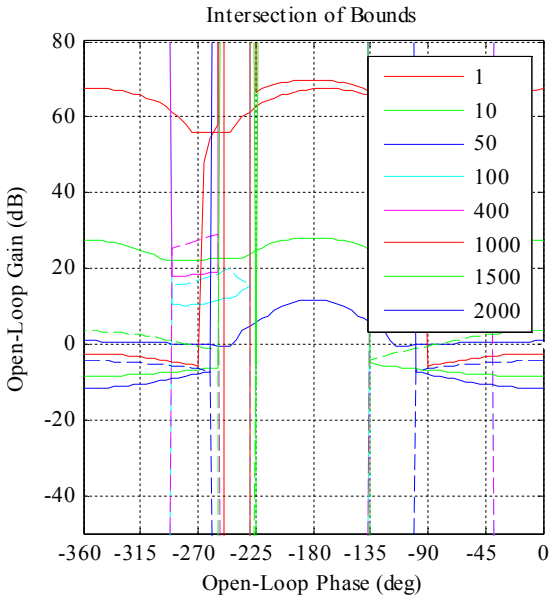

Fig. 4.13. Compilation of the bounds.

QFT loop shaping of the controller

The next step is "loop shaping" of the controller, which basically means that poles and zeros are added to the control system. The loop shaping is made by using the bounds calculated with the QFT tool and the Nichols chart, as explained previously. This is not an automated process, but has to be performed by the designer. Figure 4.14 shows $L_{\text{nom}}(s)$ without the controller, thus $C(s)=1$. The system is stable, but it can be clearly seen that it does not meet the performance criteria; it violates the stability bounds, and the open-loop transfer function of the nominal system is below the performance bounds at every frequency. The gain of the controller has to be increased and also the phase of the system has to be modified to meet the stability requirements. It is possible to adjust the gain and phase margins simply by adding poles and zeros to the control system, but in this case, we add a PID position controller of Eq. (3.24) and two lead/lag filters, Eq. (3.41), to compensate the phase reduction. The next step is to loop shape the poles and zeros given by the desired controller structure.

The result of the loop shaping procedure is shown in Fig. 4.15. It can be clearly seen that the designed controller is robust, but it still violates some performance criteria. The transfer function of the controller is

$$C_{\text{controller}}(s)=\frac{1.0\cdot10^{4}s^{4}+7.17\cdot10^{6}s^{3}+1.34\cdot10^{9}s^{2}+2.29\cdot10^{10}s+7.45\cdot10^{10}}{s^{4}+7560s^{3}+1.45\cdot10^{7}s^{2}+8.38\cdot10^{8}s} \quad (4.18)$$

There is an option to use a more complex control algorithm in attempt to meet the performance criteria. However in practice, the criteria applied in the design are too demanding for the system, the loop delay of which is more than 500 µs and the parameter variation is so large; the situation is illustrated in Fig. 4.16, where the robust sensitivity and robustness of the system with the designed controllers using the parameter uncertainties given in Table 4.3 are depicted

for the loop delays of 500 µs, 850 µs, 1100 µs, and 1600 µs, respectively, and compared to robust bounds W_1 and W_2, which are used as performance requirements for controllers. When the loop delay is 500 µs or less, it is possible to meet the performance requirements for the robust sensitivity W_2. If the loop delay is more than 500 µs, only the robust margin W_1 can be fulfilled. This guarantees that the minimum phase margin (34º) and the gain margin (4 dB) requirements are met for all loop delays.

If the values of the poles of the controller are increased, there will be a larger phase margin and the gain of the controller can be increased. However, this will result in a fact that even though the low-frequency performance is increased, also the high-frequency gain will increase, which may lead to some problems because of the limited resolution of the feedback information. The reference tracking requirement, W_6, can be assumed to be impossible to meet in practice, as can be seen in Fig. 4.17. The anti-resonance of the system substantially decreases the magnitude of the system, which is not taken into account in the reference tracking performance criteria. This is not a dramatic defect, because we know that there are no reference signals that would include such high frequencies, if the motion profile is designed properly.

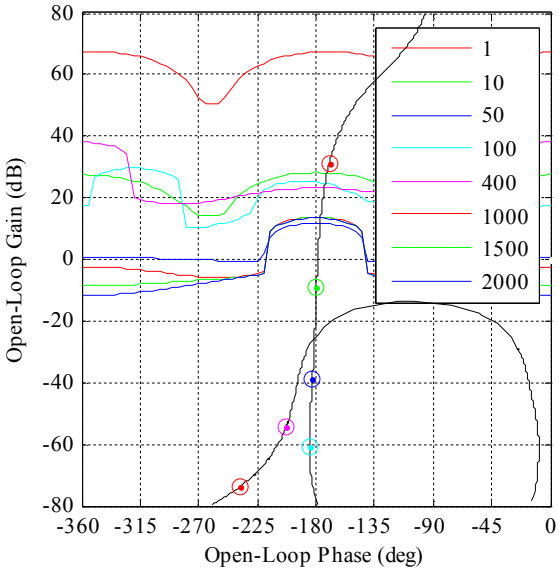

Fig. 4.14. Nichols chart of the open-loop transfer function of the nominal system when the controller $C(s) = 1$.

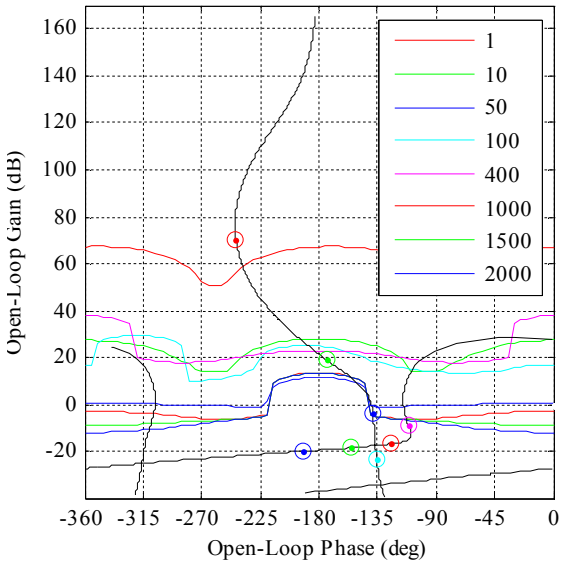

Fig. 4.15. Nichols chart of the open-loop transfer function of the nominal system with the designed controller.

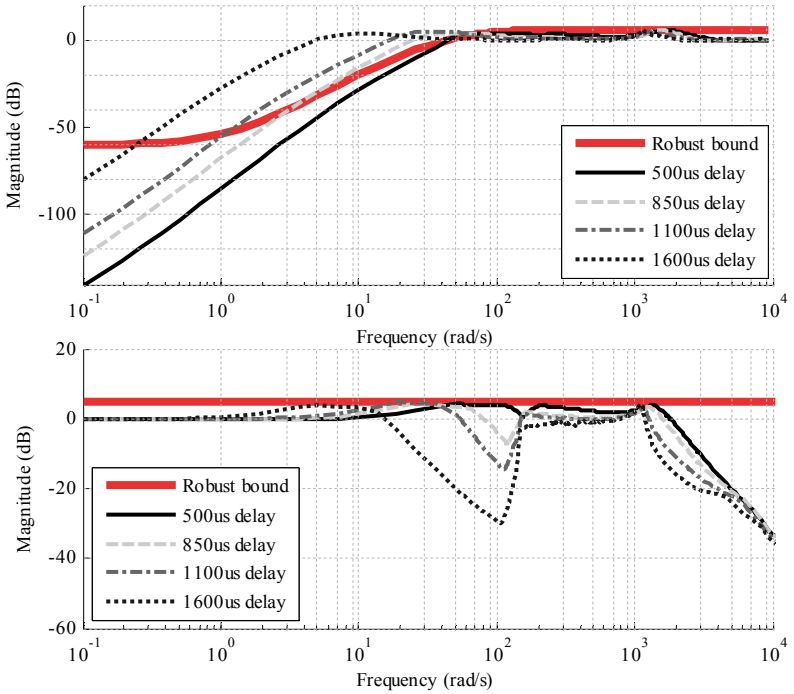

Fig. 4.16. Upper figure presents the robust margins for sensitivity, W_2, and lower figure shows the robust margin, W_1. The minimum phase and gain margin requirements (W_1) are achieved, but the sensitivity requirement (W_2) can be reached only at the loop delay of 500 µs.

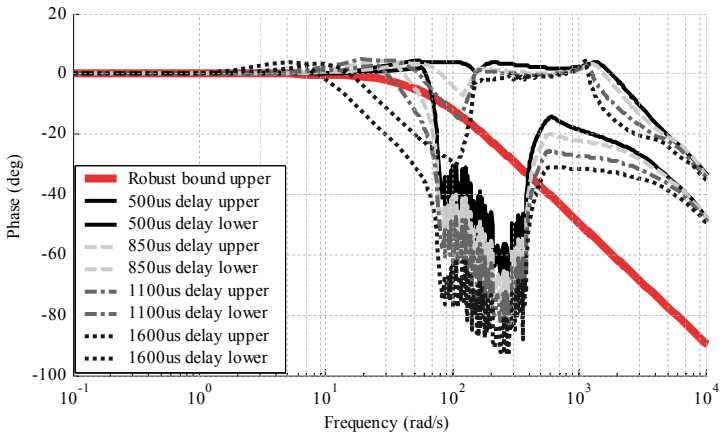

Fig. 4.17. Robust tracking capabilities of the closed-loop transfer function of the system with different loop delays compared to the robust tracking requirement W_6.

The designed controllers meet the stability requirements, but if the loop delay is over 500 µs, the performance criteria will not be met. The loop delay considerably reduces the performance of the system. The reason for this can easily be seen in Fig. 4.18, where the magnitudes and phases of the controllers are shown. The magnitude difference between the controller designed for loop delays of 500 µs and 1600 µs is about 60 dB at low frequencies. The difference decreases at frequencies above 2 rad/s, but it is still very high at the normal operating frequencies.

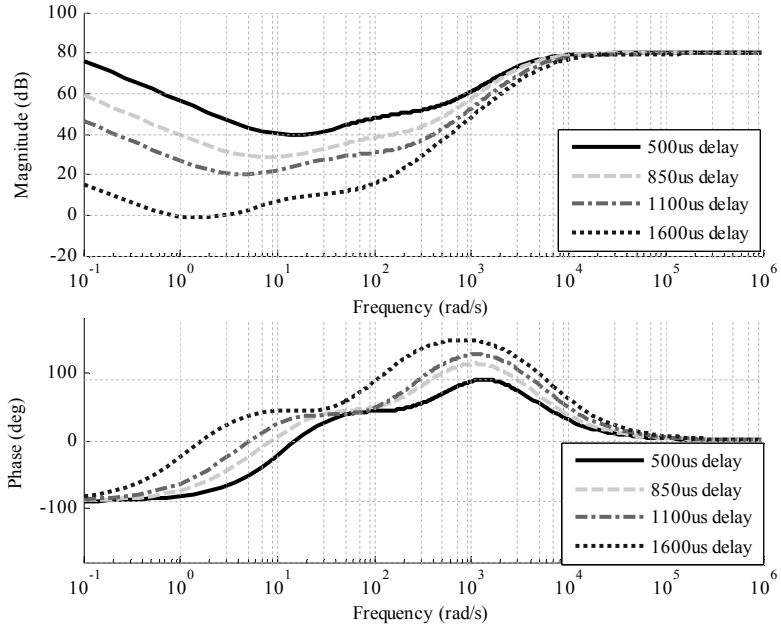

Fig. 4.18. Magnitudes and phases of robust controllers for the flexible system.

The transfer functions of the designed controllers are combinations of a PID position controller and two lead/lag filters; for practical implementation, the transfer functions should be divided into one PID controller and two lead/lag filters. Table 4.4 lists the controller parameters.

Table 4.4. Controller parameters

Delay [μs]	K_P [Nm/rad]	T_i [s]	T_d [s]	N	Lead/lag pole [rad/s]	Lead/lag zero [rad/s]
500	94	0.145	0.035	112	97.75 3493	593.4 628.8
850	26.8	0.302	0.054	188	59.83 4000	332.5 363
1100	19.5	0.507	0.100	476	30.2 4972	269 286
1600	0.85	0.687	0.303	1825	12.81 6081	97.2 128.8

Figure 4.18 shows that the designed controllers are quite moderate. The main reason for this is that a large parameter uncertainty was included in the model at the controller design phase, see Table 4.2. The performance of the controller may be increased, if additional attention is paid to minimize the parameter uncertainty. Figure 4.19 describes the effect of the uncertainty of the single parameter keeping other parameters constant. The spring constant K_{eff} is varied [4, 6, 10, 30, 50, 75] $\cdot 10^5$ N/m, the damping constant b_s [15, 25, 35, 45, 55, 65] Ns/m, the inertia of the motor J_m [0.002, 0.004, 0.006, 0.008, 0.01, 0.015] kgm^2, the mass of the load m_L [35, 40, 45, 50, 65, 75] kg, and the loop delay t_d [300, 500, 1100, 1600, 2000, 4000] μs. The controller is designed separately for each case. Figure 4.19a shows the closed-loop bandwidth (-3 dB) for each model. It is interesting to see that there is an optimum value for the spring constant. Increasing the loop time delay and the mass of the load decreases the bandwidth as was expected. However, increasing the inertia of the motor increases the closed-loop bandwidth, which is somewhat surprising and requires a more detailed analysis. Similar results can be seen in Fig 4.19b, where the bandwidth (-3 dB) of the sensitivity function is shown. Figure 4.19c shows the magnitude of the open-loop transfer function at the frequency of 0.1 rad/s. Even though the results show that the inertia of the motor should be increased to maximize the bandwidth of the system, a drawback of this would be that the system would need more torque to accelerate from zero to the velocity of 4 m/s, as can be seen in Fig 4.19d.

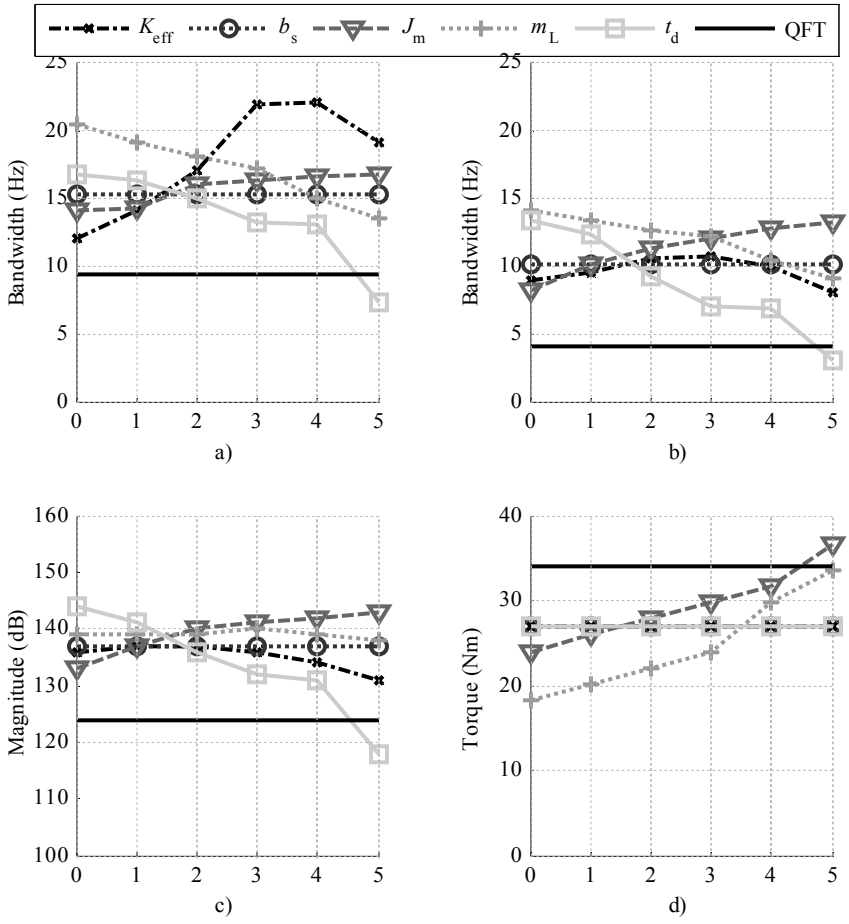

Fig. 4.19. a) Closed-loop bandwidth, b) bandwidth of the sensitivity function, c) open-loop magnitude at the frequency of 0.1 rad/s, and d) torque needed to accelerate the system from zero velocity to 4 m/s in the time of 0.209 s.

4.7.2 Reference tracking feedforward controller

The robust PID position controller designed in this work is quite moderate, and cannot thus provide accurate reference tracking. To increase the tracking capability, typically, some sort of a friction compensator and an acceleration feedforward controller are added to the control system. These feedforwards do not have any effect on the feedback sensitivity function; however, both the friction compensator and the acceleration feedforward controller decrease the position error. This thesis does not concentrate on the friction compensation methods, but only an acceleration feedforward controller is included in the study.

Figure 4.20 shows how the tracking capability changes when the acceleration feedforward controller Eq. (3.36) is included to the PID controller designed for the loop delay of 850 µs. The robust bound is the performance requirement given in Eq. (4.17), and the system with the designed controllers is compared to this robust bound. Figure 4.20 shows that the acceleration feedforward controller increases the magnitude of the closed-loop transfer function of the

system after the resonant frequency, thus, the robust performance requirement W_6 in Eq. (4.17) is not fulfilled. Figure 4.21 shows robust margins bound W_1 given in Eq. (4.15) and the robustness of the closed-loop transfer functions when the acceleration feedforward is used. We see in Fig. 4.21 that the acceleration feedforward controller increases the magnitude of the control after the lowest possible resonance frequency 100 rad/s, thus the gain and phase margins of the system is not achieved. This is caused by the fact that after the resonance frequency, the inertia that the control sees is only the motor inertia, which is less than the total inertia of the system that is used in the acceleration feedforward controller.

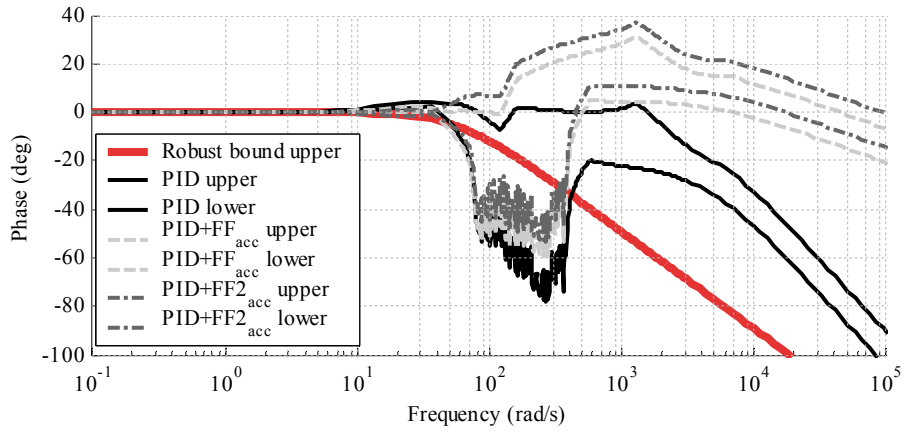

Fig. 4.20. When standard acceleration feedforward is used with the PID position controller, the robust tracking bound W_6 is not fulfilled. The standard acceleration feedforward increases the magnitude of the control after the mechanical resonance of the system. The total inertia used in FF_{acc} = 0.0158 and $FF2_{acc}$ = 0.0320.

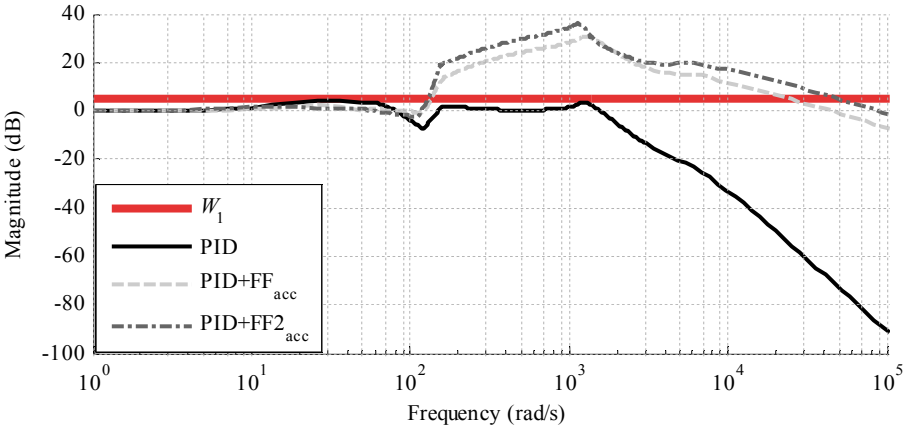

Fig. 4.21. When a robust PID position controller is used and a standard acceleration feedforward is used with this controller, the robust gain and phase margins given in the robust performance specification W_1, is not achieved. The total inertia used in FF_{acc} = 0.0158 and $FF2_{acc}$ = 0.0320.

To prevent this amplification, the acceleration feedforward controller should be designed to damp the reference signals after the resonance frequency. We could add low-pass filters of Eqs. (3.9) and (3.12), but the drawback would be the phase lag that these filters produce. The phase

lag increases the position error. Alternatively, we could add a more sophisticated feedforward controller than the acceleration controller, but it might bring some additional problems at least to the system commissioning. Because the input to the acceleration feedforward controller is the position reference or the acceleration reference depending on the structure of the function generation, the easiest way to prevent the amplification of the signal is to limit the bandwidth of the acceleration reference, shown in Section 3.1.

4.8 QFT-based robust cascaded controller design

In this section, a decentralized cascaded position controller structure is designed for a linear tooth belt drive. The actual control structure is described in Fig. 4.22a, where the motor actual position is measured and the velocity is calculated based on the position measurement. Figure 4.22b shows how the system is modeled for the QFT design procedure. It is assumed that the system consists of two separate processes $P_1(s)$ and $P_2(s)$, and the processes are closed separately with feedback controllers. In our case, the transfer function of $P_1(s)$ is from the torque reference to the motor velocity

$$P_1(s) = \frac{\omega_{\text{act}}}{T_{\text{ref}}} = \frac{1}{\tau_e s + 1} \frac{1}{\left(J_m + m_L R^2\right) s + b_1} \frac{m_L s^2 + b_s s + K_{\text{eff}}}{\frac{J_m \cdot m_L}{J_m + m_L R^2} s^2 + b_s s + K_{\text{eff}}} \quad , \tag{4.19}$$

where τ_e is the time constant of the torque controller, J_m is the inertia moment of the motor plus additional inertias that are rigidly connected to the motor shaft, m_L is the mass of the load, R is the radius of pulleys, K_{eff} is the equivalent position-dependent elasticity coefficient of the belt, ω_m *is* the angular velocity of the motor, b_s is the damping constant of the belt, b_1 is the viscous friction of the system, and T_{ref} is the torque reference to the system. The nominal values and the variation of the system parameters are given in Table 4.3. The transfer function of $P_2(s)$ is a pure integrator (from the motor velocity to the motor position)

$$P_2(s) = \frac{1}{s} \quad . \tag{4.20}$$

The total loop delay consists of both the transmitting delay $\tau_{TM}(s)$ and the feedback delay $\tau_{FB}(s)$. In Fig 4.22 it is assumed that the pre-filter is only in the outer-loop, but it is also possible to add a pre-filter to the inner-loop controller structure.

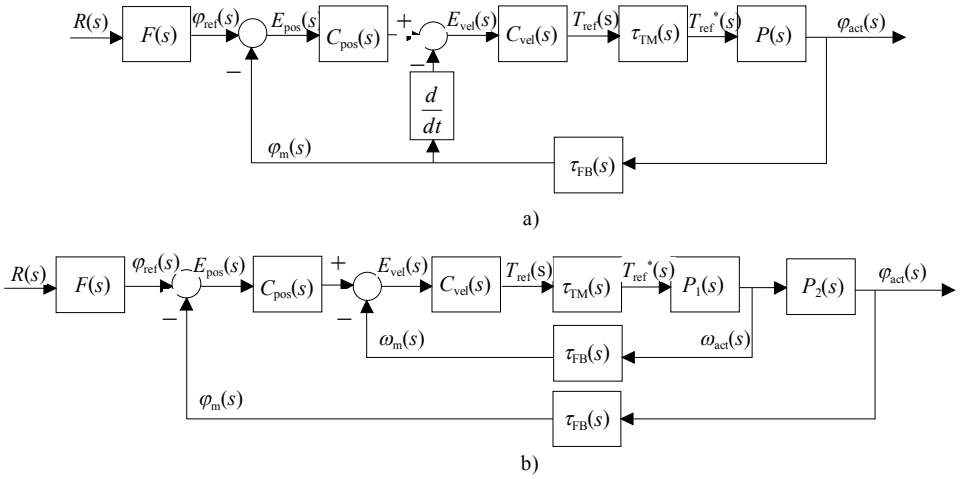

Fig. 4.22. Cascaded control structure: a) actual process and b) QFT-modeled process.

A cascade structure is preferred because it provides more design freedom compared with the PID position controller design. The velocity of the motor can be controlled independently with a separate controller when the cascaded structure is used. If needed, the feedback value for the position controller can be obtained from a different encoder than the feedback value for the velocity controller. This provides more design options. In this study, however, only the motor position is used as a feedback signal for the position controller. When a cascaded structure is designed with the QFT method, there are two different approaches available: either an inner-outer design or an outer-inner design, which means that either the inner-loop controller is designed at first and then the outer-loop controller, or vice versa. According to Wu (2000), the inner-loop is introduced mainly to reduce the bandwidth of the outer loop. If the outer controller is designed first, the dynamics of the inner controller is not included in the design, and the outer controller is not designed against the actual inner loop. This may lead to several iterations in order to design controllers that would meet the desired performance specifications. The drawback of the inner-outer method is that when the inner-loop is designed first, it has an effect on the outer-loop performance, which cannot be predicted in advance.

In this study, the inner-outer loop design is used, and the velocity controller $C_{vel}(s)$ is a PID type of Eq. (3.24) in series with a lead/lag filter of Eq. (3.41), which is added to compensate the phase shift of the loop delay. The position controller $C_{pos}(s)$ is a P controller plus a lead/lag filter. The transmitting and feedback delay is modeled using a Pade approximation and the total loop delay is 850 μs. With these assumptions, we have a similar starting point to study the performance of the cascaded design as was presented in Section 4.7 with the PID position controller design. So, the performance and differences of these control structures can be easily compared.

4.8.1 Feedback controller

First we close the inner-loop, which consists of the process $P_1(s)$, the transmitting media $\tau_{TM}(s)$ and $\tau_{FB}(s)$, and the velocity controller $C_{vel}(s)$. The template is generated using the same knowledge as in Section 4.7 where a PID position controller was designed. The template of the system is shown in Fig 4.23.

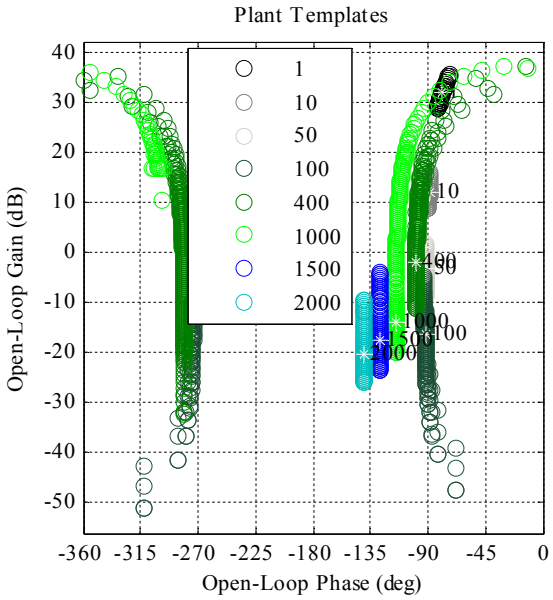

Fig. 4.23. Template of the system.

The template of the system behaves similarly as in Fig 4.8, but the magnitudes and the phases are different. Next, the robust margins and performance bounds are selected. A common rule of thumb is that the bandwidth of the inner-loop should be about three times larger than the outer-loop (Younkin 2003). Consequently, we have to give small robust margins to the inner-loop controller, which ensures a higher gain and a larger sensitivity bandwidth than when the larger robust margins are used. To test this assumption, we designed robust velocity controllers using robust margins $M_T = 1.7$, $M_T = 1.25$, and $M_T = 1.05$. These margins give us 4.0 dB and 34º, 5.1 dB and 47º, and 5.8 dB and 57º magnitude and phase margins, respectively. The sensitivity requirement is the same as with the PID position controller

$$\left|\frac{1}{1+L(j\omega)}\right| < W_2(j\omega) = \left|\frac{\left(\frac{j\omega}{M_S^{1/n}}+\omega_b\right)^n}{\left(j\omega+\omega_b\cdot A^{1/n}\right)^n}\right|, \tag{4.21}$$

where M_S gives the robust sensitivity margin, ω_b is the desired bandwidth, and A is the attenuation at the zero frequency. In this study $n = 2$, which gives a 40 dB/decade roll-off rate at low frequencies. The structure of the PID controller ensures a 40 dB/decade roll-off rate at low frequencies. We use $A = 0.0001$. The frequency of ω_b is chosen to be 10 Hz, which corresponds to half of the minimum resonance frequency and the robust sensitivity margin $M_S = 2$. Figure 4.24 shows the robust boundaries when applying the robust sensitivity requirements given above and when $M_T = 1.05$. We see in Fig. 4.24 that the parameter uncertainties give large templates for the frequencies between 400 rad/s and 1000 rad/s.

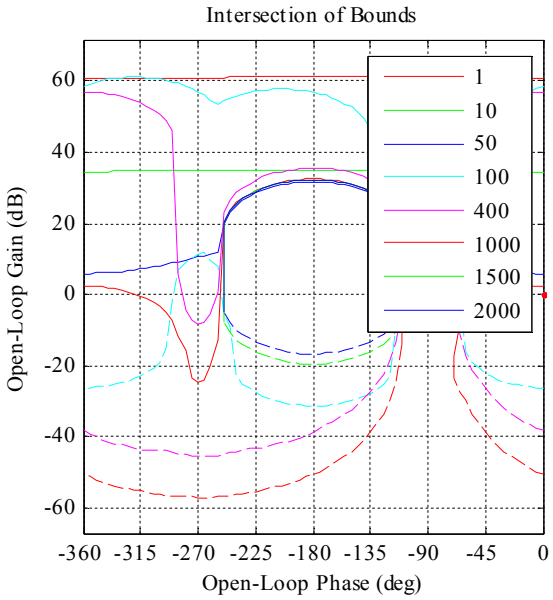

Fig. 4.24. Robust bounds for the velocity controller.

QFT loop shaping of the velocity controller

When the robust performance boundaries are calculated, the next step is to "loop shape" the controller. We used a pre-determined PID velocity controller of Eq. (3.24) and a lead/lag filter structure of Eq. (3.41) as a velocity controller. The open-loop Nichols envelope of the "loop-shaped" velocity controller with the robust margin $M_T = 1.05$ is shown in Fig 4.25. The performance of the PID velocity controller plus the lead/lag filter do not meet the sensitivity performance requirements given in Eq. (4.21), if the $M_T < 1.7$, which can be seen in Fig. 4.26, where the closed-loop robust sensitivity margins of the system with designed controllers are shown. Larger robust phase and gain margins (W_1) decrease the bandwidth of the sensitivity function S; however, the bandwidth of the complementary sensitivity function T is not decreased, as can be seen in Fig. 4.27, the robust tracking capability of the designed velocity controllers are compared to the robust tracking requirement W_6.

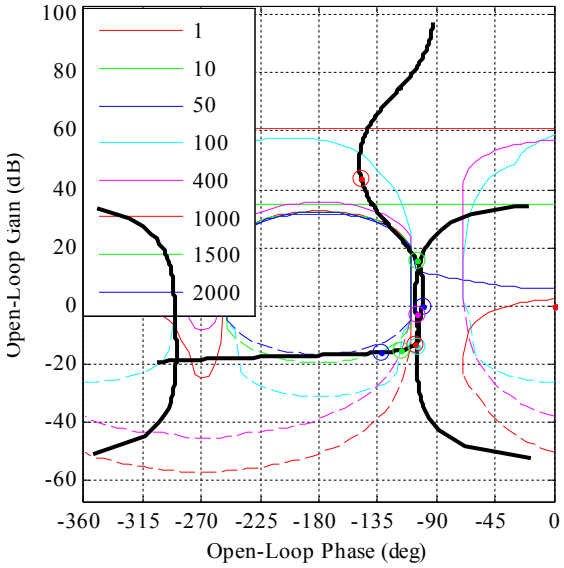

Fig. 4.25. QFT loop-shaped velocity controller, $M_T = 1.05$.

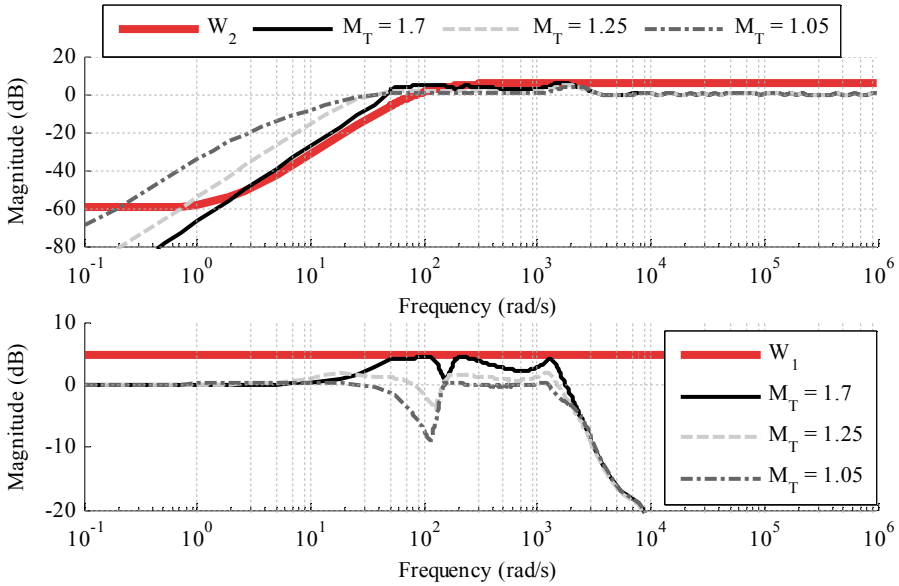

Fig 4.26. Upper figure describes the robust sensitivities of the designed controllers and are compared to the performance requirement of the system W_2. The bandwidth of the robust sensitivity requirement is 10Hz. Lower figure shows the robust phase and gain margins of the system compared to the performance specification of $W_1 = M_T = 1.7$.

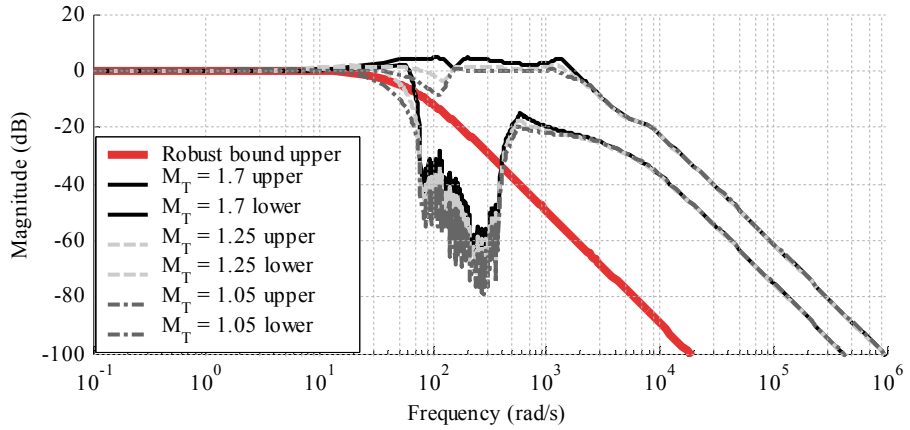

Fig. 4.27. Robust tracking capability of the designed velocity controllers compared to the robust tracking requirement W_6.

The robust margin M_T has a significant effect on the magnification of the controller. Figure 4.28 shows that when $M_T = 1.7$, the controller amplifies the frequency of 0.1 rad/s at 60 dB, but if M_T is 1.05, the magnification is only 30 dB. Also the phases of the controller behave differently. The parameters of the PID velocity controllers are gathered in Table 4.5.

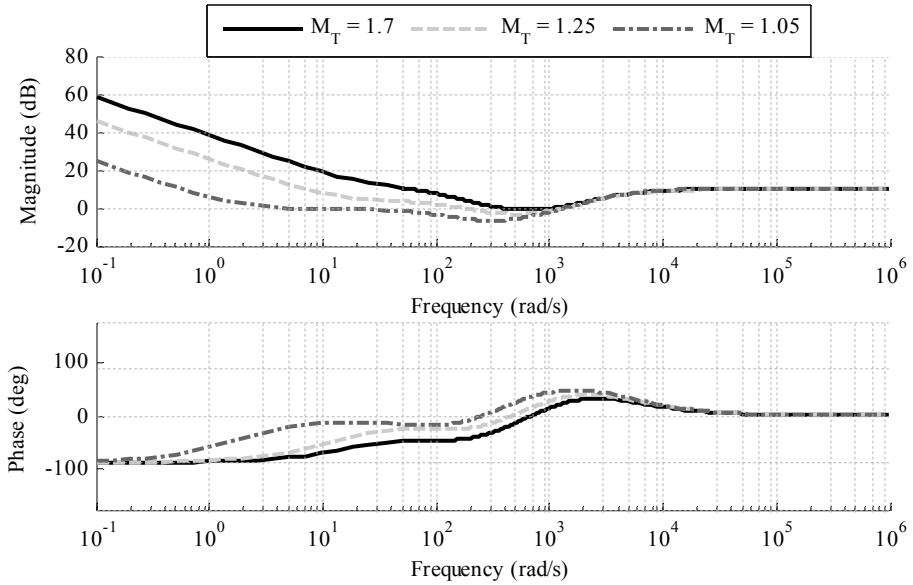

Fig. 4.28. Magnitudes and phases of the designed velocity controllers.

Table 4.5. Parameters of the PID velocity controllers.

M_T	K_V [Nms/rad]	T_i [s]	T_d [s]	N	Lead/lag pole [rad/s]	Lead/lag zero [rad/s]
1.7	3.72	0.046	0.0014	6.39	81.0	717.5
1.25	1.58	0.083	0.0020	9.24	120.8	642.2
1.05	0.95	0.573	0.0035	15.15	82.9	405.3

After the inner-loop controller is closed and the velocity controller is designed, the outer-loop will be closed. First, the template of the system is generated. Figure 4.29 shows the template of the outer-loop when the robust margin of the velocity controller is M_T = 1.05. The velocity controller $C_{vel}(s)$ tries to compensate the uncertainties of the process P_1. As we can see, the controller is effective at low frequencies, but after the frequency of 50 rad/s the controller cannot compensate the uncertainties.

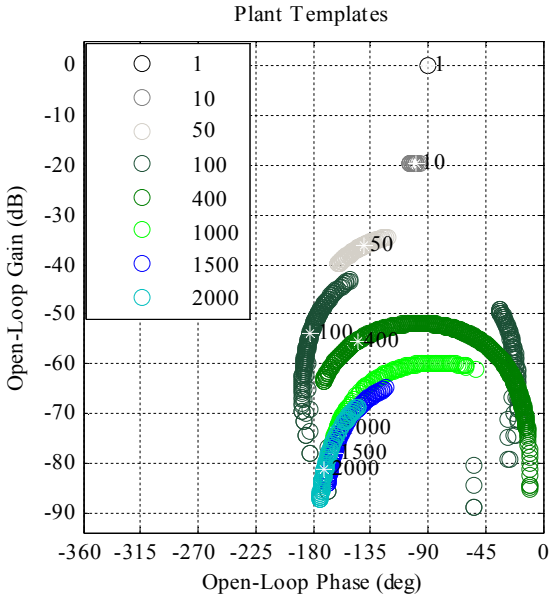

Fig. 4.29. Template of the cascaded position controller, when the velocity controller was designed using the robust phase and gain margins of $W_1 = M_T = 1.05$.

Now the robust margins for the position controller have to be determined. The robust margin is the same as when the PID position controller was designed. Hence, the robust margin for the complementary sensitivity functions is

$$\left|\frac{L(j\omega)}{1+L(j\omega)}\right| < W_1 = M_T = 1.7\,. \tag{4.22}$$

And for the sensitivity function

$$\left|\frac{1}{1+L(j\omega)}\right| < W_2(j\omega) = \left|\frac{\left(\frac{j\omega}{M_s^{1/n}}+\omega_b\right)^n}{\left(j\omega+\omega_b\cdot A^{1/n}\right)^n}\right|, \tag{4.23}$$

where $M_s = 2$, $\omega_b = 6$ Hz, and $A = 0.0001$. The order $n = 2$, which gives a 40 dB/decade roll-off rate at low frequencies. The structure of the P position controller ensures that only 20 dB/ can be achieved. Figure 4.30 shows the robust bounds for the cascaded position controller, and Fig. 4.31 shows the designed P position controller with a lead/lag filter when the velocity controller was designed with the margins $M_T = 1.05$.

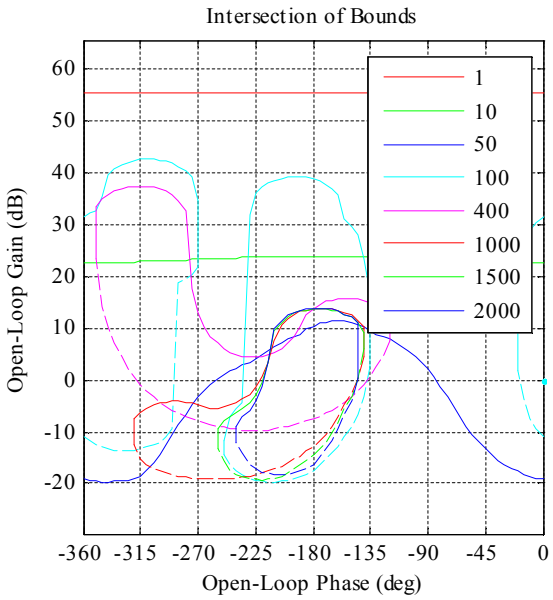

Fig. 4.30. Robust bounds for the cascaded position controller.

We see in Fig. 4.31 that the robust sensitivity functions of the system with designed controllers do not meet the robust sensitivity requirements at low frequencies, because the P position controller could only achieve the 20 dB/deg roll-off rates. The roll off-rate 40 dB/deg could be achieved if an integrator were added. Figure 4.32 shows clearly that the best sensitivity reduction will be obtained when the velocity controller is designed with $M_T = 1.05$. The robust reference tracking capability is shown in Fig. 4.33, and the magnitudes and phases of the designed controllers are shown in Fig. 4.34. We see, that the highest gain of the position controller can be achieved when the M_T of the velocity controller were 1.05. This means that the smallest position error for the reference is also achieved when the velocity controller is designed with $M_T = 1.05$

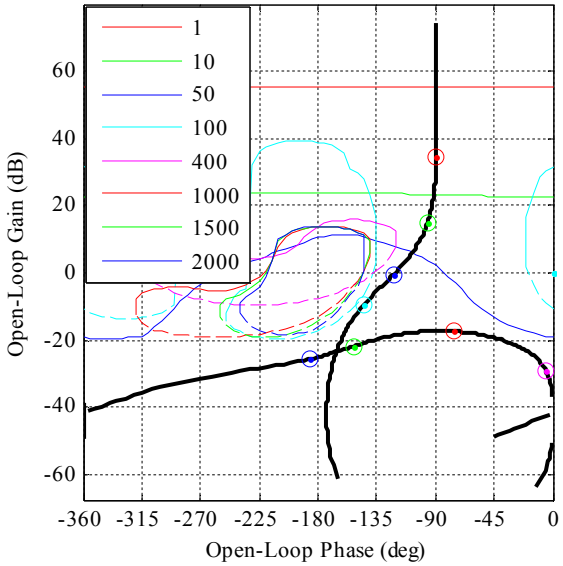

Fig. 4.31. Designed position controller, when the velocity controller was designed using the robust phase and gain margins of $W_1 = M_T = 1.05$.

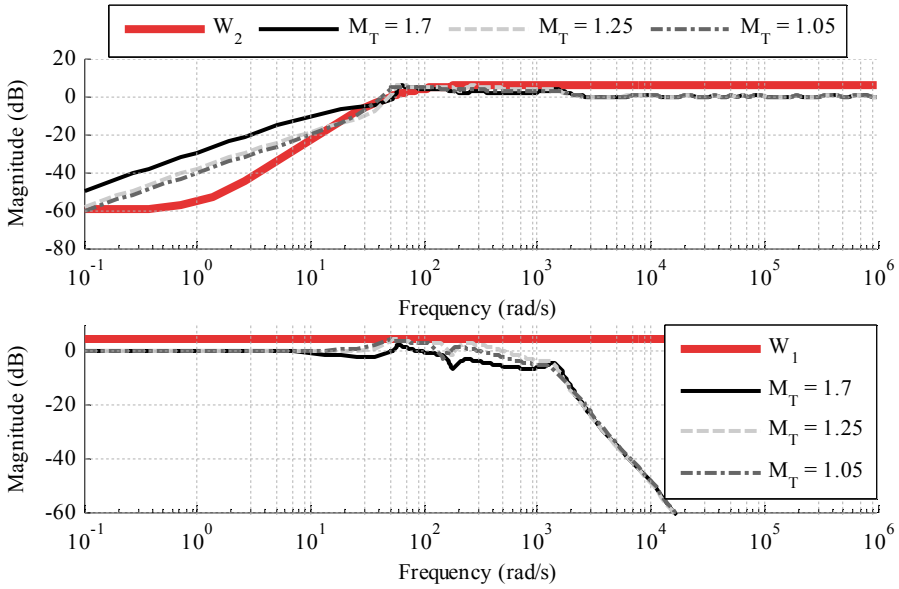

Fig. 4.32. Upper figure describes the robust sensitivity of the system, when the velocity controller is designed using the robust phase and gain margins of $M_T = 1.7$, $M_T = 1.25$, and $M_T = 1.05$, respectively, and the cascaded position controller is designed using the robust phase and gain margins of $W_1 = 1.7$. Lower figure shows the robust gain and phase margins of the system using same robust performance requirements.

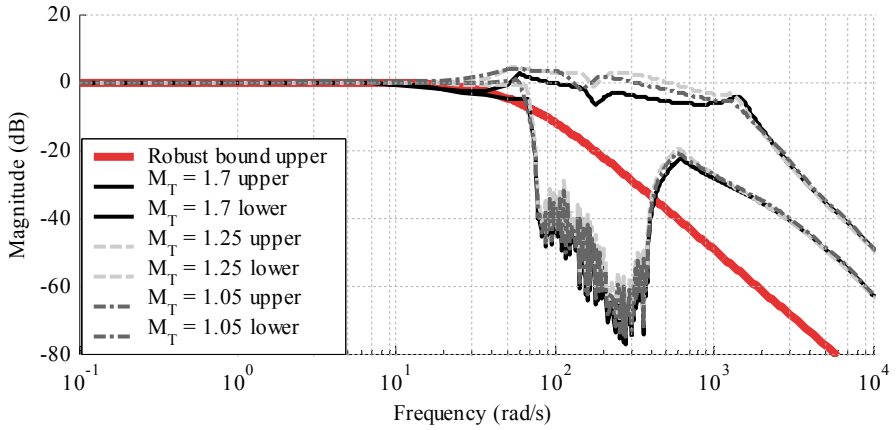

Fig. 4.33. Robust tracking capability of the cascaded position controller when the velocity controller is designed using the robust phase and gain margins of M_T = 1.7, M_T = 1.25, and M_T = 1.05, respectively, and the cascaded position controller is designed using the robust phase and gain margins of W_1 = 1.7. The robust bound is the robust tracking requirement given in W_6.

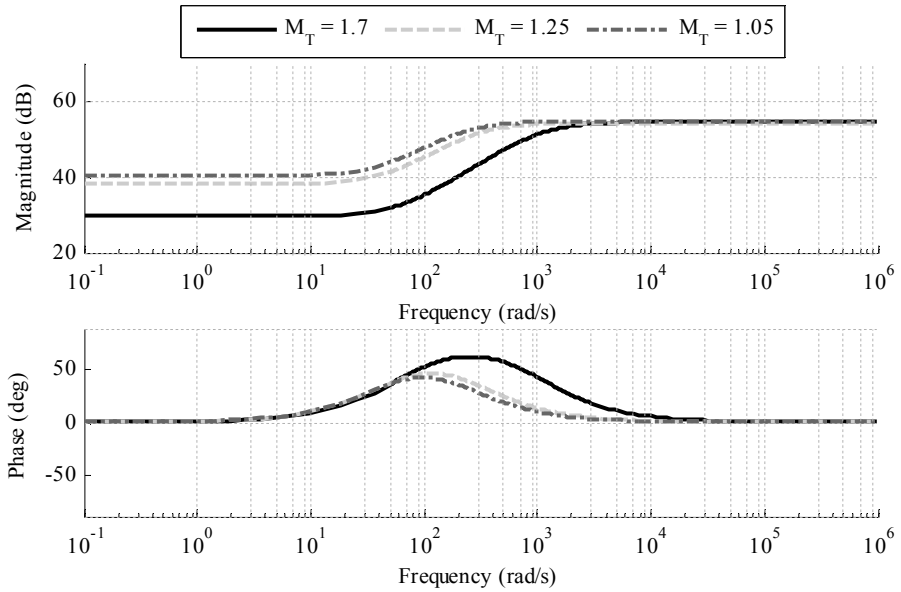

Fig. 4.34. Magnitudes and phases of robust cascaded position controllers using different robust margins in the design of the velocity controller.

Table 4.6 lists the parameters of the position controller. As can be seen, the gain of the position controller can be increased significantly if the velocity controller is designed with larger robust margins. Also the importance of the lead/lag filter of the position controller decreases if the velocity controller is designed with larger robust margins.

Table 4.6. Parameters of the position controller.

M_T	K_P [1/s]	Lead/lag pole [rad/s]	Lead/lag zero [rad/s]
1.7	30	1084	61.85
1.25	80	296.3	46.55
1.05	102	225.6	42.75

As was shown in Fig 4.19, the performance of the PID-position-controlled process may be improved, if additional attention is paid to minimize the parameter uncertainty. Figure 4.35 illustrates the effect of the uncertainty of a single parameter keeping other parameters constant, when the control structure is a cascaded P position controller with a lead or lag filter, and the velocity controller is a PID controller with a lead or lag filter. The parameters are varied so, that the spring constant K_{eff} is [4, 6, 10, 30, 50, 75] $\cdot 10^5$ N/m, the damping constant b_s [15, 25, 35, 45, 55, 65] Ns/m, the inertia of the motor J_m [0.002, 0.004, 0.006, 0.008, 0.01, 0.015] kgm^2, the mass of the load m_L [35, 40, 45, 50, 65, 75] kg, and the loop delay t_d [300, 500, 1100, 1600, 2000, 4000] µs. The controller is designed separately for each case. Figure 4.35a shows the closed-loop bandwidth (-3 dB) for each model.

Unlike in the case of the PID position control structure, in a cascaded structure, an optimal value cannot be found for the spring constant. Increasing the loop time delay and the mass of the load decreases the bandwidth as was expected. However, increasing the inertia of the motor increases the closed-loop bandwidth, but not as much as in the case of the PID position controller; see Fig. 4.19. Similar results can be seen in Fig 4.35b, where the bandwidth (-3 dB) of the sensitivity function is shown. Figure 4.35c shows the magnitude of the open-loop transfer function at the frequency of 0.1 rad/s and Fig. 4.35d shows the torque that is needed to accelerate the system from zero velocity to 4 m/s in the time of 0.209 s.

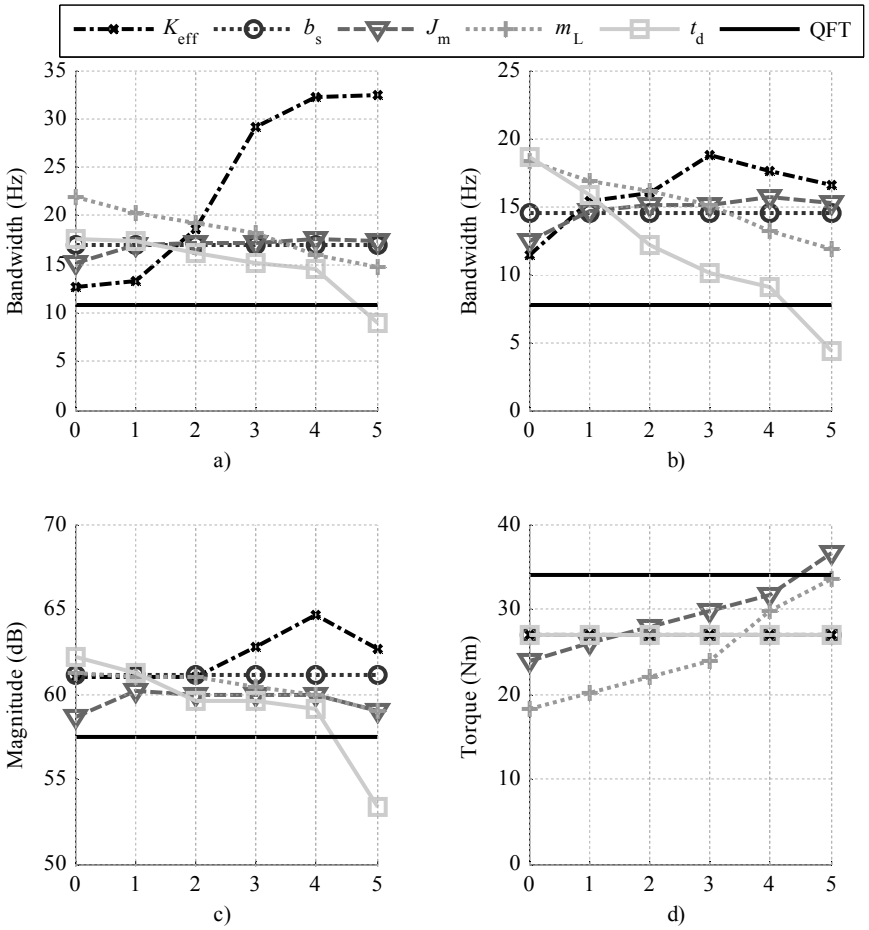

Fig. 4.35. a) Closed-loop bandwidth, b) bandwidth of the sensitivity function, c) open-loop magnitude at the frequency of 0.1 rad/s, and d) torque needed to accelerate the system from zero velocity to 4 m/s in the time of 0.209 s.

4.8.2 Reference tracking feedforward controller

The robust cascaded P position and PID velocity controller designed in this work is quite moderate, and cannot thus provide accurate reference tracking compared with the PID position controller. To increase the tracking capability, typically, a velocity feedforward controller $FF_{vel}(s)$ of Eq. (3.37) is added to the position control. The velocity feedforward does not increase the feedback sensitivity functions; however, the velocity feedforward controller significantly decreases the position error. Of course, an acceleration feedforward controller could also be used in the velocity loop, but it has the same drawbacks as the ones shown in Section 4.7.2 where an acceleration feedforward controller is designed in the PID position control loop. Figures 4.36 and 4.37 show that the velocity feedforward controller amplifies the frequencies from 20 rad/s to above (P+FF_{vel}). This amplification may cause some overshooting and, thus, may produce some problems in industrial applications. The high frequency overshooting can be reduced if the transmitting time delay is compensated from the velocity feedforward signal, (P+$FF2_{vel}$).

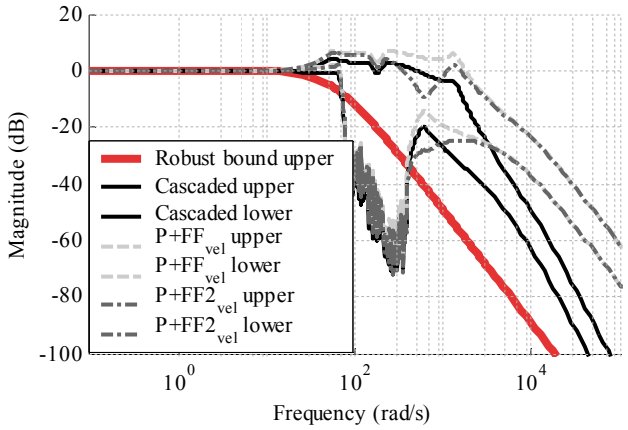

Fig. 4.36. Robust tracking performance, when a robust cascaded structure is used and a standard velocity feedforward is used with this structure. The robust bound is performance specification given in W_6.

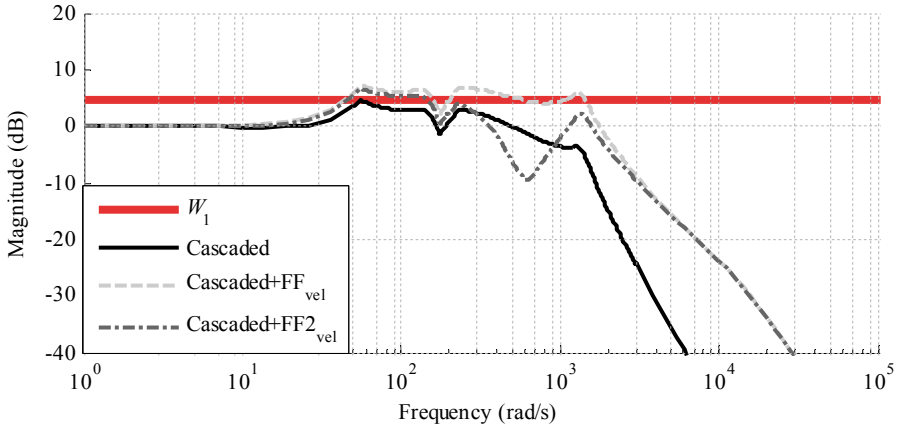

Fig. 4.37. Robustness of the closed-loop system when a robust cascaded structure is used and a standard velocity feedforward is used with this structure. W_1 is the robust performance requirement for the gain and phase margins.

4.9 PID position controller versus the cascaded controller structure, conclusions

Section 3.2 showed how to design a robust PID position controller and a robust cascaded P position controller with a PID velocity controller. In both control structures, two lead/lag filters are used to compensate the phase reduction produced by the loop delay and also to compensate the phase shifts of the mechanical resonances and anti-resonances. As was previously stated, both structures are very common in industry, and both have some advantages and drawbacks. This section illustrates the differences between the controller structures and sums up some important knowledge of the tuning procedure of these structures.

The main difference between the controller structures is that the PID position controller is capable of integrating the constant velocity error off during motion, while the cascaded structure cannot integrate the error off. Of course this is not the issue, if the position controller of the cascaded structure is a PI controller. Both the structures ensure zero end point position error. The PID position controller has greater overshoot than the cascaded controller, which is mainly caused by the integrator of the PID position controller, and this overshoot can be reduced if the integrator is reset every time when the position error changes direction. Some industrial applications apply this method.

Figure 4.38 compares the sensitivity functions S (upper figure) and robust margins (lower figure) of the PID position controller and the cascaded structure using the nominal model of the process, an 850 µs loop delay, and the velocity controller of the cascaded structure, which is loop shaped using robust the margin $M_T = 1.25$. We can see that the PID position controller structure gives a better performance at low frequencies. This means that the PID position controller gives better results when there are low frequency references or disturbances. If the cascaded structure is used, the bandwidth of the sensitivity function is greater than the bandwidth of the PID position controller. This can be seen also in Fig. 4.39, where the tracking capability of the controller structures is shown.

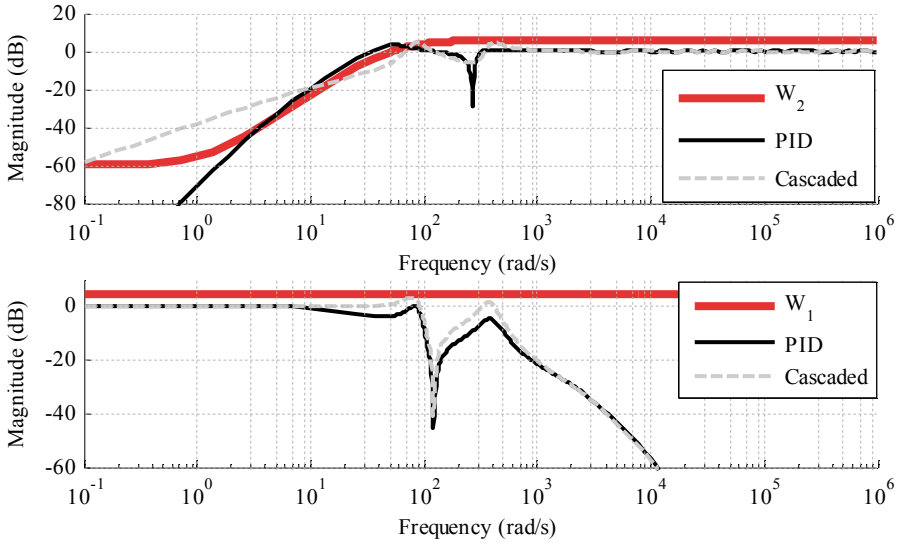

Fig. 4.38. Sensitivity functions and robust margins when using the PID position controller and the cascaded structure. W_1 is the robust margin requirement of the complementary sensitivity function and W_2 is the robust margin requirement of the sensitivity function.

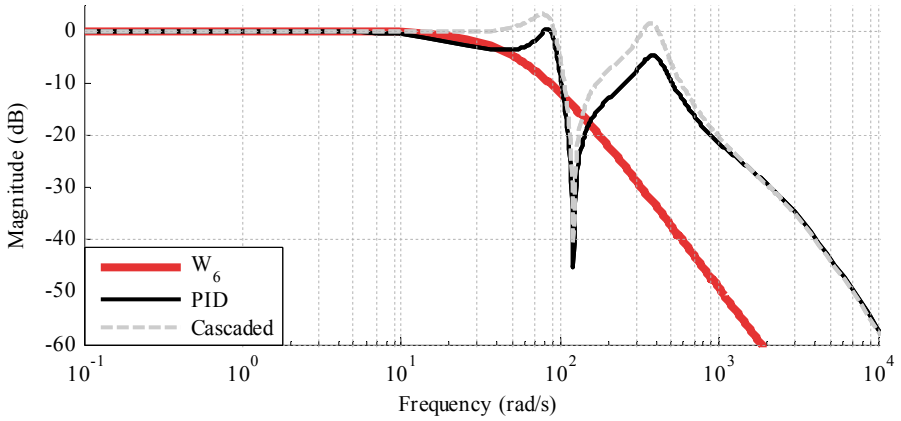

Fig. 4.39. Tracking capability when using the PID position controller and the cascaded structure. W_6 is the robust performance requirement.

When lead/lag filters are used to compensate the phase shifts, there will be some problems, which has to be taken into account. The first one is that the lead filter increases the magnitude (a zero increases the phase by 90 deg/decade and the magnitude by 20 dB/decade, and a pole decreases the phase by 90 deg/decade and the magnitude by 20 dB/decade). This means that the difference between placements of the zeros and poles cannot be too large or the high frequencies are amplified too much. When a cascaded structure is used, the controller designer must choose where the lead/lag filters are used; in a position loop, in a velocity loop, or in both loops as in this thesis. Each of these alternatives needs a high-frequency limit of its own.

Because accurate reference tracking has to be achieved in motion control applications, velocity and acceleration feedforwards have to be used. The feedback controller cannot provide good enough tracking performance. When the cascaded structure is used, it is easy to include a velocity feedforward in the position loop as was shown in Section 3.2.4. The velocity feedforwards significantly increase the reference tracking performance. If a PID position controller is used, the same kind of feedforward cannot be used because of the lack of the velocity controller. Figures 4.40 and 4.41 show a case where the velocity feedforward is added to the cascaded structure and the structure is compared with the PID position structure. In both structures there can be an acceleration compensation, which decreases the acceleration error. The drawbacks of the acceleration compensation are discussed in Sections 4.7.2 and 4.8.2.

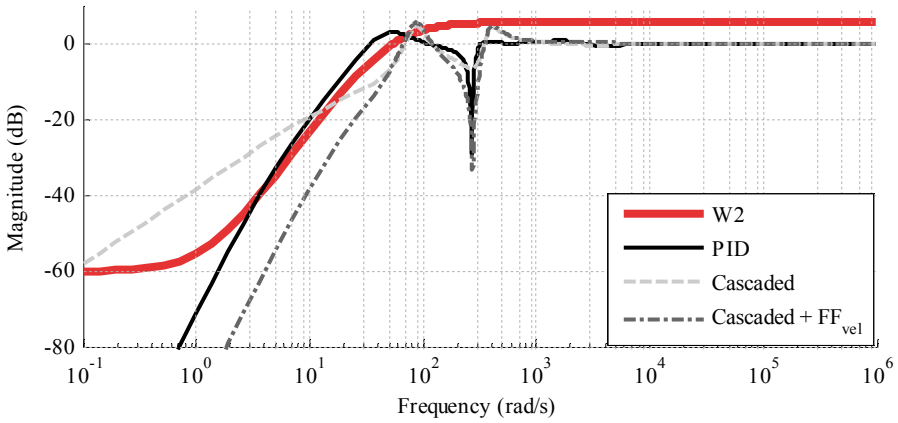

Fig. 4.40. Sensitivity from the reference to the error of the position controller between the PID position controller, the cascaded structure, and the cascaded structure with the velocity feedforward. W_2 is the sensitivity requirement for the system.

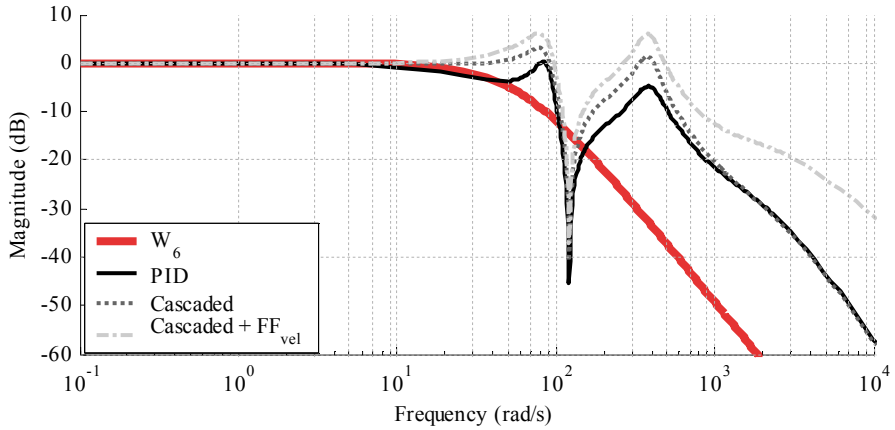

Fig. 4.41. Tracking capability between the PID position controller, the cascaded controller, and the cascaded controller with velocity feedforward. W_6 is the robust tracking requirement for the system.

Figure 4.42 shows that if the velocity feedforward is used, it will amplify some frequencies too much and cause overshooting. Adding acceleration feedforwards to the PID position controller and the cascaded structure with a velocity feedforward, we can see in Fig. 4.42 that there is too large amplification at the resonance frequency, and the advantage of the acceleration feedforward seems to be quite small. If the acceleration feedforward is used, the reference must be designed to be smooth and band limited.

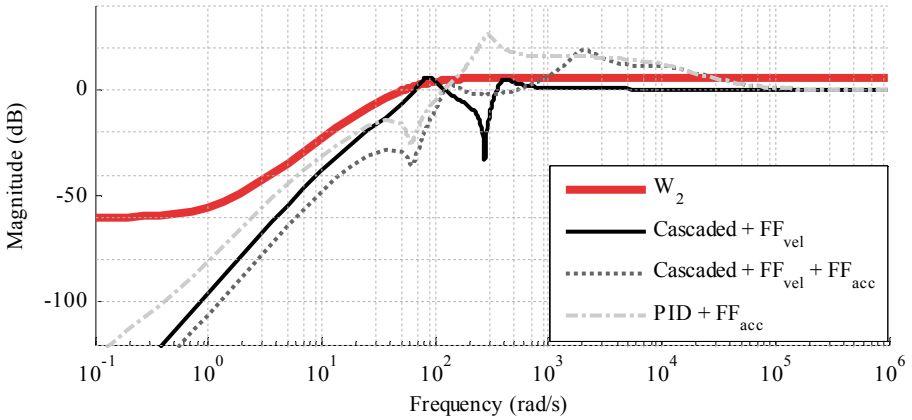

Fig. 4.42. Sensitivity from the reference to the error of the position controller when the simplest feedforwards are used with PID position controller and the cascaded structure. W_2 is the robust performance requirement for the sensitivity of the system.

5 EXPERIMENTAL RESULTS

The designed control structures were tested in the laboratory using the test setup described in Section 2.2. The movement and performance of the *x*-axis were studied. Both the motor angle and linear movement of the *x*-axis cart were measured with encoders; however, the sampling time of the linear band encoder was too low (1.8 ms) to be used in the performance analysis. The sampling times of the linear band encoder were reduced by the *K*-bus that connects the encoder modules to the embedded PC. It should also be mentioned that the measurement of the motor angle was delayed by the 410 µs because of the delay of the feedback signal.

Even though the maximum length of the movement of the *x*-axis was 1600 mm, the movement was reduced to 900 mm because of the safety margins of the movement. We used limit switches to activate the deceleration, if the cart was too close to the end of the tooth belt guide. The deceleration needs a 350 mm distance to ensure zero velocity before the end of the guide at the velocity of 3.5 m/s.

First, we tested how the designed feedback controllers perform from the fastest position ramp that can be used safely. The fastest position ramp means that the cart is accelerated and decelerated using the largest force that the belt can handle safely, and the constant velocity time is minimized. The acceleration and deceleration were 15 m/s^2 (Fig 2.10, line-E), and the jerk of the movement was set to 100 m/s^3 to provide a smooth profile (Fig 3.2). However, the designed feedback controllers would allow the use of jerky references and still provide smooth motion. The velocity of the cart was limited to 2.5 m/s by the length of the movement. The maximum velocity is actually more than the maximum velocity value that the connection shaft would allow (Fig. 2.11), but as the measurements show there are no visible complications at the velocity of 2.5 m/s.

Figure 5.1 shows the position references of the system, position errors, motor velocities, and the torque reference using both the PID position control structure and the cascaded P position controller and the PID velocity controller, when applying different robust margins of the velocity controller. The parameters of the PID position controllers are shown in Table 4.4 (delay of 850 µs) and the cascaded structure in Tables 4.5 and 4.6. The movement is from the end of the guide (the "flexible" part of the axes) to the start of the guide (the "rigid" part of the axes). Figure 5.2 shows the same movement but the moving direction is opposite (from the "rigid" part to the "flexible" part).

As we can see in the figures, even though the cart velocity is more than the connection shaft would allow, there are no visible problems. The shaft resonance is not excited. The performance difference can be seen in the position errors. The smallest maximum error is achieved with the PID position controller while the largest position error is achieved when using the cascaded structure and when the velocity controller is tuned with the smallest robust margins. The PID position controller has a significant overshoot, which is not always tolerable. These results are as expected. Even though the smallest position error is achieved when the velocity controller is loop shaped using the largest robust margin $M_T = 1.05$ in the cascaded structure, a closer look reveals that the settling time of the system is large because of the large integrator time constant of the velocity controller. The same large settling time can also be seen when the PID position controller is used. When the velocity controller is loop shaped using the robust margin $M_T = 1.25$, the maximum position error is not significantly increased and the integrator time constant of the velocity controller is not considerably reduced, which ensures a faster settling time. The best overall performance of the studied cascaded structure can be achieved if the robust margin

M_T = 1.25. This is the reason why the other measurements are performed with this robust margin.

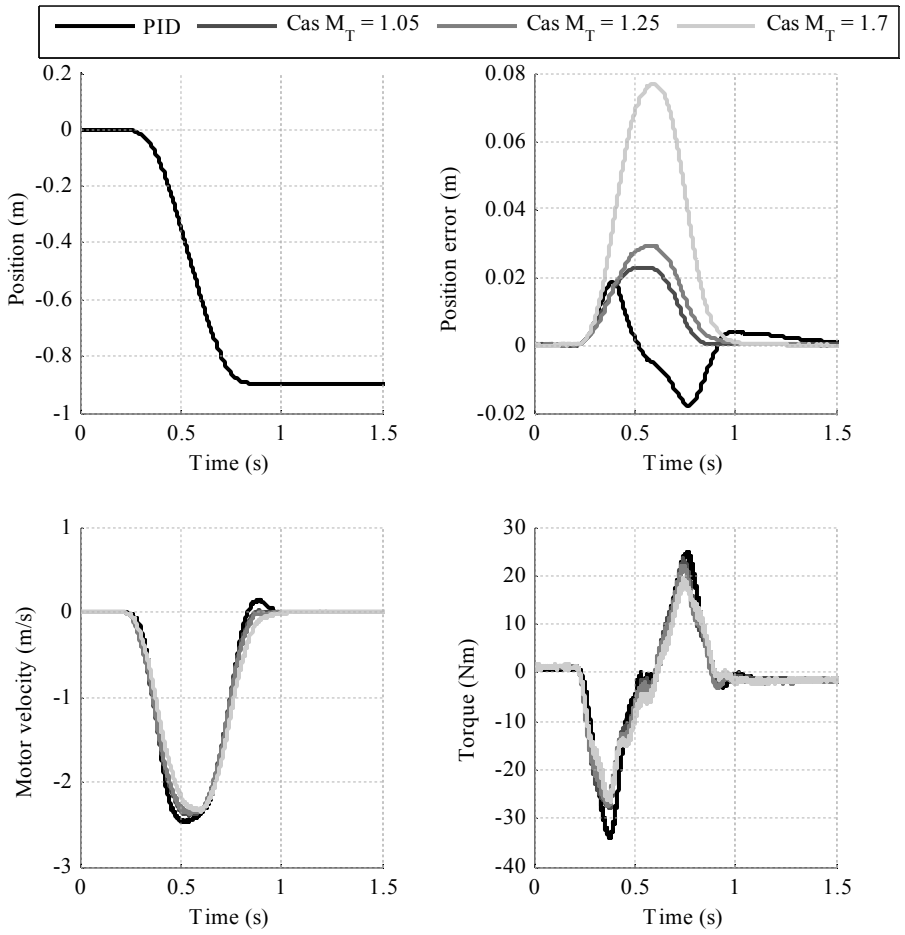

Fig. 5.1. Cascaded structure compared with the PID position controller using maximum acceleration and deceleration (15 m/s^2) and a velocity of 2.5 m/s. The cart is moved from flexible to rigid positions.

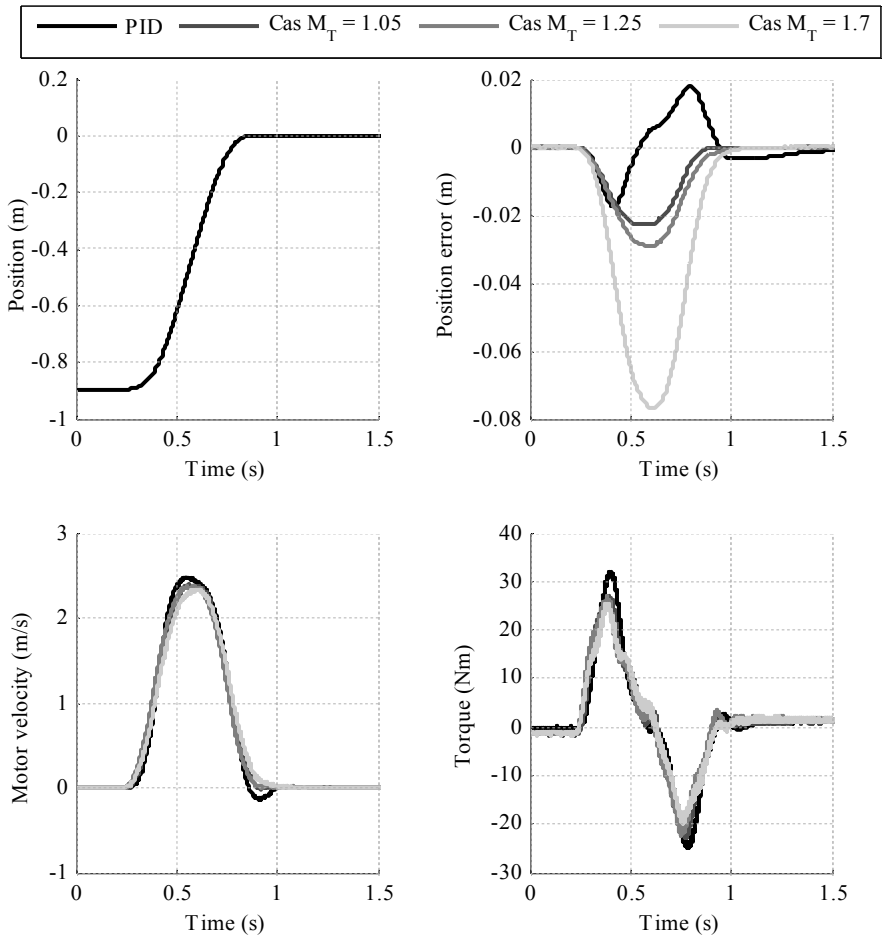

Fig. 5.2. Cascaded structure compared with the PID position controller using maximum acceleration and deceleration (15 m/s^2) and a velocity of 2.5 m/s. The cart is moved from rigid to flexible positions.

The velocity of the cart was varied to be 0.5 m/s, 1.0 m/s, and 1.5 m/s, the acceleration and deceleration of the system were kept constant at 250 m/s^2 during the measurement, and the jerk of the movement was set to 100 m/s^3. The velocity of the movement affects the performance of the system. Figure 5.3 shows the position references, motor velocities, position errors, and torque references during these motion references when using the cascaded structure. Figure 5.4 shows the same measurements with the PID position controller. Again, the main differences of these control structures can be seen. The faster movement gives a larger constant speed error when the cascaded structure is used, but with the PID position controller, the increased velocity does not increase the maximum position error. Figure 5.5 shows that we get opposite results if the acceleration and deceleration of the system are changed and the velocity is kept constant. The acceleration and deceleration rates do not seem to have any effect on the maximum error if the cascaded structure is used, but with the PID controller, the position error is increased if the acceleration and deceleration rates are increased.

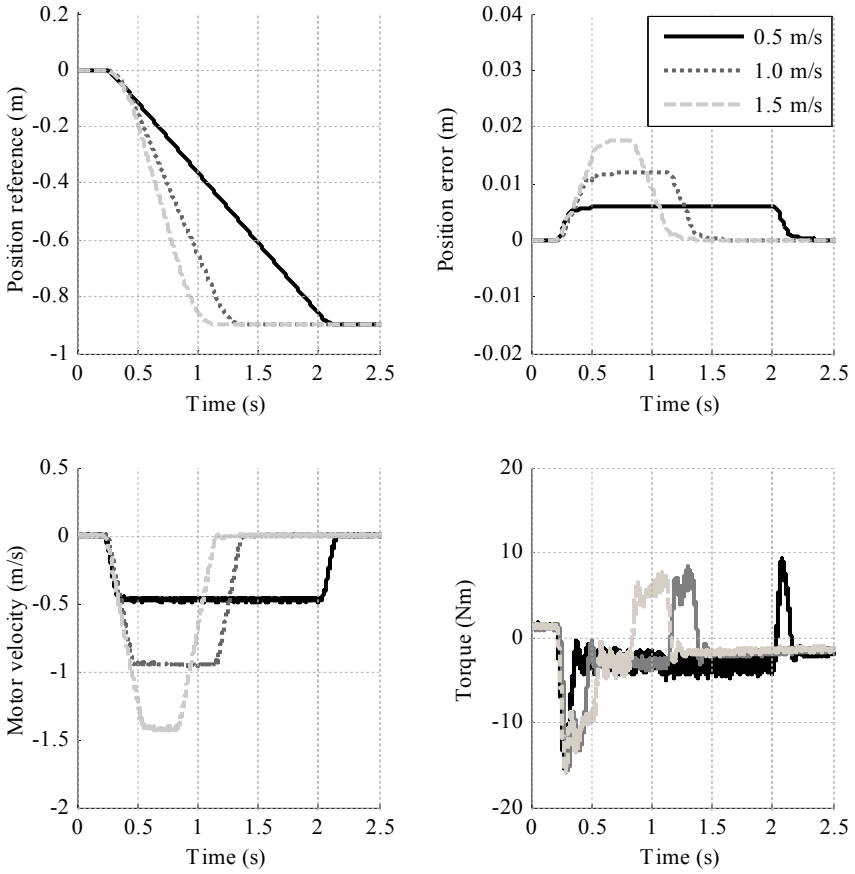

Fig. 5.3. Cascaded control structure $M_T = 1.25$ using different velocity values. The cart is moved from flexible to rigid position.

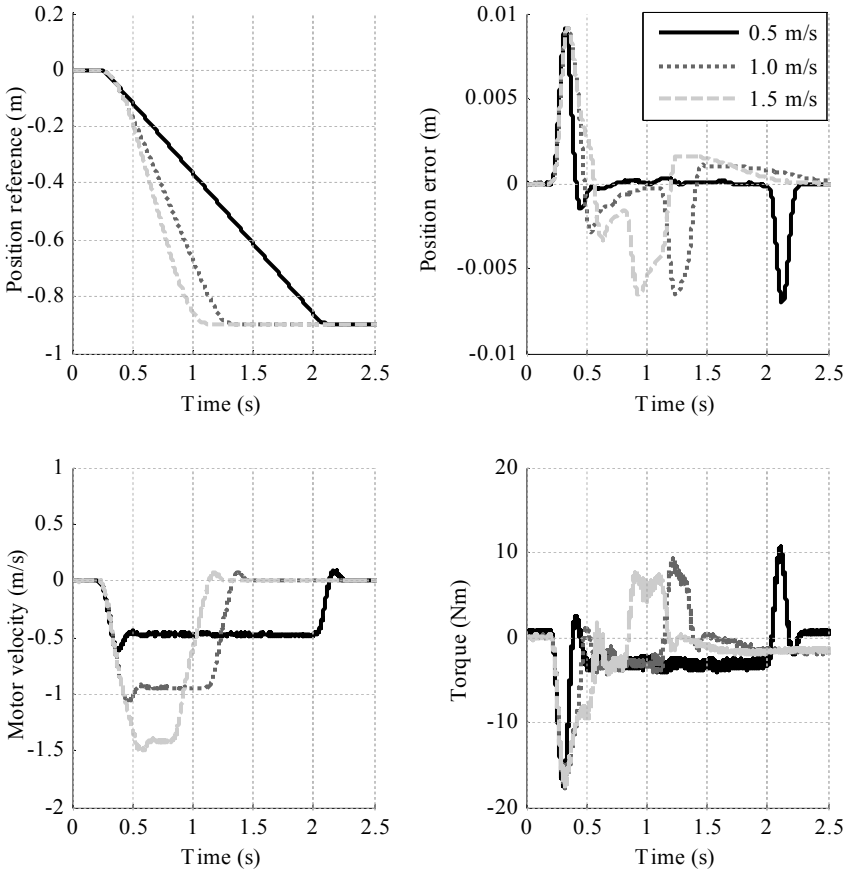

Fig. 5.4. PID position control structure using different cart velocity values. The cart is moved from flexible to rigid position.

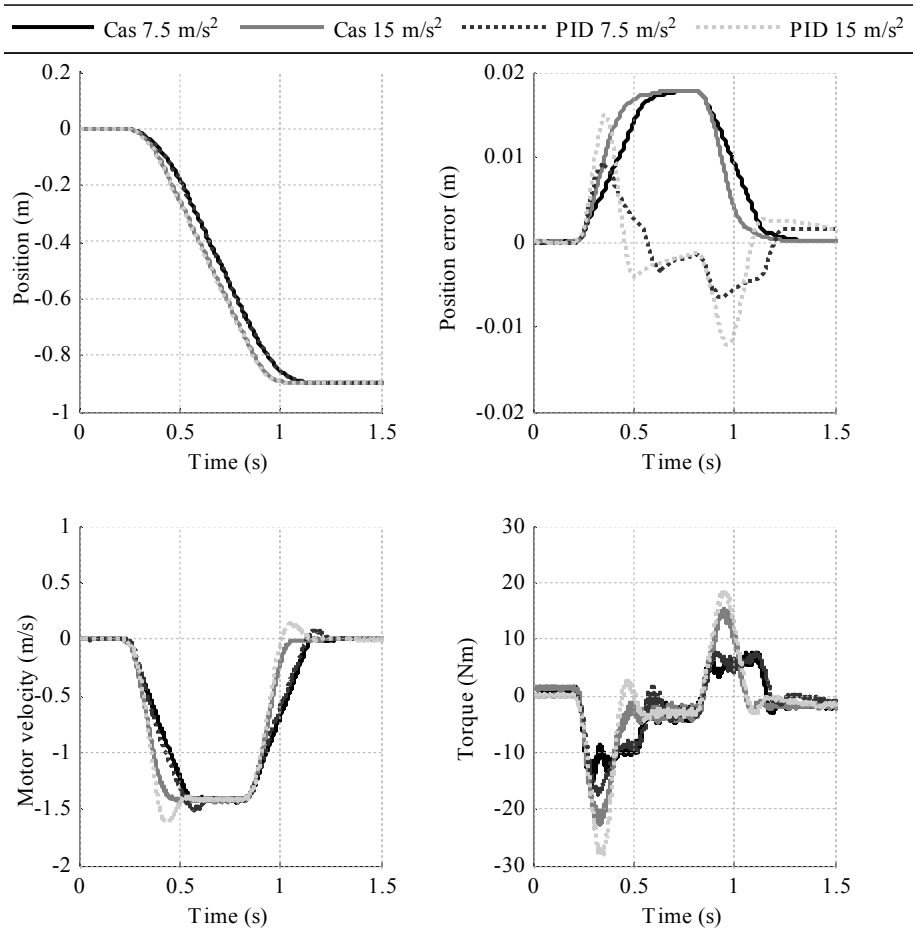

Fig. 5.5. Effect of the acceleration value when using the cascaded structure and the PID position controller. The cart is moved from flexible to rigid position.

The effect of jerk is shown in Fig. 5.6. The upper left-hand figure shows the motor velocity using the cascaded structure, the lower left-hand figure shows the motor velocity using the cascaded structure with both acceleration and velocity feedforwards, the upper right-hand figure shows the motor velocity when the PID position controller is used, and finally, the lower right-hand figure depicts the PID position controller with an acceleration feedforward. The jerk of the movement is varied between 100 m/s^3, 500 m/s^3, and 5000 m/s^3 and the control structures are compared. The jerk of 100 m/s^3 is small enough so that it does not excite any resonance frequency of the system, while the jerk of 500 m/s^3 may excite the resonance of the connection shaft but not the belt resonance, and finally, the jerk of 5000 m/s^3 excites all the resonances if there are some. It can be seen that if no feedforwards are used, the motor velocity does not have any significant resonances, but if the feedforwards are used, a larger jerk excites the resonance of the system and causes an additional force to the belt, which may lead to a situation where the belt force is larger than the holding force, and consequently, the belt will jump over one tooth.

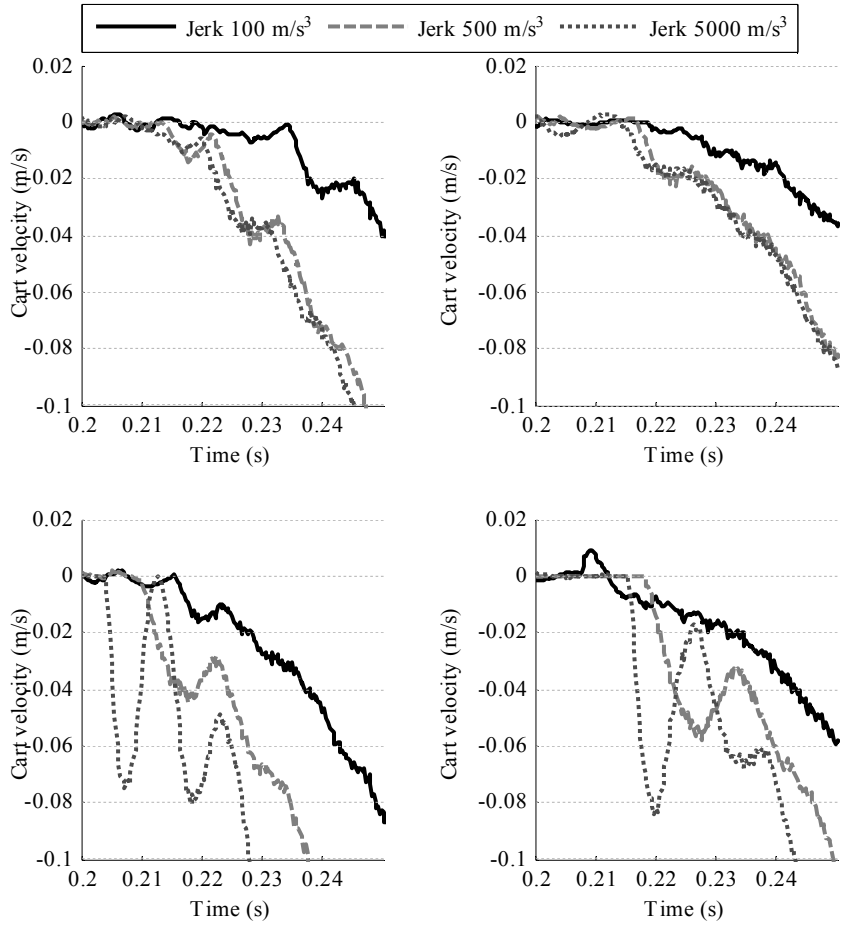

Fig. 5.6. Motor velocities with different control structures. Upper left: Cascaded structure, upper right: PID position controller, lower left cascaded with velocity and accelerations feedforwards and lower right PID position controller with an acceleration feedforward.

Because the oscillation of the system is not desired, the jerk of the movement must be reduced to 100 m/s^3 if an acceleration feedforward is used. Figure 5.7 shows the advantage of the feedforwards. Using the acceleration feedforward with the PID position controller, the maximum position error is reduced from 90 mm to 30 mm with the motion profile of 1.5 m/s velocity and 7.5 m/s^2 acceleration and deceleration rates. If the cascaded structure is used with both acceleration and velocity feedforwards, the maximum position error is reduced from 18 mm to 0.5 mm.

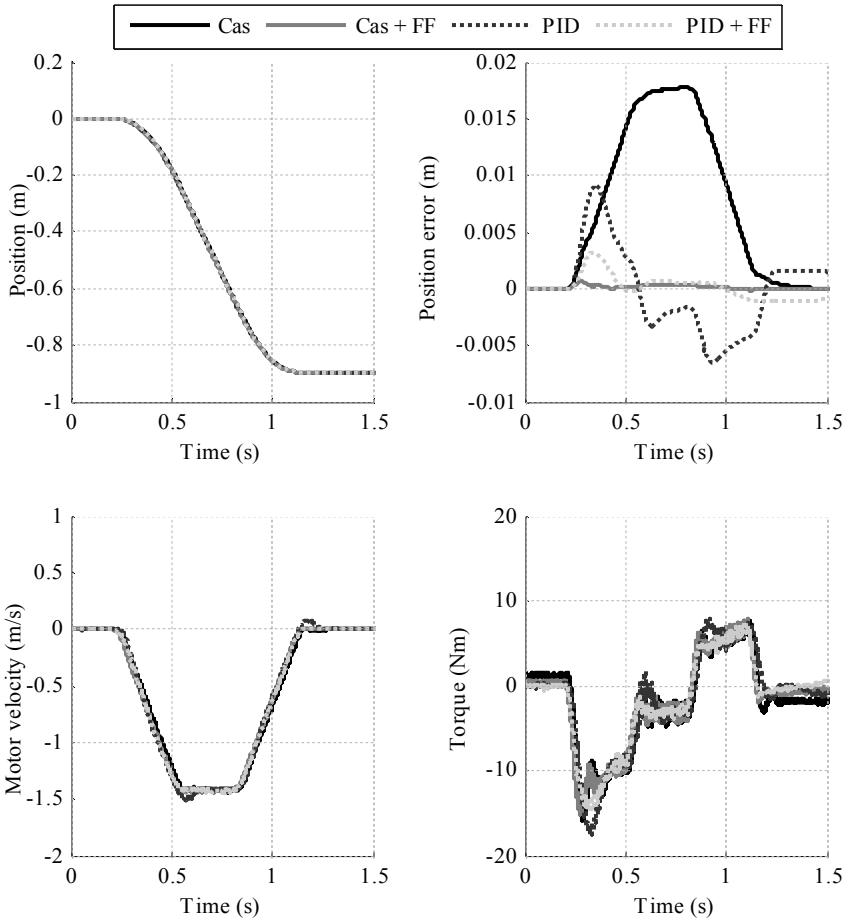

Fig. 5.7. Cascaded structure versus a PID position controller with and without feedforwards.

6 CONCLUSION

In the course of this doctoral thesis it became obvious to the author that if a high-performance motion control system were to be designed, the whole process should be understood in detail. There are a great variety of parameters and characteristics of the process that have a significant influence on the performance of the process. The tuning and design rules that are commonly used in industry are not valid, if the characteristics of the total process are taken into account. The traditional control structures such as a PID position controller with a reference feedforward or a P position controller cascaded with a PID velocity and feedforwards may work properly if the reference is frequency band limited and there are no significant disturbances in the system. Nevertheless, the tuning of these controllers is still a challenging task. In this study, the quantitative feedback theory was used to design a robust feedback and reference feedforward control structure. With the QFT method, a robust and accurate position controller can be achieved.

The test setup used in the study was a Cartesian robot, which uses tooth belt drives for the *x*, *y*, and *z* movements. The x-axis was the most critical one, and a lot of effort was put to understand the behavior and limitations of the drive. The results were very promising: Accurate tracking capability was achieved, and knowledge was obtained on how these drives should be driven, how the references should be made, what kind of properties the fieldbus should have if the system were controlled in a centralized manner. However, these results are not valid only with linear tooth belt drives. Results can be utilized in most of the processes, where resonant frequencies are present.

There is still a lot of work to be done in this field: Because the resonance frequency of the tooth belt drive varies between the operations, the controller is very difficult to tune so that it would give a good and robust performance at the same time. It would be interesting to investigate whether a vibration controller or a disturbance observer could linearize the model in such a way that the feedback controller would be easier to tune. Also the delay compensation should be studied in more detail, because the lead/lag filters used in this study to compensate the phase distortion of the loop delay increase the high-frequency magnification and may amplify the measurement excessively.

REFERENCES

ABB, 2008, [Online], Available at http://www.expo21xx.com/automation21xx/13869_st3_robotics/3_p4_3x3.jpg, [Accessed 10 December 2008].

ABB, 2010, [Online], Available at http://www.abb.fi/product/seitp327/0fdf4cb76bdf4dfec12575070045ed16.aspx?productLanguage=fi&country=FI&tabKey=2 [Accessed 11 April 2010].

ABB Review, 2008, "Picking a winner and packing a punch," *ABB Review* 4/2008, pp. 29–33.

Ahn K.K. and Chau N.H.T., 2007, "Design of a robust force controller for the new mini motion package using quantitative feedback theory," *Mechatronics*, Vol. 17, pp. 532–550.

Armstrong Jr, R.W., 1998. "Load to Motor Inertia Mismatch: Unveiling the Truth," presented at *Drives and Controls Conference*, Telford, England. [Online], Available at http://www.diequa.com/download/articles/inertia.pdf, [Accessed 4 May 2010].

Borghesani C., Chait Y., and Yaniv O., 2003, *The QFT Frequency Domain Control Design Toolbox for Use with MATLAB®*, [Online], Available at http://www.terasoft.com/qft/QFTManual.pdf, [Accessed 10 February 2010].

Bose B.K., 1985, "Motion Control Technology – Present and Future," *IEEE Transaction on Industry Applications*, Vol. 1A-21, No. 6, November/December, pp. 1337–1342.

Byrne G., Dornfeld D., and Denkena B., 2003, "Advancing Cutting Technology," *CIRP Annals-Manufacturing Technology*, Vol. 52, Issue 2, pp. 383–507.

Chen S. L., Tan K.K., and Huang S.N, 2007,"Friction Modelling of Servomechanical Systems with Dual-relay Feedback," In *Proceedings of the IEEE Industrial Electronics Society*, *Annual Meeting*, pp. 557–562.

Craig J., 1986, *Introduction to Robotics Mechanics & Control,* New York: Addison-Wesley Publishing Company, 1986.

Cusimano G., 2007, "Optimization of the choice of the system electric drive-device – transmission for mechatronic applications," *Mechanism and Machine Theory*, Vol. 42, pp. 48–65.

Dornfeld D., and Lee D.E., 2008, *Precision Manufacturing*, New York, New York: Springer Science+Business Media, LCC.

Ellis G., and Lorenz R.D., 1999, "Comparison of Motion Control Loops for industrial applications," In *Proceedings of the IEEE Industry Applications Society, Annual Meeting*, Vol. 4, pp. 2599–2605.

Ellis G., 2000, *Control system design guide, second edition*, Boston: Academic Press.

Ellis G., Lorenz R.D., 2000, "Resonant Load Control Methods for Industrial Servo Drives," In *Proceedings of the IEEE Industry Applications Society*, *Annual Meeting*, Vol. 3, pp. 1438–1445.

Ellis G., and Gao Z., 2001, "Cures for Low-Frequency Mechanical Resonance in Industrial Servo Systems," In *Proceedings of the IEEE Industry Applications Society*, *Annual Meeting*, Vol. 1, pp. 252–258.

Erkorkmaz K. and Altintas Y., 2000, "High speed CNC system design Part I: jerk limited trajectory generation and quintic spline interpolation," *International Journal of Machine Tools & Manufacture*, Vol. 41, pp. 1323–1343.

Faanes A. and Skogestad S., 2003, "Feedforward control under the presence of the plant uncertainty," *European Control Conference, ECC' 03*, Cambridge, UK, September 1–4, 2003.

Fan K. C. and Chen M. J., 2000, "A 6-degree-of-freedom measurement system for the accuracy of X-Y stages," *Precision Engineering*, Vol. 24, pp. 15–23.

Festo, 2006, Ordering documentation of the test system.

Festo, 2003, "Repair Instructions Electrical Linear Axis With Toothed Belt And Roller Guide," Product Management Technical Support.

García-Sanz M., Guillén J.C., and Ibarrola J.J., 2001, "Robust controller design for uncertain system with variable time delay," *Control Engineering Practice 9*, pp. 961–972.

Graham K. S., 1996, *Theory and problems of mechanical vibrations*, New York: The McGraw-Hill Company.

Hace A., Jerernik K., Curk B., and Terbuc M., 1998, "Robust Motion Control of XY Table for Laser Cutting Machine," In *Proceedings of the IEEE IECON*, *Annual Meeting,* Vol. 2., pp. 1097– 1102.

Hace A., Jezernik K., and Terbuc M., 2001, "VSS motion control for a laser-cutting machine," *Control Engineering Practice 9*, pp. 67-77.

Hace A., Jezernik K., and Sabanovic A., 2004, "A New Robust Position Control Algorithm for a Linear Belt-Drive," In *Proceedings of the IEEE international Conference on Mechatronics*, pp. 358–363.

Hace A., Jezernik K., and Sabanovic A., 2005, "Improved Design of VSS Controller for a Linear Belt-Driven Servomechanism," *IEEE/ASME Transactions on Mechatronics*, Vol. 10, No. 5. pp. 385–390.

Hearns G., and Grimble M.J., 2002, "Quantitative Feedback Theory for Rolling Mills," In *Proceedings of the IEEE International Conference on Control Applications*, pp 367–372.

Hibbard S.C., 1995, "Open Drive Interfaces for Advanced Machining Concepts," [Online], Available at http://www.sercos.com/literature/pdf/open_drive_interfaces.pdf, [Accessed 28 April 2010].

Horowitz I. 1982, “Quantitative feedback theory,” *Proceedings of Control Theory and Applications*, Vol. 129, Issue 6., pp. 215–226.

Horowitz I., 2001, “Survey of quantitative feedback theory (QFT),” *International Journal of Robust and Nonlinear Control*, Vol 11., Issue 10., pp. 887–921.

Houpis C., Rasmussen S., and Garcia-Sanz M., 2006, *Quantitative Feedback Theory*: *fundamentals and applications*, Boca Raton (FL): Taylor & Francis Group.

IEC 61491, 2002, “International standard – Electrical equipment of industrial machines Serial data link for real-time communication between controls and drives,” Reference number *CEI/IEC 61491:2002*. Geneva: International Electrotechnical Commission.

Jinkun L., and Yuzhu H., 2007, “QFT control based on zero phase error compensation for flight simulator,” *Journal of System Engineering and Electronics*, Vol. 18, No. 1, pp. 125–131.

Jokinen M., Kosonen A., Niemela M., Ahola J., and Pyrhönen J., 2007, “Disturbance Observer for Speed-Controlled Process With Non-Deterministic Time Delay of Feedback Information,” In *Proceedings of the IEEE Power Electronics Specialists Conference*, pp. 2751–2756.

Jokinen M., Niemelä M., Pyrhönen J., and Kosonen A., 2006, “Implementation of Disturbance Observers in Speed Controlled Electric Drives,” *Nordic Workshop on Power and Industrial Electronics (NORPIE)*, 12–14, June, Lund, Sweden.

Jovane F., Koren Y., and Boer C.R., 2003, “Present and Future of Flexible Automation: Towards New Paradigms,” *CIRPS Annals*, Vol. 52. pp. 543–560.

Karpenko M., Sepehri N., 2006, “QFT Synthesis of a Position Controller for a Pneumatic Actuator in the Presence of Worst-Case Persistent Disturbances,” *American Control Conference*, 14–16, June, Minneapolis, the U.S.A.

Katoaka H., Ohishi K., Miyazaki T., Katsura S., and Takuma H., 2008, ”Motion Control Strategy of Industrial Robot for Vibration Suppression and Little Positioning Phase Error,” *IEEE Workshop on Advanced Motion Control*, Trento, Italy, pp. 661–666.

Kiel E., 2008, *Drive Solutions mechatronics for production and Logistic*, Berlin, Heidelberg: Springer-Verlag.

Kiong T.K., Heng L.T., and Sunan H., 2008, *Precision Motion Control Design and Implementation, second edition*, Berlin, Heidenlberg: Springer-Vertag.

Kynast R., 2005, *Specification SERCOS interface Version 2.4 (Update 02.05)*, *SERCOS International e.V*.

Laribi M. A., Romdhane L., Zeghloul S., 2007, “Analysis and dimensional synthesis of the DELTA robot for a prescribed workspace,” *Mechanism and Machine Theory*, Vol 42, Issue 7, pp. 859–870.

Lewis F. L., Dawson D. M., Abdallah C. T., 2004, *Robot Manipulator Control: Theory and Practice, Second Edition, Revised and Expanded*, New York: Marcel Dekker Inc.

Liu Z. Z. and Luo F. L., 2005, "Robust and Precision Motion Control System of Linear-Motor Direct Drive for High-Speed X-Y Table Positioning Mechanism," In *Proceedings of the IEEE Transactions on Industrial Electronics*, Vol. 52, No. 5, October 2005, pp. 1357–1363.

MANU*FUTURE* High Level Group, 2004, *Manufuture a Vision for 2020*, , [Online], Available at http://www.manufuture.org/manufacturing/wp-content/uploads/manufuture_vision_en1.pdf, [Accessed 22 April 2010].

McCarthy K., 1991, "Accuracy in Positioning Systems," *Reprinted from The Motion Control Technology Conference Proceedings*, March 19–21, 1991. [Online], Available at http://www.dovermotion.com/Downloads/KnowledgeCenter/Accuracy.pdf, [Accessed 28 December 2010].

Neugebauer R, Denkena B., Wegener K., 2007, "Mechatronic Systems for Machine Tools," *CIRPS Annals*, Vol. 56, Issue 2, pp. 657–686.

Niiranen J., 2009, "Applications for Industry – practical point of view & future needs," post-graduate course *Estimation of electrical-machine models*, Helsinki University of Technology, Espoo, Finland, 11–16 May 2009.

Olabi A., Béarée R., Gibaru O., 2010, "Feedrate planning for machining with industrial six-axis robots," *Control Engineering Practice*. Vol 18, Issue 5, pp. 471–482.

Olsson H., Åström K.J., Canudas de Wit C., Gäfvert M., and Lischinsky P., 1997, *Friction Models and Friction Compensation*, [Online], Available at http://www.lag.ensieg.inpg.fr/canudas/publications/friction/dynamic_friction_EJC_98.pdf, [Accessed 1 March 2010].

Ott H. W., 1988, *Noise Reduction Techniques in Electronic Systems*, Chichester: John Wiley & Sons, 2nd edition.

Parallemic, 2010, [Online], Available at http://www.parallemic.org/Material/FlexPicker.gif, [Accessed 11 April 2010].

Pettersson M., 2008, *Design Optimization in Industrial Robotics Methods and Algorithms for Drive Train Design*, Dissertations, No. 1170, Linköping University Institute of Technology, Sweden.

PLCopen, 2010, [Online], Available at http://www.plcopen.org, [Accessed 2 September 2010].

Puranen J., 2006, *Induction motor versus permanent magnet synchronous motor in motion control applications: a comparative study*, Dissertation, Acta Universitatis Lappeenrantaensis 249, Lappeenranta University of Technology, Lappeenranta.

Rahman M., Heikkala J., and Lappalainen K., 2000, "Modeling, measurement and error compensation of multi-axis machine tools. Part I: theory," *International Journal of Machine Tools & Manufacture*, Vol. 40, pp. 1535–1546.

Ramesh R., Mannan M.A., and Poo A.N., 2005, "Tracking and contour error control in CNC servo systems," *International Journal of Machine Tools & Manufacture*, Vol. 45, pp. 301–326.

Roos F., 2007, *Towards a Methodology for Integrated Design of Mechatronic Servo Systems*, Doctoral thesis, Royal Institute of Technology, Stockholm, Sweden.

Schmidt P., Rehm T., 1999, "Notch Filter Tuning for Resonant Frequency Reduction in Dual Inertia Systems," In *Proceedings of the IEEE Industry Applications Conference, Annual Meeting*, Vol. 3, pp. 1730–1734.

Schneiders M.G.E, van de Molengraft M.J.G, Steinbuch M., 2003, "Introduction To an Integrated Design For Motion Systems Using Over-Actuation," In *Proceedings of the European Control Conference 2003*.

Schwenke H., Knapp W., Haitjema H., Weckenmann A., Schmitt R., and Delbressine F., 2008, "Geometric error measurement and compensation of machines – an update," *CIRP Annals – Manufacturing Technology*, Vol. 57, pp. 660–675.

Singhose W., 1997, *Command Generation for Flexible Systems*, D.Sc (Tech) dissertation, Massachusetts Institute of Technology.

Skogestad S., Postlethwaite I., 2005, *Multivariable Feedback Control Analysis and Design,* Second edition, Chichester, England: John Wiley & Sons.

SKS, 1999, "Design guide for a tooth belt drive (Hammashihnakäytön suunnitteluopas)," datasheet in Finnish, [Online], Available at http://www.sks.fi, [Accessed 20 April 2008].

Stenerson J, 1999, *Fundamentals of Programmable Logic Controllers, Sensors, and Communications*, Second Edition, Upper Saddle River (N.J.): Prentice-Hall.

Stephens L., 2007, "What goes wrong when inertias aren't right," [Online], Available at http://machinedesign.com/article/what-goes-wrong-when-inertias-arent-right-0524 [Accessed on 30 July 2007].

Suh S.-H., Kang S.-K., Chung D.-H., and Stound I., 2008, *Theory and Design of CNC Systems*, London: Springer-Verlag.

Taghirad H.D. and Rahimi H., 2005, "Composite QFT controller Design for Flexible Joint Robots," In *Proceedings of the IEEE Conference on Control Applications*, pp. 583–588.

Tao Z., Changhou L., and Zhuyan X., 2006, "Modeling and Simulation of Nonlinear Friction in XY AC Servo Table," In *Proceedings of the IEEE International Conference on Mechatronics and Automation*, pp. 616–622.

Tomizuka M., 1987, "Zero Phase Error Tracking Algorithm for digital Control," *Journal of dynamic systems, Measurement and Control*, Vol 109, pp. 65–68.

Van de Straete H., Degezelle P., De Schutter J., 1998, "Servo Motor Selection Criterion for Mechatronic Applications," *IEEE/ASME Transactions on Mechatronics*, Vol. 3, No. 1, pp. 43–50.

Voss W., 2007, *A Comprehensible Guide to Servo Motor Sizing*, Massachusetts: Copperhill Technologies Corporation.

Wontrop C., 2010, "How Today's Flexible Digital Servo Drives Help OEMs Build a Better Machine, Faster," [Online], Available at http://kollmorgen.com/website/common/download/document/2-20100216-20475672.pdf, [Accessed 15 April 2010].

Wu W., 2000, "A New QFT Design Method for SISO Cascaded-loop Design," In *Proceedings of the IEEE American Control Conference*, Vol. 6, pp. 3827–3831.

Yaniv O., 1999, *Quantitative Feedback Design of Linear and Nonlinear Control Systems*, Massachusetts: Kluwer Academic Publishers.

Yaniv O. and Nagurka M., 2004, "Design of PID controllers satisfying gain margins and sensitivity constraints on a set of plants," *Automatica,* Vol. 40, pp. 111–116.

Yaniv O. and Nagurka M., 2005, "Automatic Loop Shaping of Structured Controllers Satisfying QFT Performance," *Transactions of the ASME*, Vol. 127, pp. 472–477, September, 2005.

Yaskawa 2005, "Comparison of Higher Performance AC Drives and AC Servo Controllers," [Online], Available at http://www.yaskawa.com/site/Industries.nsf/reportFiles/AN.AFD.05, [Accessed 25 July 2005].

Younkin G., 2004, "Compensating Structural Dynamics For Servo Driven Industrial Machines with Acceleration Feedback," In *Proceedings of the IEEE Industry Applications, Annual Meeting*, Vol. 3, pp. 188–1890.

Younkin G., 2003, *Industrial Servo Control Systems Fundamentals and Applications*, 2nd edition Revised and Expanded, New York: Marcel Dekker.

Younkin G., McGlasson W.D., Lorenz R.D., 1991, "Considerations for Low Inertia AC Drives in Machine Tool Axis Servo Applications", *IEEE transactions on industry applications*, Vol. 27, No. 2, pp. 262–267.

Ziegler J. G. and Nichols N. B., 1942, "Optimum settings for automatic controllers," *Transactions of the A. S. M. E.*, November 1942. pp. 759–768.

Zolotas A.C., Halikias G.D., 1999, "Optimal design of PID controllers using the QFT method," In *Proceedings of the IEE Control Theory Applications.* Vol 146, No. 6, pp. 585–589.

Åström K. J., Hägglund T., 1995, *PID Controllers: Theory, Design, and Tuning*, 2nd edition, Research Triangle Park (N.C.): Instrument Society of America.

Åström K. J., Wittenmark B., 1995, *Adaptive Control,* 2nd edition, 1995, New York: Addison-Wesley Publishing Company.

ACTA UNIVERSITATIS LAPPEENRANTAENSIS

365. POLESE, GIOVANNI. The detector control systems for the CMS resistive plate chamber at LHC. 2009. Diss.

366. KALENOVA, DIANA. Color and spectral image assessment using novel quality and fidelity techniques. 2009. Diss.

367. JALKALA, ANNE. Customer reference marketing in a business-to-business context. 2009. Diss.

368. HANNOLA, LEA. Challenges and means for the front end activities of software development. 2009. Diss.

369. PÄTÄRI, SATU. On value creation at an industrial intersection – Bioenergy in the forest and energy sectors. 2009. Diss.

370. HENTTONEN, KAISA. The effects of social networks on work-team effectiveness. 2009. Diss.

371. LASSILA, JUKKA. Strategic development of electricity distribution networks – Concept and methods. 2009. Diss.

372. PAAKKUNAINEN, MAARET. Sampling in chemical analysis. 2009. Diss.

373. LISUNOV, KONSTANTIN. Magnetic and transport properties of II-V diluted magnetic semiconductors doped with manganese and nickel. 2009. Diss.

374. JUSSILA, HANNE. Concentrated winding multiphase permanent magnet machine design and electromagnetic properties – Case axial flux machine. 2009. Diss.

375. AUVINEN, HARRI. Inversion and assimilation methods with applications in geophysical remote sensing. 2009. Diss.

376. KINDSIGO, MERIT. Wet oxidation of recalcitrant lignin waters: Experimental and kinetic studies. 2009. Diss.

377. PESSI, PEKKA. Novel robot solutions for carrying out field joint welding and machining in the assembly of the vacuum vessel of ITER. 2009. Diss.

378. STRÖM, JUHA-PEKKA. Active du/dt filtering for variable-speed AC drives. 2009. Diss.

379. NURMI, SIMO A. Computational and experimental investigation of the grooved roll in paper machine environment. 2009. Diss.

380. HÄKKINEN, ANTTI. The influence of crystallization conditions on the filtration characteristics of sulphathiazole suspensions. 2009. Diss.

381. SYRJÄ, PASI. Pienten osakeyhtiöiden verosuunnittelu – empiirinen tutkimus. 2010. Diss.

382. KERKKÄNEN, ANNASTIINA. Improving demand forecasting practices in the industrial context. 2010. Diss.

383. TAHVANAINEN, KAISA. Managing regulatory risks when outsourcing network-related services in the electricity distribution sector. 2010. Diss.

384. RITALA, PAAVO. Coopetitive advantage – How firms create and appropriate value by collaborating with their competitors. 2010. Diss.

385. RAUVANTO, IRINA. The intrinsic mechanisms of softwood fiber damage in brown stock fiber line unit operations. 2010. Diss.

386. NAUMANEN, VILLE. Multilevel converter modulation: implementation and analysis. 2010. Diss.

387. IKÄVALKO, MARKKU. Contextuality in SME ownership – Studies on owner-managers´ ownership behavior. 2010. Diss.

388. SALOJÄRVI, HANNA. Customer knowledge processing in key account management. 2010. Diss.

389. ITKONEN, TONI. Parallel-operating three-phase voltage source inverters – Circulating current modeling, analysis and mitigation. 2010. Diss.

390. EEROLA, TUOMAS. Computational visual quality of digitally printed images. 2010. Diss.

391. TIAINEN, RISTO. Utilization of a time domain simulator in the technical and economic analysis of a wind turbine electric drive train. 2010. Diss.

392. GRÖNMAN AKI. Numerical modelling of small supersonic axial flow turbines. 2010. Diss.

393. KÄHKÖNEN, ANNI-KAISA. The role of power relations in strategic supply management – A value net approach. 2010. Diss.

394. VIROLAINEN, ILKKA. Johdon coaching: Rajanvetoja, taustateorioita ja prosesseja. 2010. Diss.

395. HONG, JIANZHONG. Cultural aspects of university-industry knowledge interaction. 2010. Diss.

396. AARNIOVUORI, LASSI. Induction motor drive energy efficiency – Simulation and analysis. 2010. Diss.

397. SALMINEN, KRISTIAN. The effects of some furnish and paper structure related factors on wet web tensile and relaxation characteristics. 2010. Diss.

398. WANDERA, CATHERINE. Performance of high power fiber laser cutting of thick-section steel and medium-section aluminium. 2010. Diss.

399. ALATALO, HANNU. Supersaturation-controlled crystallization. 2010. Diss.

400. RUNGI, MAIT. Management of interdependency in project portfolio management. 2010. Diss.

401. PITKÄNEN, HEIKKI. First principles modeling of metallic alloys and alloy surfaces. 2010. Diss.

402. VAHTERISTO, KARI. Kinetic modeling of mechanisms of industrially important organic reactions in gas and liquid phase. 2010. Diss.

403. LAAKKONEN, TOMMI. Distributed control architecture of power electronics building-block-based frequency converters. 2010. Diss.

404. PELTONIEMI, PASI. Phase voltage control and filtering in a converter-fed single-phase customer-end system of the LVDC distribution network. 2010. Diss.

405. TANSKANEN, ANNA. Analysis of electricity distribution network operation business models and capitalization of control room functions with DMS. 2010. Diss.

406. PIIRAINEN, KALLE A. IDEAS for strategic technology management: Design of an electronically mediated scenario process. 2010. Diss.